Molecular Characterization of EspB: A Phospholipid Binding *Mycobacterium tuberculosis* Virulence Factor

A Thesis Submitted to the
College of Graduate and Postdoctoral Studies
In Partial Fulfillment of the Requirements
For the Degree of Master of Science
In the Department of Biochemistry, Microbiology and Immunology
University of Saskatchewan
Saskatoon

By

Beatrice Chung

PERMISSION TO USE

In presenting this thesis in partial fulfillment of the requirements for a Postgraduate degree from the University of Saskatchewan, I agree that the Libraries of this University may make it freely available for inspection. I further agree that permission for copying of this thesis in any manner, in whole or in part, for scholarly purposes may be granted by the professor who supervised my thesis work or, in their absence, by the Head of the Department or the Dean of the College in which my thesis work was done. It is understood that any copying or publication or use of this thesis or parts thereof for financial gain shall not be allowed without my written permission. It is also understood that due recognition shall be given to me and to the University of Saskatchewan in any scholarly use which may be made of any material in my thesis.

Requests for permission to copy or to make other uses of materials in this thesis in whole or part should be addressed to:

Head of the Department of Biochemistry, Microbiology and Immunology
GA20.12, Health Sciences
107 Wiggins Road
University of Saskatchewan
Saskatoon, Saskatchewan S7N 5E5
Canada

OR

Dean
College of Graduate and Postdoctoral Studies
116 Thorvaldson Building, 110 Science Place
University of Saskatchewan
Saskatoon, Saskatchewan S7N 5C9
Canada

ABSTRACT

Mycobacterium tuberculosis (*M. tb*) is the causative agent of tuberculosis (TB), a severe lung infection that causes 1.4 million deaths per year. During infection, *M. tb* is able to subvert host immune responses and survive within the macrophage by using its type-7 early secreted antigenic target (ESAT-6) system 1 (ESX-1) to secrete virulence protein effectors including EspB. A previously published study showed that EspB has a virulence function distinct from other ESX-1 secreted proteins that may be dependent on phospholipid binding. The objective of this thesis project is to determine the molecular basis of EspB-phospholipid interactions and whether oligomerization of EspB is critical for its interaction with phospholipids and consequently important for its virulence function.

Amino acids in EspB predicted to be critical for phospholipid binding (R17, H223, F159, and I246) or oligomerization (W176, K259, and K267) were replaced. Recombinant EspB variants ($EspB^{R17A/H223A}$, $EspB^{F159R/I246R}$, $EspB^{W176R}$, and $EspB^{K259A/K267A}$) were produced in *Escherichia coli* (*E. coli*) and were assessed for oligomerization and phospholipid binding.

Two EspB variants, $EspB^{R17A/H223A}$ and $EspB^{F159R/I246R}$ were shown to form hyper-oligomers in native polyacrylamide gel electrophoresis (native-PAGE), dynamic light scattering, and transmission electron microscopy analyses. $EspB^{W176R}$ and $EspB^{K259A/K267A}$ did not appear to have significant differences in oligomerization compared to $EspB^{WT}$. Replacement of the residues R17 and H223 in $EspB^{R17A/H223A}$ abolished its phospholipid binding ability, whereas the replacement of residues in F159 and I246 in $EspB^{F159R/I246R}$ appeared to enhance phospholipid binding. $EspB^{W176R}$ was able to bind phospholipids similarly to $EspB^{WT}$ and $EspB^{K259A/K267A}$ was shown to have reduced binding. Addition of purified $EspB^{R17A/H223A}$ to the *M. tb* 5'Tn::*pe35* strain was able to enhance the induction of THP-1 macrophage cytotoxicity similarly to $EspB^{WT}$.

The residues R17 and H223 appear to be important for phospholipid binding. However, mutation in predicted critical oligomeric sites of EspB did not have a significant impact on its phospholipid binding ability. Although phospholipid binding ability was predicted to affect the virulence function of EspB, purified $EspB^{R17A/H223A}$ was still able to induce cytotoxicity in THP-1

macrophages similarly to $EspB^{WT}$, suggesting that phospholipid binding may not be the sole factor in EspB virulence.

ACKNOWLEDGEMENTS

I would first like to thank my supervisor, Dr. Jeffrey Chen, for the support and guidance throughout the course of my degree. I would also like to thank my committee members, Dr. Linda Chelico, Dr. Harold Bull, and Dr. Scot Stone for advising me throughout my project and providing me with invaluable feedback. I would also like to thank my peers from VIDO and especially from the Chen lab for their support and for all of their contributions to my project.

I would like to acknowledge LaRhonda Sobchishin and Dr. Eiko Kawamura at the WCVM for assisting me with my work on TEM imaging. I would also like to thank Dr. Michal Boniecki at the PCCF for helping me with obtaining and interpreting my DLS data.

Lastly, I would like to thank my friends and family for their tremendous support and encouragements these past few years.

The work presented in this thesis was supported by a grant from the National Sanitarium Association and Devolved Graduate Scholarships from the Department of Biochemistry, Microbiology, and Immunology, and the College of Graduate and Postdoctoral Studies at the University of Saskatchewan.

PERMISSION TO REPRODUCE

All previously published figures within this document have been reproduced with permission from the journals in which they were published.

Figure 1.2: Pai, M., Behr, M.A., Dowdy, D., Dheda, K., Divangahi, M., Boehme, C.C., Ginsberg, A., Swaminathan, S., Spigelman, M., Getahun, H., et al. (2016). Tuberculosis. Nat. Rev. Dis. Prim. 2, 1–23.

Figure 1.3: Poirier, V., and Av-Gay, Y. (2012). *Mycobacterium tuberculosis* modulators of the macrophage's cellular events. Microbes Infect. 14, 1211–1219.

Figure 1.4: Gröschel, M.I., Sayes, F., Simeone, R., Majlessi, L., and Brosch, R. (2016). ESX secretion systems: Mycobacterial evolution to counter host immunity. Nat. Rev. Microbiol. 14, 677–691.

Figures 1.6, 1.7, 1.8, and 1.10: Chen, J.M., Zhang, M., Rybniker, J., Boy-Röttger, S., Dhar, N., Pojer, F., and Cole, S.T. (2013). *Mycobacterium tuberculosis* EspB binds phospholipids and mediates EsxA-independent virulence. Mol. Microbiol. 89, 1154–1166.

Figure 4.3: Korotkova, N., Piton, J., Wagner, J.M., Boy-Röttger, S., Japaridze, A., Evans, T.J., Cole, S.T., Pojer, F., and Korotkov, K. V. (2015). Structure of EspB, a secreted substrate of the ESX-1 secretion system of *Mycobacterium tuberculosis*. J. Struct. Biol. 191, 236–244.

TABLE OF CONTENTS **PAGE**

LIST OF TABLES **PAGE**

LIST OF FIGURES **PAGE**

LIST OF ABBREVIATIONS

AEC	Airway Epithelial Cell
AM	Alveolar Macrophage
ATCC	American Type Culture Collection
BCA	Bicinchoninic Acid
BCG	Bacille Calmette-Guérin
BSA	Bovine Serum Albumin
CF	Culture Filtrate
CFP-10	Culture Filtrate Protein-10
CL	Cell Lysate
DC	Dendritic Cell
DLPA	1,2-dilauroyl-sn-glycero-3-phosphate
DLS	Dynamic Light Scattering
DMEM	Dulbecco's Modified Eagle's Medium
DMSO	Dimethyl Sulfoxide
DPPS	1,2-dipalmitoyl-sn-glycero-3-phosphoserine
Ecc	Esx conserved-component
ESAT-6	Early Secretory Antigenic Target-6
Esp	ESX-1 specific-protein
ESX	ESAT-6 Secretion System
FBS	Fetal Bovine Serum
GFP	Green Fluorescent Protein
IDT	Integrated DNA Technologies
IFN	Interferon
LB	Luria-Bertani
LEW	Lysis-Equilibrium-Wash
MOI	Multiplicity Of Infection

MTBC	*Mycobacterium tuberculosis* Complex
MycP1	Mycosin-1 Protein
Ni-IDA	Nickel-Iminodiacetic Acid
OD	Optical Density
PA	Phosphatidic Acid
PAGE	Polyacrylamide Gel Electrophoresis
PBS	Phosphate Buffered Saline
PDI	Polydispersity Index
PE	Proline-Glutamate
PIP	Phosphatidylinositol Phosphate
PMA	Phorbol 12-myristate 13-acetate
PPE	Proline-Proline-Glutamate
PS	Phosphatidylserine
RD-1	Region of Difference 1
RPMI	Roswell Park Memorial Institute
TB	Tuberculosis
TBS	Tris Buffered Saline
TEM	Transmission Electron Microscopy
V-ATPase	Vesicular-H+-ATPase
WxG	Tryptophan-x-Glycine
YxxxD	Tyrosine-x-x-x-Aspartate

1. Introduction

1.1. *Mycobacterium tuberculosis*

Mycobacterium tuberculosis (*M. tb*) is the causative agent of tuberculosis (TB) in humans, which is one of the major causes of death due to a single infectious disease agent in the world. In addition to *M. tb*, TB can be caused by other members of the *Mycobacterium tuberculosis* complex (MTBC) such as *Mycobacterium bovis* (*M. bovis*) and *Mycobacterium africanum* (*M. africanum*) (Forrellad et al., 2013; de Jong et al., 2010). TB primarily affects the lungs but can spread to any other organ in the body (Pai et al., 2016). Each year, approximately 10 million people fall ill with TB and 1.5 million people die due to this disease (Geneva: World Health Organization, 2020).

Infection with *M. tb* can lead to several outcomes: clearance of the infection, latent disease, or active disease (Lin and Flynn, 2018) (Figure 1.1). Some infected individuals may be able to

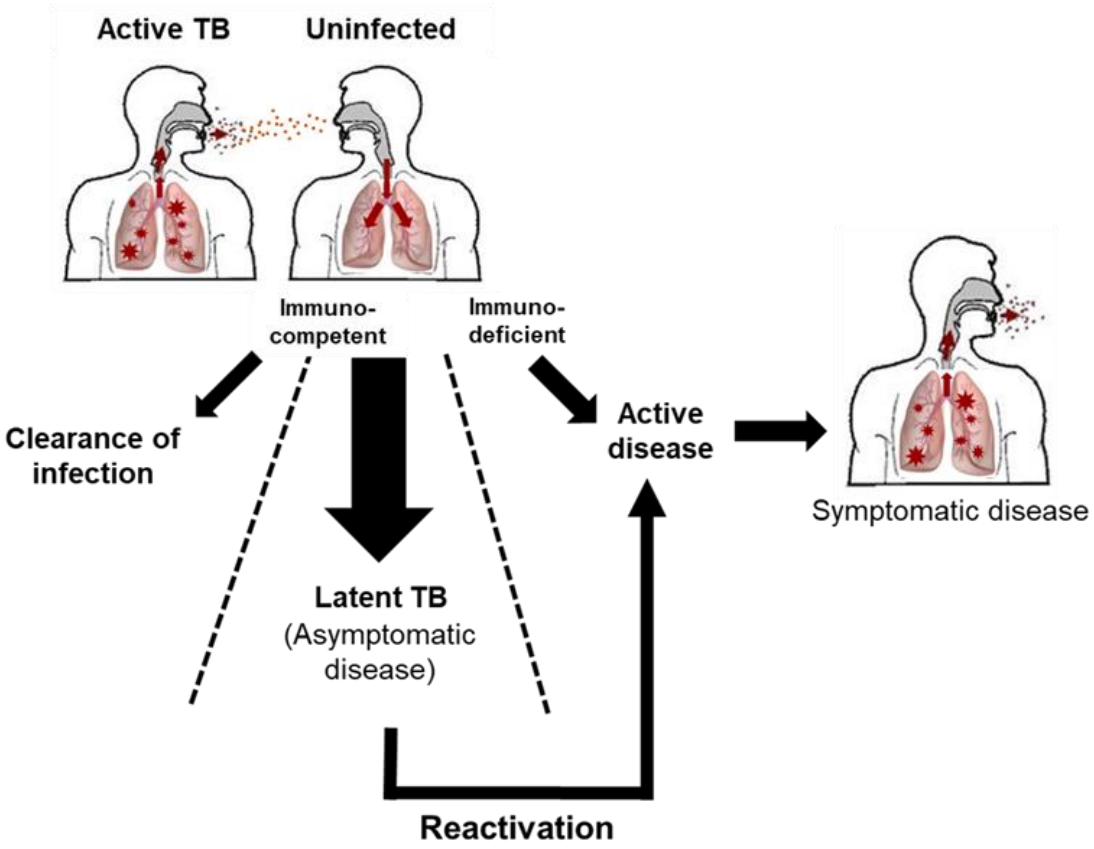

Figure 1.1. Possible outcomes of TB disease in humans. In immunocompetent individuals, there is a chance of bacterial clearance. However, most individuals develop latent disease, which is an asymptomatic, non-transmissible state. Individuals who are immuno-deficient may develop active disease, which is symptomatic and transmissible.

clear the bacteria and do not progress to active TB (Lin and Flynn, 2018). In most cases, the individual can develop latent TB, which is an asymptomatic, non-transmissible state of infection (Delogu and Fadda, 2009; Ernst, 2018; Flynn and Chan, 2001). Often times, latent TB can go unnoticed for many years (Lin and Flynn, 2018; Silva Miranda et al., 2012). In this case, *M. tb* is able to survive within the host and evade the immune response (Lin and Flynn, 2018; Silva Miranda et al., 2012). Individuals with latent TB become a reservoir for the bacteria with a 10% chance of reactivation into active disease (Silva Miranda et al., 2012). Reactivation is especially likely in immunocompromised individuals such as human immunodeficiency virus (HIV)-positive patients, older individuals, and individuals with other underlying medical conditions including malnutrition and diabetes (Silva Miranda et al., 2012). In active TB, clinical symptoms are present and the infection is transmissible to other individuals. Some of the symptoms of active TB include fever, weight loss, fatigue, persistent cough, and hemoptysis (Pai et al., 2016).

Although there is an established treatment for TB, the drug treatment has remained unchanged for the last 50 years (Lin and Flynn, 2018). In addition, treatment of TB involves a 4 – 6 month regimen of 4 antibiotics: isoniazid, rifampin, pyrazinamide and ethambutol (Pai et al., 2016). Even with the established treatment of TB, there is a rising problem with drug-resistant *M. tb*. Since this treatment is accompanied with severe side effects, this could lead to poor patient compliance (Iacobino et al., 2020). Furthermore, poor drug regimen selection and sometimes the lack of availability of drugs especially in smaller, more isolated countries can lead to the inability of the patient to finish the treatment, contributing to the rise in drug resistant *M. tb* (Iacobino et al., 2020). Approximately half a million people fall ill and 180,000 die from drug-resistant *M. tb* each year (Geneva: World Health Organization, 2020). The current vaccine available against TB is the Bacille Calmette-Guerin (BCG) vaccine, which is a live attenuated strain derived from *Mycobacterium bovis* (*M. bovis)*(Andersen and Doherty, 2005). This vaccine has its advantages and limitations. BCG is most commonly administered to infants soon after birth and is effective in protecting young children against severe forms of TB such as miliary TB and meningeal TB (Andersen and Doherty, 2005; Mattow et al., 2003). However, protectiveness of the vaccine against pulmonary TB is poor in adults (Andersen and Doherty, 2005). In addition, there is a wide range of variability in the protectiveness of BCG due to differences in culturing methods in laboratories worldwide (Andersen and Doherty, 2005; Davenne and Mcshane, 2016). Due to the

poor efficacy of BCG and the harsh treatments of TB, more research is needed on the pathogenesis of *M. tb* in order to develop an improved vaccine and treatment regimen.

1.2. Pathogenesis of tuberculosis

M. tb enters the body through inhalation of aerosols and the bacterium travels through the lower respiratory tract to the alveoli (Lerner et al., 2015). Within the alveoli, *M. tb* is able to infect a variety of local and recruited immune cells in the alveoli including alveolar macrophages (AMs), dendritic cells (DCs), neutrophils, and type-2 airway epithelial cells (AECs) (Figure 1.2) (Lerner et al., 2015). Type-2 AECs infected by *M. tb* can act as an immune sentinel where they can activate mucosal-associated invariant T-cells and induce production of protective cytokines such as tumour necrosis factor-α (TNF-α) and interferon-γ (IFN-γ), which are important for *M. tb* clearance (Lawn and Zumla, 2011; Lerner et al., 2015; de Martino et al., 2019). DCs are another type of immune cell that can be infected by *M. tb* and is crucial for bridging the innate immune response and the adaptive immune response (Barber-Mayer and Barber, 2015; Lerner et al., 2015; Poirier and Av-Gay, 2012). Following uptake of *M. tb*, DCs process the surface antigens of the bacteria and present them on the DC surface via major histocompatibility complex I and II (MHC-I or II) to prime T-

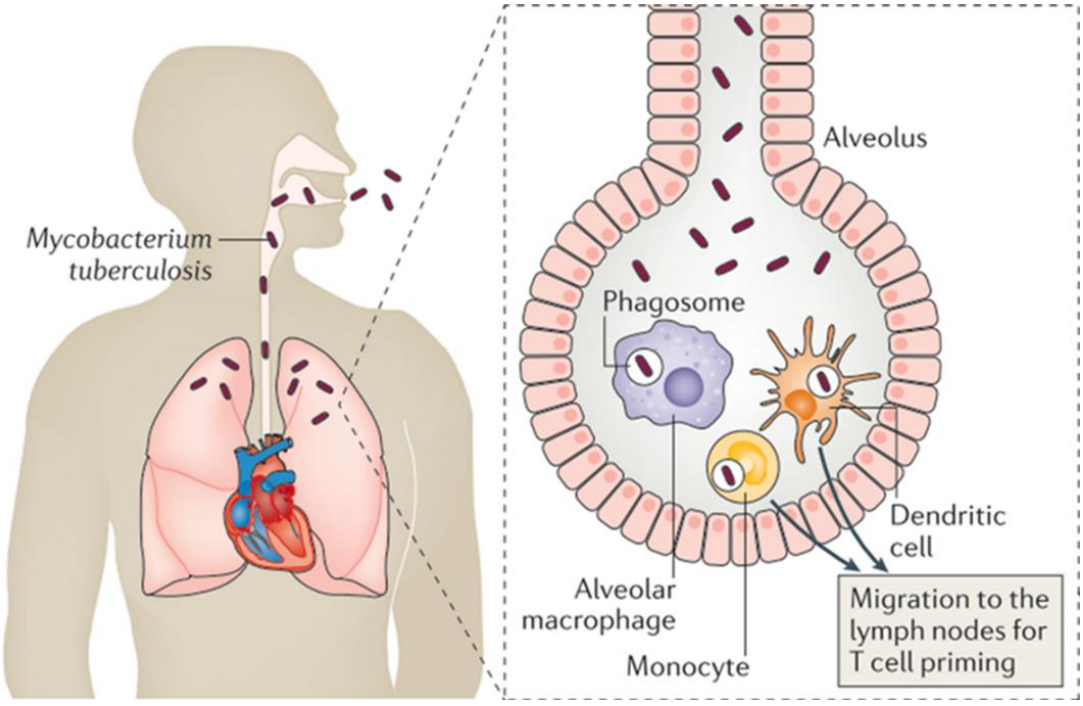

Figure 1.2. *M. tb* infects multiple cell types in the alveoli. Within the alveoli, *M. tb* is able to infect several types of cells including AMs, DCs, neutrophils as well as type-2 AECs (Pai et al., 2016).

cells in local draining lymph nodes and initiate an adaptive immune response (Barber-Mayer and Barber, 2015; Lerner et al., 2015). Neutrophils play a role in enhancing *M. tb* killing by infected macrophages as well as modulating DC trafficking to the draining lymph node in order to prime $CD4^+$ T-cells (Barber-Mayer and Barber, 2015).

Following DC migration into the lymph node, DCs prime naïve $CD4^+$ T cells through 3 signals: antigen presentation via MHC, costimulatory signal and a cytokine signal, interleukin-12 (IL-12) (de Martino et al., 2019). The $CD4^+$ T cells then undergo activation and expansion of T cells specific against *M. tb* antigens and produce IFN-γ (de Martino et al., 2019). IFN-γ plays a key role in controlling *M. tb* infection and its production heavily relies on $CD4^+$ T cells and some $CD8^+$ T cells (de Martino et al., 2019). In turn, this can lead to *M. tb* evasion of the immune response, formation of granulomas and the development of latent disease (de Martino et al., 2019). Mounting an adaptive immune response can either be protective or damaging (Barber-Mayer and Barber, 2015). It is evident that in HIV co-infected patients, the lack of $CD4^+$ T cells leads to the inability to control *M. tb* infection (Barber-Mayer and Barber, 2015). Alternatively, in HIV negative patients, $CD4^+$ T cells can also mediate immunopathology and lung tissue damage (Barber-Mayer and Barber, 2015). Currently, an immune response that is protective against *M. tb* is not fully understood. However, it appears that a balance of both innate immunity and adaptive immunity is necessary.

1.2.1. *M. tb* subversion of innate immunity in macrophages

AMs are one of the first immune cells that *M. tb* encounters when infecting the lungs. The macrophages use cell surface receptors to recognize antigens on the surface of *M. tb* as pathogen associated molecular patterns for internalization of the bacteria into a phagosome (Dey and Bishai, 2014; Glickman and Jacobs, 2001; Lerner et al., 2015). After internalization of the bacteria, the phagosome interacts with the endosomal pathway where each step enables the phagosome to acquire endocytic and membrane components to progress the phagosomal maturation process (Figure 1.3) (Poirier and Av-Gay, 2012). These acquired components include vesicular-H^+-ATPase (V-ATPase), proteolytic enzymes (lysosomal hydrolases) and initiation of reactive oxygen species production (Poirier and Av-Gay, 2012). This results in the degradation of the bacteria and the antigens are processed by the macrophage for presentation (Poirier and Av-Gay, 2012). Markers of phagosomal maturation include Rab7, Rab9, lysobisphosphatidic acid,

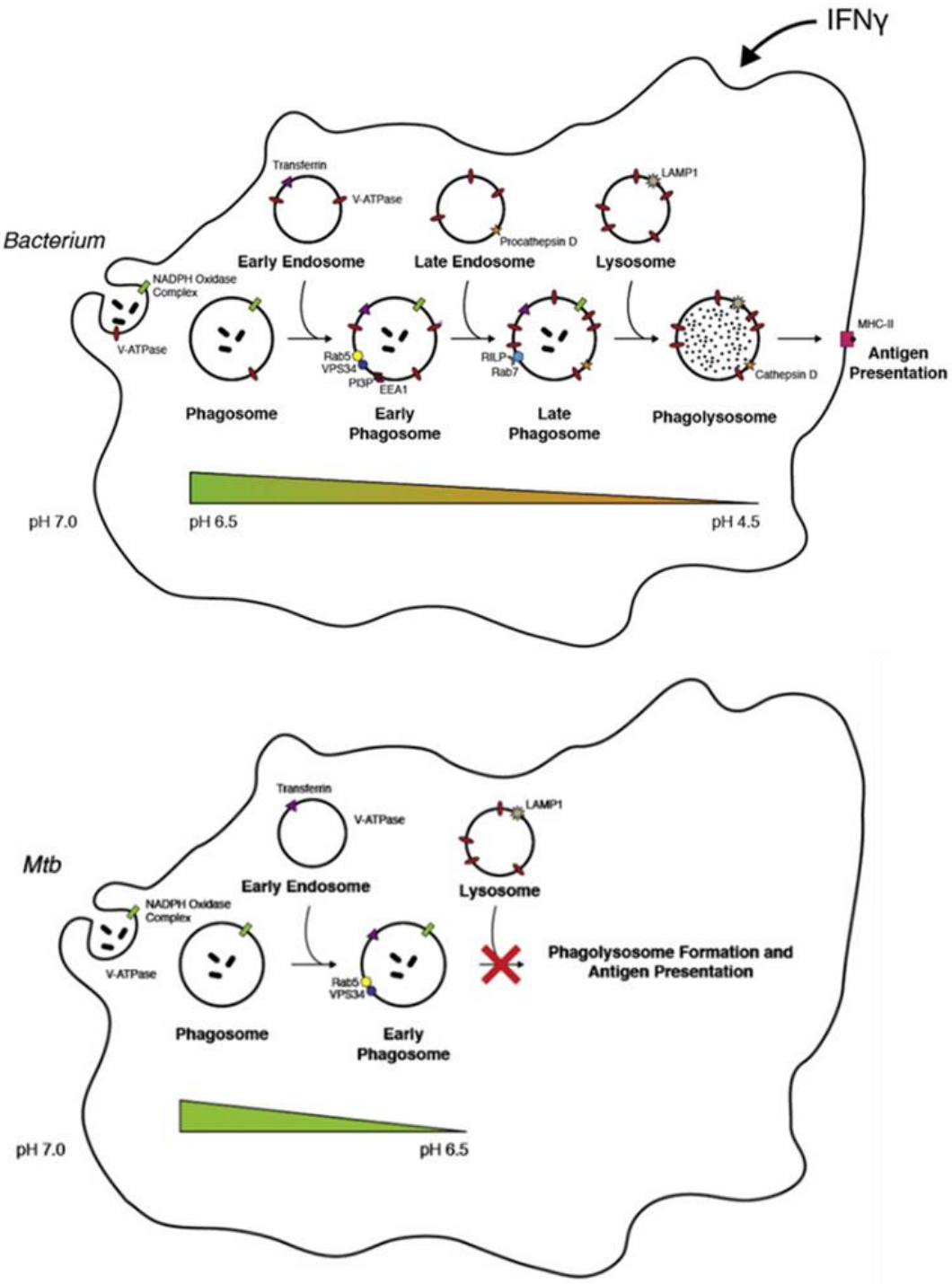

Figure 1.3. Steps of phagosomal maturation in macrophages. Phagocytosis of a foreign bacteria by a macrophage leads to interaction of the compartment with early endosomes, late endosomes, and lysosomes to result in phagosome maturation and ultimately elimination of the bacteria, processing and presentation of bacterial antigens. However, infection with *M. tb* results in premature arrest of phagosome maturation, leading to bacterial escape into macrophage cytosol (Poirier and Av-Gay, 2012).

mannose-6-phosphate receptor and lysosomal-associated membrane proteins (Poirier and Av-Gay, 2012; Vieira et al., 2002).

In turn, *M. tb* is able to subvert the macrophage response in several ways: 1) escape the phagosome and take over the cell as its replicative niche, 2) modulate host cell type-1 IFN signaling, 3) downregulate autophagy and prevent antigen presentation, and 4) reprogram host cell death (Stutz et al., 2017). *M. tb* is able to escape bacterial killing by the macrophage by disrupting the phagosomal membrane and inhibiting phagosomal maturation (Gröschel et al., 2016; Stutz et al., 2017). It was shown that phagosomes containing *M. tb* did not fuse with lysosomes as markers of phagosomal maturation were absent in infected macrophages (Poirier and Av-Gay, 2012). *M. tb* is able to utilize its early secretory antigenic target-6 (ESAT-6) system-1 (ESX-1) secretion apparatus to escape the phagosome and mediate virulence (Gröschel et al., 2016). One particular way that *M. tb* may be able to halt phagosome maturation is to disrupt the V-ATPase acquired by the phagosome (Gröschel et al., 2016). In addition, it was found in *M. marinum* that two ESX-1 secreted substrates, EsxA and EsxB, (also known as early secretory antigenic target-6 (ESAT-6) and culture filtrate protein-10 (CFP-10) respectively) were involved in breaching the phagosomal membrane and enabling escape of the bacteria (Gröschel et al., 2016; Tan et al., 2006). In doing so, *M. tb* is able to survive in the macrophage and avoid antigen processing and presentation required to initiate an adaptive immune response (Poirier and Av-Gay, 2012).

A critical step in the phagosomal maturation process that *M. tb* disrupts is the acidification of the phagosome through recruitment of the V-ATPase (Gröschel et al., 2016; Stutz et al., 2017). This enables *M. tb* to utilize its host cell as its replicative niche (Stutz et al., 2017). *M. tb* infection was also found to inhibit host-protective cytokines, dampening IFN-γ response, and induce immunosuppressive interleukin-10 (IL-10) (Stutz et al., 2017). The host cell also uses autophagy in order to remove and degrade damaged organelles (Bento et al., 2016; Huang and Bao, 2016). In addition, autophagy induced by IFN-γ can overcome disruption of the phagosomal maturation process by *M. tb* (Huang and Bao, 2016). However, it was found that *M. tb* downregulates autophagy possibly through inhibition of IFN-γ by an ESX-1 substrate, ESX-specific protein B (EspB) (Huang and Bao, 2016). *M. tb* is also able to manipulate antigen presentation by impairing DC maturation which can lead to the delay of adaptive immunity (Stutz et al., 2017). As a defence against *M. tb* infection, the host cell attempts to contain the bacteria within the phagosome, form

cytoplasmic blebs and enable uptake of the apoptotic cell by other phagocytes in order to prevent the spread of the pathogen (Elmore, 2007; Stutz et al., 2017). However, *M. tb* is able to upregulate anti-apoptotic proteins B cell lymphoma-2 and myeloid cell leukemia-1 (Spier et al., 2019). Additionally, *M. tb* was found to induce necrotic death of the host cell by causing mitochondrial damage and fragmentation (Spier et al., 2019; Wiens and Ernst, 2016). Induction of necrotic cell death in the host cell is beneficial for *M. tb* as the integrity of the host cell membrane is lost and can promote extracellular spread of *M. tb* (Moraco and Kornfeld, 2014).

1.3. *M. tb* ESX secretion systems

Due to the thick mycobacterial cell envelope, specialized secretion systems called ESX systems are utilized in mycobacteria for transport of substrates across the cell envelope (Gröschel et al., 2016; Houben et al., 2012). These ESX systems are present in mycobacteria and other genera within the Actinobacteria phylum (Gröschel et al., 2016). There are similarities in all of the *esx* loci in that they contain genes encoding small secreted proteins approximately 100 amino acids in length (Gröschel et al., 2016). These proteins contain a conserved Trp-X-Gly (WxG) motif involved in the helix-turn-helix structure as well as a secretion signal that is present in many of these proteins (Gröschel et al., 2016; Houben et al., 2014). The ESX systems are comprised of several groups of proteins: core ESX-conserved component (Ecc) proteins that are structural transmembrane components that assemble into the secretion machinery, accessory ESX-specific proteins (Esp) that are secreted virulence effectors, and a conserved mycosin protein (MycP), which is a subtilisin serine-like protease involved in substrate processing and regulation of ESX secretion (Gröschel et al., 2016; Houben et al., 2014; Ohol et al., 2010; Stoop et al., 2012). Despite these similarities, the functions of the ESX systems can vary greatly.

At least 3 of the 5 ESX systems are required for full virulence of *M. tb*, namely: ESX-1, ESX-3, and ESX-5 (Gröschel et al., 2016). The ESX-3 system is involved in mycobactin-mediated iron acquisition, whereas the ESX-5 system is involved in secretion of Pro-Glu (PE) and Pro-Pro-Glu (PPE) proteins required for immune evasion and virulence of *M. tb* (Beckham et al., 2017; Gröschel et al., 2016). The ESX-3 system is conserved among many mycobacterial species and plays an important role in the viability of both environmental and pathogenic mycobacteria (Gröschel et al., 2016). Expression of the *esx*-3 genes are dependent on the presence of iron or zinc which demonstrates its role in metal acquisition and metabolism (Gröschel et al., 2016). Its

importance in bacterial growth was determined by the inability to recover *M. tb* strains deficient in ESX-3 for many years (Gröschel et al., 2016). In addition to its role in metal homeostasis, ESX-3 appears to be important during infection (Gröschel et al., 2016). EsxH secreted by the ESX-3 system strongly induces IFN-γ secretion in T-cells (Gröschel et al., 2016). It is also able to interact and disrupt the endosomal sorting complex required for transport (ESCRT) of the infected host cell (Gröschel et al., 2016). The ESX-1 and the ESX-5 secretion systems share similar core structural proteins that were shown to have approximately 30% amino acid identity (Beckham et al., 2017; Gröschel et al., 2016). Therefore, , determining the structure of the ESX-5 system may provide more information on the structure and assembly of the ESX-1 system (Beckham et al., 2017).

In contrast to the 3 aforementioned ESX systems, the functions of the ESX-2 and ESX-4 systems are largely unknown. Given that *Mycobacterium leprae* and *Mycobacterium lepromatosis* have lost their *esx*-4 locus and have a non-functional ESX-2 system, it appears that these ESX systems are not essential for *in vivo* growth or virulence of mycobacteria (Gröschel et al., 2016).

1.3.1. *M. tb* type-7 ESX-1 secretion system

The type-7 ESX-1 system is the most well studied of the 5 ESX systems present in *M. tb*. Using this secretion system, *M. tb* is able to disrupt phagosomal maturation and evade killing (Chen et al., 2013). Through comparison studies between BCG and *M. tb*, it was shown that BCG was lacking a region of difference (RD-1), which was present in *M. tb* as the *esx*-1 locus (Gröschel et al., 2016; Kroesen et al., 2019). The key functions of the ESX-1 secretion system includes phagosomal rupture, which enables the release of the pathogen into the cytosol (Gröschel et al., 2016; Simeone et al., 2012). In addition, it is involved in host cell invasion, intracellular replication, cellular inflammation, host-cell death, and dissemination of the bacteria (Chen et al., 2013). The ESX-1 secretion machinery is assembled by core Ecc proteins and is able to secrete virulence effectors such as Esx and Esp proteins (Gröschel et al., 2016; Stoop et al., 2012). In addition, MycP1 is also a part of the ESX-1 system that is responsible for substrate processing and secretion regulation (Gröschel et al., 2016).

1.4. ESX-1 secreted effectors

The ESX-1 system is encoded by the *esx*-1 locus as well as an upstream *espACD* operon (Figure 1.4) (Gröschel et al., 2016). These genes include the core Ecc proteins as well as accessory Esp proteins. Core Ecc proteins of the ESX-1 system including EccC, EccB, EccD, and EccE assemble into the ESX-1 secretion machinery (Figure 1.5) (Gröschel et al., 2016; Stoop et al., 2012). The ESX-1 system shares some of these core components with the ESX-5 system with approximately 30% identical amino acids, and therefore structural studies of the ESX-5 system may be useful in determining the assembly and structure of the ESX-1 system (Gröschel et al., 2016). Two of the main ESX-1 substrates, EsxA and EsxB, are crucial for the full virulence of *M. tb* (Forrellad et al., 2013; Gröschel et al., 2016; Simeone et al., 2009). It was shown that EsxA and EsxB are co-secreted by the bacterium as homo- and hetero-dimers and were found to dissociate under acidic conditions, allowing EsxA to induce pores in the phagosomal membrane (Chen et al., 2013; Forrellad et al., 2013; Ma et al., 2015; Zhang et al., 2016). This was further confirmed as *M. tb* that is defective in EsxA is unable to disrupt phagosomal maturation of the infected host cell, leading to bacterial clearance (Wong, 2017).

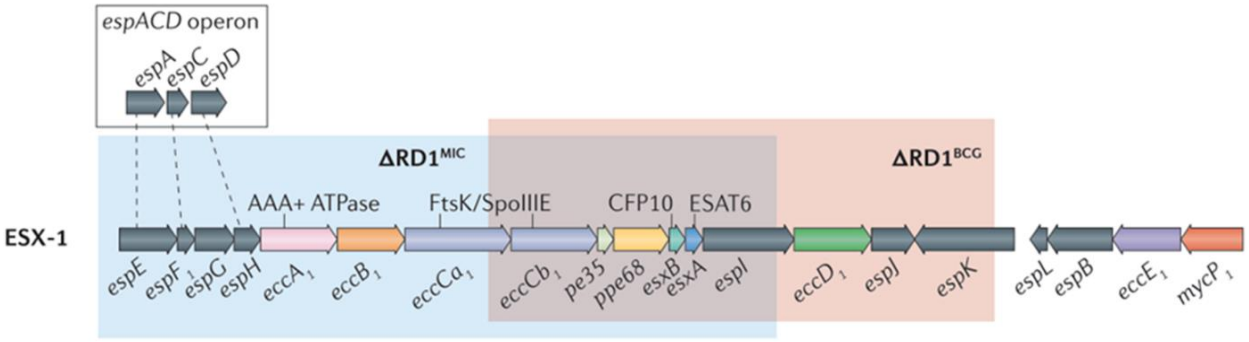

Figure 1.4. The *esx*-1 locus and upstream *espACD* operon encode genes that make up the ESX-1 secretion system of *M. tb*. The $\Delta RD1^{BCG}$ indicate the genes that are absent in BCG (Gröschel et al., 2016).

Other secreted virulence factors are the Esp proteins, some of which are encoded on the *esx*-1 locus itself, whereas others are encoded on the upstream *espACD* operon (Forrellad et al., 2013; Gröschel et al., 2016). As with EsxA and EsxB, these secreted effectors are shown to be interdependent with each other, which demonstrates how complex the ESX-1 secretion system is (Gröschel et al., 2016). For instance, EspA and EspC are co-secreted with EsxA and EsxB (Chen et al., 2013; DiGiuseppe Champion et al., 2009). Furthermore, EspC interacts with the ESX-1 core

components to facilitate the secretion of EsxA and EsxB (Chen et al., 2013; DiGiuseppe Champion et al., 2009). EspD secretion was shown to be largely ESX-1 independent, but its expression is required for EsxA and EsxB secretion, as well as stabilizing the intracellular levels of EspA and EspC (Chen et al., 2012, 2013). Expression of EsxB is also required for EspB expression and secretion (Chen et al., 2013). During EspB secretion, it also interacts with MycP1 for processing of its C-terminus end (Chen et al., 2013; Ohol et al., 2010).

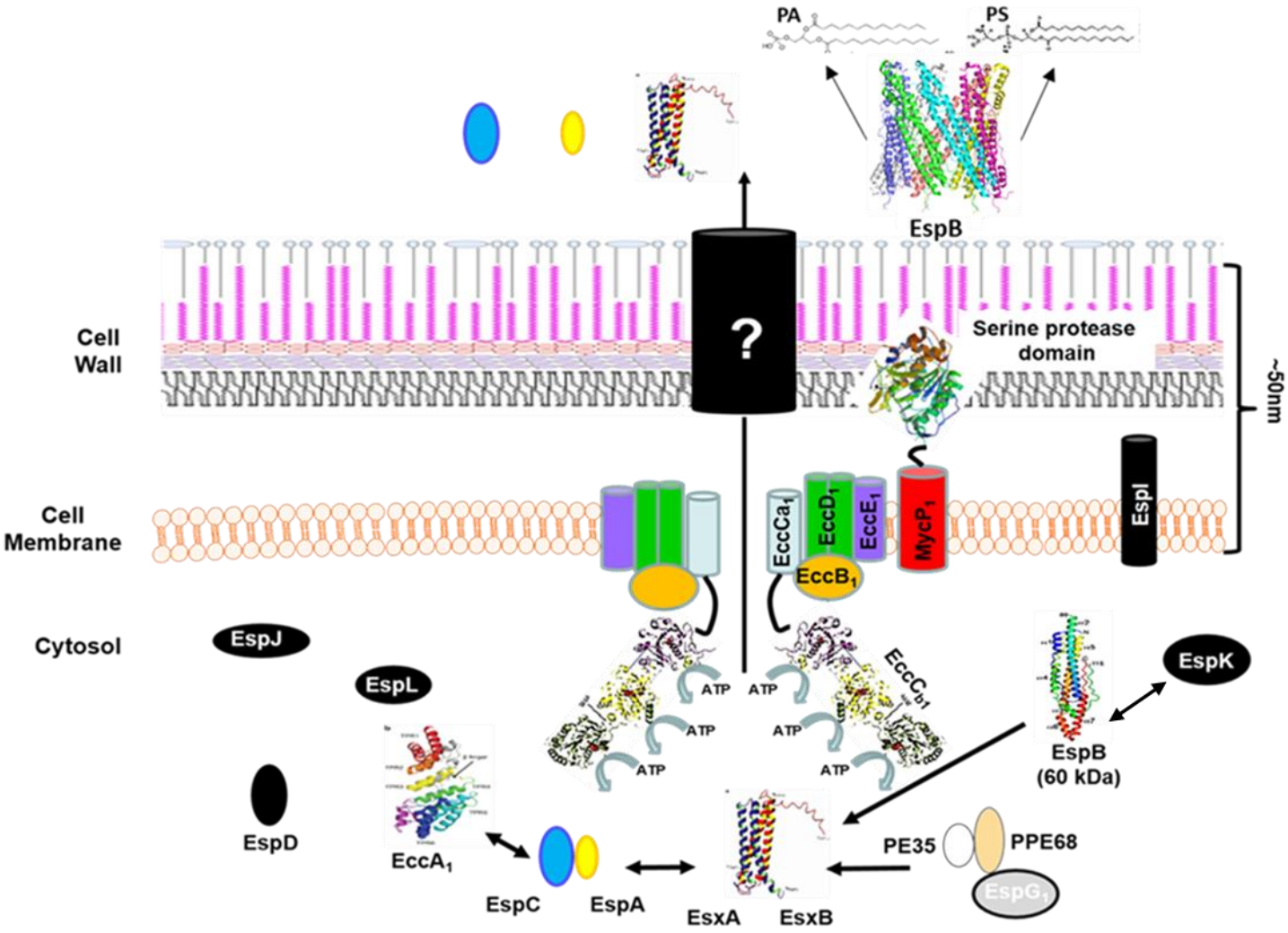

Figure 1.5. Assembly of the ESX-1 secretion system of *M. tb*. This schematic shows a working model of the assembly of the core Ecc proteins and secretion of Esx and Esp proteins from the ESX-1 secretion system.

1.4.1. PE/PPE proteins of *M. tb*

The ESX systems from mostly pathogenic mycobacterial species are known to secrete proteins that are a part of the PE/PPE protein family (Daleke et al., 2012). Approximately 10% of

the *M. tb* genome is made up of *pe* and *ppe* genes, whereas non-pathogenic mycobacteria were reported to encode fewer *pe/ppe* genes in comparison (Ekiert and Cox, 2014). These are small proteins that serve a variety of functions such as nutrient transport, pathogenesis of TB, and possibly antigenic variability of *M. tb* (Ekiert and Cox, 2014; Majlessi et al., 2015; Solomonson et al., 2015; Wang et al., 2020). Consistent with the interdependency between the ESX substrates, PE/PPE proteins were shown to interact with other ESX substrates (Ekiert and Cox, 2014). For example, EspG of the ESX-5 system was shown to be a chaperone for the PE25/PPE41 complex to prevent self-aggregation of the PE/PPE proteins (Ekiert and Cox, 2014; Solomonson et al., 2015). In addition, many of these PE/PPE proteins are associated with the outer layer of the mycobacterial cell envelope for a variety of functions including nutrient transport (Ekiert and Cox, 2014; Wang et al., 2020). Interestingly, PE and PPE proteins appear to be only stable in a PE/PPE complex (Strong et al., 2006). Other Esx and Esp proteins also have structures resembling PE/PPE and can similarly form homo- or hetero-dimeric complexes (Solomonson et al., 2015). For example, EsxAB heterodimer and monomeric EspB have structures resembling the PE25/PPE41 complex (Solomonson et al., 2015). Therefore, studies of these PE/PPE structures may be helpful in determining structures of other ESX-1 substrates.

1.5. EspB

The protein of interest in this project is EspB which is expressed and secreted through the ESX-1 secretion system. EspB is expressed as a 60 kDa protein within the bacterium and is cleaved during its secretion by MycP1 into 50 kDa (Ohol et al., 2010). Truncation of EspB is required for full virulence of *M. tb* (Solomonson et al., 2015). It was shown that the cleaved C-terminus of EspB has roles in regulating ESX-1 secretion, such as maintaining intracellular levels of EsxA and secretion of EsxA and EsxB (Ohol et al., 2010; Solomonson et al., 2015). EspB was also shown to interact with the C-terminal region of EspK, where EspK may be serving as a chaperone (McLaughlin et al., 2007; Mishra et al., 2019). This further demonstrates the interconnectedness of the ESX-1 substrates. However, the functions of both intracellular and secreted EspB is currently unclear.

1.5.1. Prior characterization of EspB and identification of its distinct virulence functions

Two previously published *M. tb* transposon mutants: *M. tb espA*::Tn and *M. tb* 5'Tn::*pe35* were constructed and studied (Chen et al., 2012, 2013). These mutants contain a single Tn5370

transposon insertion at the *espA* gene (*espA*::Tn) or upstream of the *pe35* gene (5'Tn::*pe35*) (Chen et al., 2013). The *M. tb espA*::Tn mutant was found to be deficient in EspA, EspC, and EspD expression and was unable to secrete EsxA and EsxB (Chen et al., 2012, 2013). Whereas, the *M. tb* 5'Tn::*pe35* mutant was found to have lower mRNA levels of *pe35, ppe68, esxB, esxA, espI,* and $eccD_1$, leading to the shutdown of the ESX-1 secretion system (Brodin et al., 2006; Chen et al., 2013) Both transposon mutants were found to be disrupted in the functionality of their ESX-1 systems when infecting THP-1 macrophages (Figure 1.6) (Chen et al., 2013). In comparison to WT *M. tb* infected macrophages, both transposon mutants induced lower levels of cytotoxicity (Chen et al., 2013). However, *M. tb espA*::Tn was able to induce higher levels of cytotoxicity compared to *M. tb* 5'Tn::*pe35* (Chen et al., 2013). The phenotypes of these transposon mutants were demonstrated in both THP-1 cells and MRC-5 cells with consistent results (Chen et al., 2013).

Interestingly, upon analyzing the secretion profiles of the transposon mutants using culture filtrate (CF) and cell lysate (CL), the *M. tb espA*::Tn mutant was revealed to express and secrete EspB whereas *M. tb* 5'Tn::*pe35* was able to express but not secrete EspB (Figure 1.7) (Chen et al.,

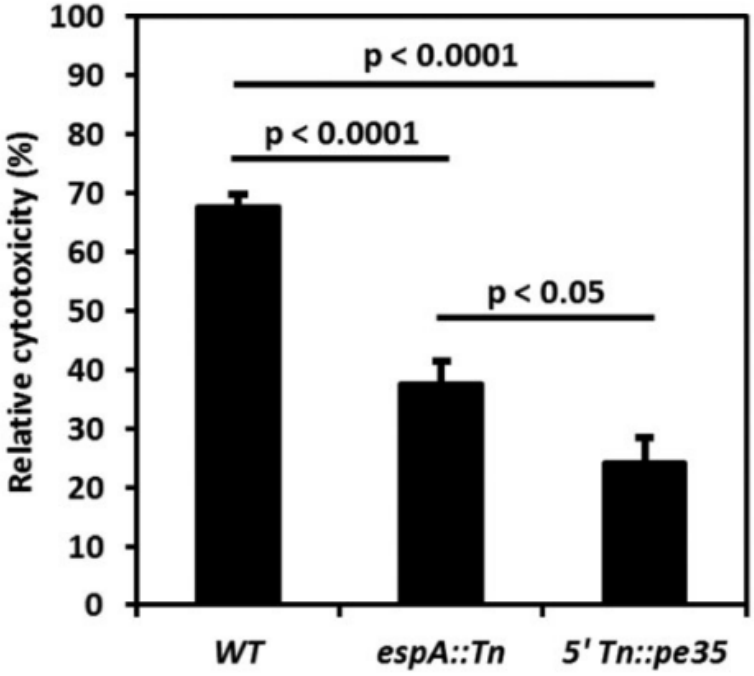

Figure 1.6. Percent relative cytotoxicity of *M. tb* strains infecting THP-1 macrophages. THP-1 macrophages were infected with WT *M. tb*, *M. tb espA*::Tn, or *M. tb* 5'Tn::*pe35* (Chen et al., 2013).

2013). In addition, *M. tb espA*::Tn expressed but did not secrete EsxA and EsxB, whereas the *M. tb* 5'Tn::*pe35* lacked expression of both EsxA and EsxB (Chen et al., 2013). This also revealed that disruption of EsxA and EsxB expression blocks EspB secretion but not its expression (Chen et al., 2013).

Addition of purified mature (50 kDa) EspB with *M. tb* 5'Tn::*pe35* mutant to infect THP-1 macrophages restored the virulence of this strain to the same level as *M. tb espA*::Tn mutant (Figure 1.8) (Chen et al., 2013). However, addition of purified EspB to THP-1 macrophages without the presence of bacteria was not able to induce cytotoxicity (Chen et al., 2013). This demonstrates that EspB was responsible for the gap in virulence between *M. tb espA*::Tn and *M. tb* 5'Tn::*pe35* strains and that the presence of *M. tb* is essential for the virulence function of EspB (Chen et al., 2013). This study revealed that EspB has a distinct virulence function independent of EsxA and EsxB, which prompted further investigation on how secreted EspB functions to induce cytotoxicity in THP-1 macrophages.

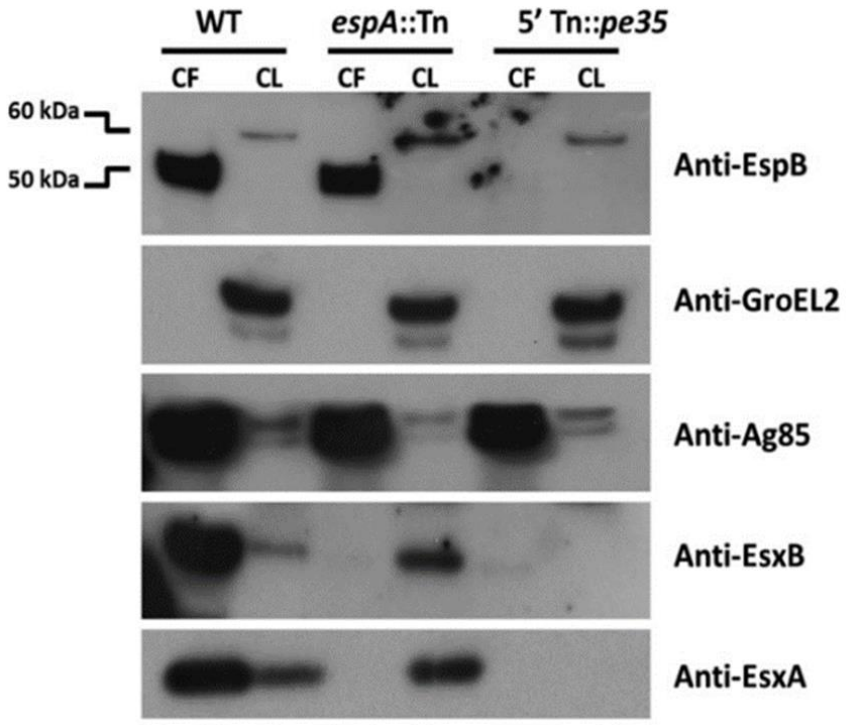

Figure 1.7. Secretion profile analysis of WT *M. tb*, *M. tb espA*::Tn, and 5'Tn::*pe35*. A western blot of the secreted proteins in the culture filtrate (CF) and expressed proteins in the cell lysate (CL) was performed (Chen et al., 2013).

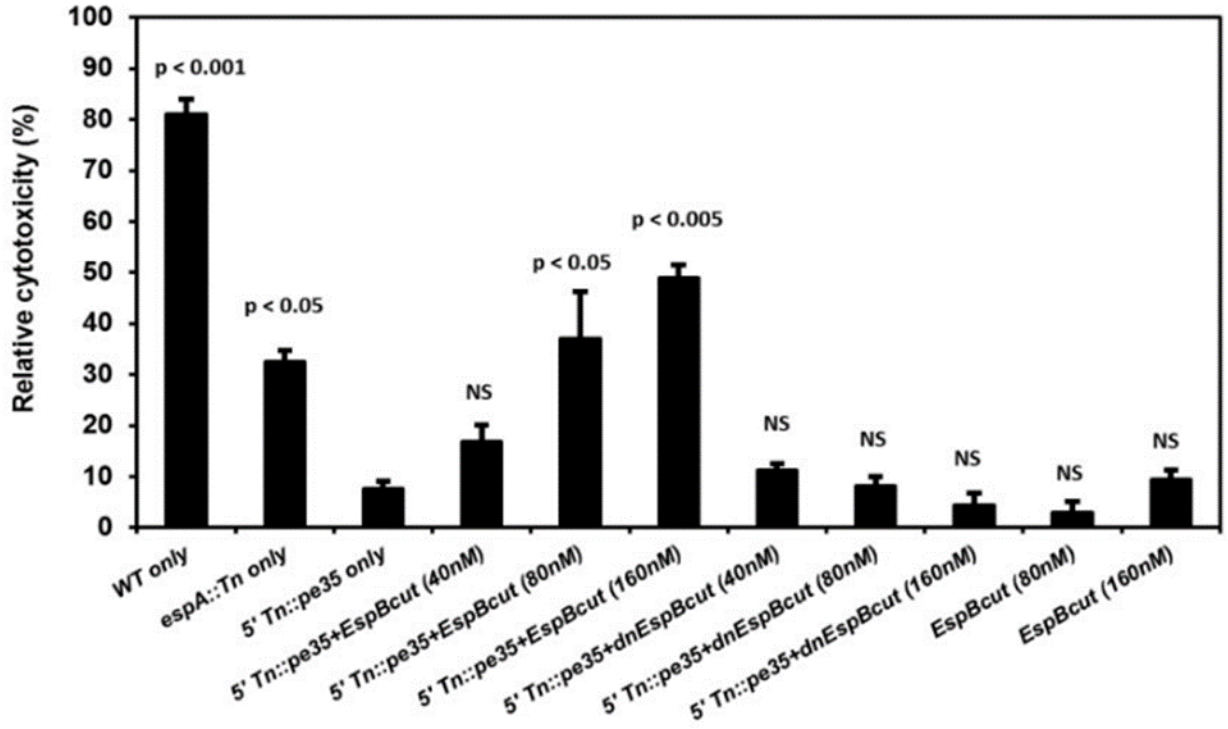

Figure 1.8. Addition of purified mature EspB to *M. tb* 5'Tn::*pe35* induces cytotoxicity to *M. tb espA*::Tn levels in THP-1 macrophages. Various concentrations of purified mature EspB (EspBcut) or denatured EspB (dnEspBcut) added to *M. tb* 5' Tn::*pe35* to infect THP-1 macrophages. Compared to cytotoxicity induced by WT *M. tb*, *M. tb espA*::Tn or EspB alone infecting THP-1 macrophages (Chen et al., 2013).

1.5.2. Structure of EspB

The structure of secreted EspB (50 kDa form) was recently solved by two independent research groups. The primary structure of EspB consists of a PE and PPE domain with a linker in between (Figure 1.9) (Solomonson et al., 2015). The monomer assembles into a PE/PPE-like fold that resembles the structure of PE25/PPE41 from the ESX-5 system (Solomonson et al., 2015). This hairpin-like structure is stabilized by a WxG and Tyr-x-x-x-Asp (YxxxD) motif, which also serves as a bipartite secretion signal (Piton et al., 2020; Solomonson et al., 2015). Residues in the export arm of EspB were shown to be identical to the sequence in $EsxB_{TB}$ that is essential for interaction with EccCb1 (Solomonson et al., 2015). Mutation of the YxxxD motif or deletion of EccCb1 was found to disrupt EspB secretion (Solomonson et al., 2015). In addition, two hydrophobic pockets were identified on the EspB monomer that was predicted to bind the fatty acid regions of phospholipids (Korotkova et al., 2015). The residues within the hydrophobic

pockets were identified at helices α1 and α2 (L60, F159, and L163) and helices α6 and α7 (L232, I246, Y236, and Y250) (Figure 1.10) (Korotkova et al., 2015).

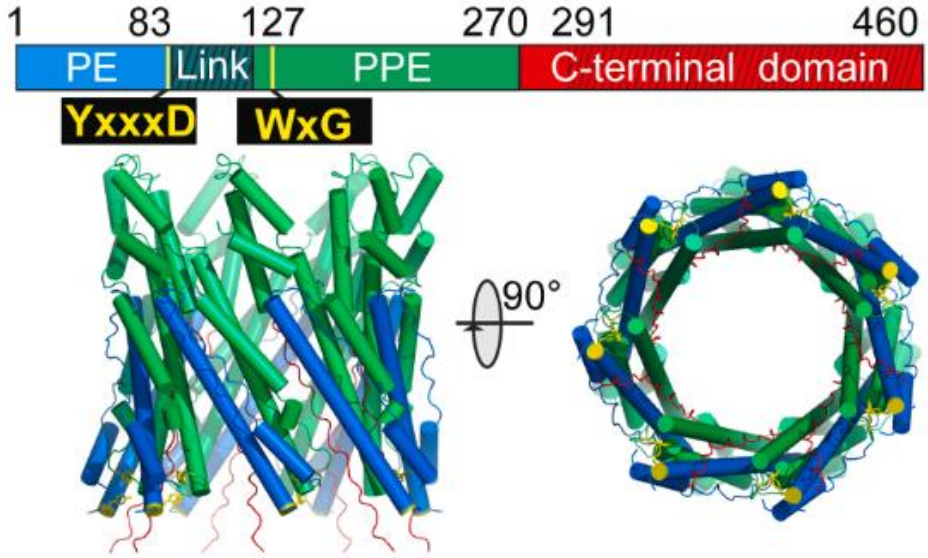

Figure 1.9. Schematic of EspB protein domains and structure of EspB oligomer. EspB contains a PE and PPE domain with a linker in between the YxxxD and WxG motif. The protein assembles into a heptameric oligomeric structure (Piton et al., 2020).

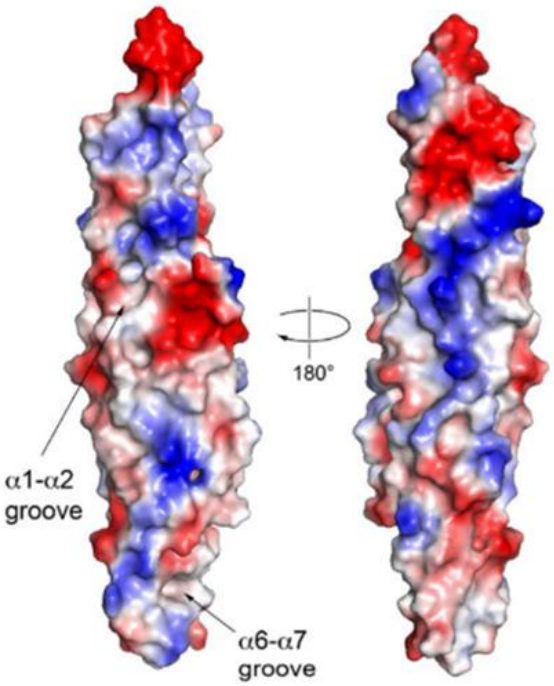

Figure 1.10. Hydrophobic grooves identified on EspB monomer. Hydrophobic grooves on the EspB monomer are indicated as α1- α2 groove and α6- α7 groove (Korotkova et al., 2015)

1.5.3. EspB binds phospholipids

EspB was previously shown to bind acidic phospholipids, specifically phosphatidic acid (PA) and phosphatidylserine (PS) (Chen et al., 2013). It was shown that purified mature EspB bound to PA and PS on a lipid membrane overlay assay (Figure 1.11) (Chen et al., 2013). Whereas purified, unprocessed EspB did not bind to PA or PS on the lipid spotted membrane (Chen et al., 2013). However, the residues within EspB responsible for binding these phospholipids are currently unknown. Since PA and PS play important roles in the mammalian host cell, it is possible that phospholipid binding plays a role in the virulence function of EspB.

Given that *M. tb* is able to induce mitochondrial damage of the host cell during infection, it is possible that interactions of EspB with PA on the mitochondrial membrane can contribute to mitochondrial damage. PA was shown to have important roles in regulating mitochondrial fusion and fission (Yang and Frohman, 2012). Mitochondrial fusion is important in energy production of the cell and fission allows for damaged mitochondrial components to be recycled via autophagy (Yang and Frohman, 2012). Therefore, interaction of EspB with PA may interfere with PA regulation of mitochondrial fission and fusion. In addition, as *M. tb* is able to induce mitochondrial damage as well as downregulate autophagy by the host cell, this collectively disrupts with the defence mechanisms of the host cell.

One of the signals of an apoptotic cell is PS on the outer leaflet of the cell membrane (Bohdanowicz and Grinstein, 2013). PS is primarily localized at the inner leaflet of mammalian cells but when exposed to the outer leaflet, it serves as an "eat me" signal for uptake by other phagocytes (Bohdanowicz and Grinstein, 2013). As discussed above, apoptosis is one of the defense mechanisms that macrophages utilize to contain the bacteria and prevent spread of the infection (Spier et al., 2019). It is possible that *M. tb* uses its ESX-1 effectors to interact and inhibit PS exposure to the outer leaflet and disrupting this apoptotic signal.

In addition to mitochondrial damage and inhibition of apoptosis, *M. tb* infection also causes disruption in the phagosomal maturation process. The process of phagocytosis and phagosomal maturation involves many precisely coordinated steps of membrane trafficking and recruitment of components to facilitate in the acidification of the compartment (Bohdanowicz and Grinstein, 2013). Soon after phagocytosis of the pathogen, phosphatidylinositol 3-phosphate (PI(3)P)

accumulates at the phagosomal membrane and plays a critical role in the maturation process of phagosomes (Levin et al., 2015). Therefore, disruption of this phospholipid may lead to failure to accumulate PI(3)P to the phagosomal membrane, resulting in its arrest in an immature state (Levin et al., 2015).

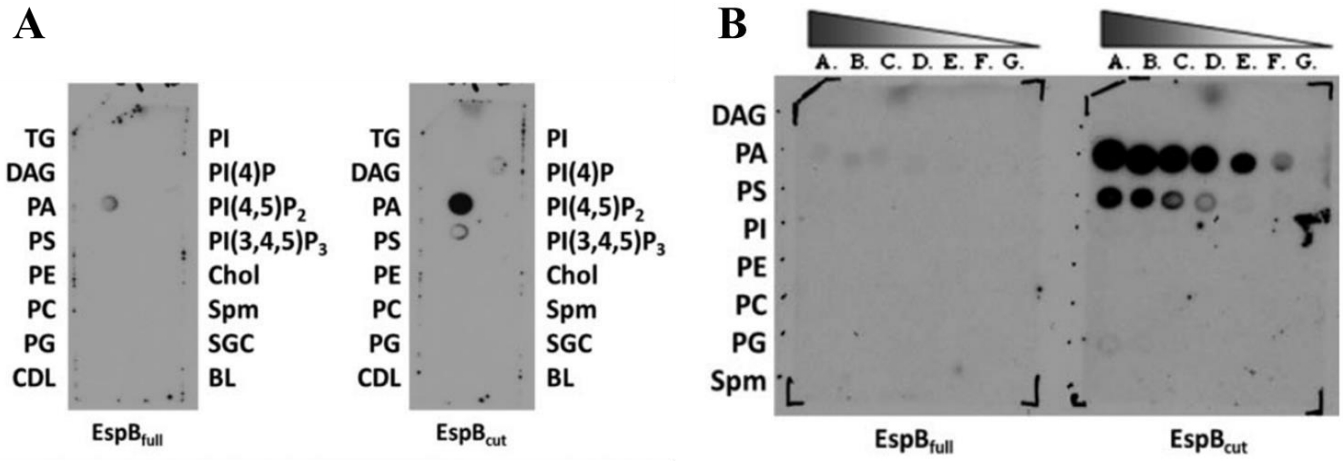

TG	Triglyceride	**PI**	Phosphatidylinositol
DAG	Diacylglycerol	**PI(4)P**	Phosphatidylinositol-4-monophosphate
PA	Phosphatidic acid	**PI(4,5)P_2**	Phosphatidylinositol-4, 5-diphosphate
PS	Phosphatidylserine	**PI(3,4,5)P_3**	Phosphatidylinositol-3, 4, 5-triphosphate
PE	Phosphatidylethanolamine	**Chol**	Cholesterol
PC	Phosphatidylcholine	**Spm**	Sphingomyelin
PG	Phosphatidylglycerol	**SGC**	3-sulfogalactosylceramide
CGL	Cardiolipin	**BL**	Blank

Figure 1.11. Purified mature EspB binds to PA and PS. Mature EspB ($EspB_{cut}$) was shown to bind to PA and PS using **A.** membrane lipid overlay strips and **B.** arrays containing decreasing concentration of phospholipids spotted on the membrane. Whereas unprocessed EspB ($EspB_{Full}$) did not bind to the phospholipids (Chen et al., 2013).

2. Rationale, Hypothesis, and Objectives

2.1. Rationale

EspB was shown to be able to induce cytotoxicity in macrophages with the presence of *M. tb* (Chen et al., 2013). This was demonstrated by the addition of purified EspB to *M. tb* 5'Tn::*pe35*, which resulted in induction of cytotoxicity in infected macrophages to the same level as *M. tb espA*::Tn (Chen et al., 2013). In addition, EspB was found to bind to phospholipids (Chen et al., 2013). The interaction was demonstrated to be specific to PA and PS which are important for macrophage function (Chen et al., 2013). Furthermore, structural studies revealed potential PA and PS binding domains on EspB (Korotkova et al., 2015). These studies also showed that EspB adopts a heptameric barrel oligomer (Korotkova et al., 2015; Piton et al., 2020; Solomonson et al., 2015). Collectively, these data lead to the hypothesis that the virulence function of EspB may be dependent on its ability to bind phospholipids (PA and PS). Additionally, oligomerization of EspB may play an important role in its ability to interact with phospholipids. Therefore, the goal of this project was to further characterize the phospholipid interactions and oligomerization of EspB and how these relate to its virulence function.

2.2. Hypothesis

The distinct virulence property of secreted EspB in its 50 kDa mature form is dependent on phospholipid binding.

2.3. Objectives

1. I will construct EspB variants containing mutations in residues predicted to be important for EspB function. The constructed variants will be characterized using phospholipid binding assays and oligomerization assays to determine if these phenotypes are critical for the virulence function of EspB.

2. The EspB variants will be added to the *M. tb* 5' Tn::*pe35* strain to infect THP-1 macrophages to assess their ability to enhance cytotoxicity of the macrophages. Cell viability will be measured using a resazurin-based assay.

3. Materials and Methods

3.1. Mapping of targeted residues on 3D model of EspB

Molecular graphics and analyses were performed using the UCSF Chimera program developed by the Resource for Biocomputing, Visualization, and Informatics team at the University of California, San Francisco, with support from NIH P41-GM103311 (Pettersen et al., 2004). The 3D structural file of EspB was obtained from the protein data bank (PDB) (access number 6XZC) from a previously published structural paper (Piton et al., 2020). The PDB file was opened using the UCSF Chimera 1.13.1 molecular modelling system. Residues that were targeted for mutagenesis were labelled with the residue one letter code and position number. These residues were also colour coded for clarity. Each EspB variant that were labelled and colour coded were saved as separate files.

3.2. Construction of *espB* mutations

The variants *espB*$^{R17A/H223A}$ and *espB*$^{K259A/K267A}$ were constructed by site-directed mutagenesis of the *espB*^{WT} gene that was already cloned into pET28a plasmid. The variants *espB*^{W176R} and *espB*$^{F159R/I246R}$ on the other hand, were synthesized and cloned into a vector, pUCIDT (Kan^{R}) by Integrated DNA Technologies (IDT). The forward and reverse primers used for each variant are summarized in Table 1. All EspB variants that were constructed in this project contained a 6X His-tag and was not removed after purification. Experimental details are described below.

Table 1: Primers used for *espB* variant constructs.

Mutation	Direction	Primers used for Plasmid Constructs
WT	Forward	5’ – CAG CAT ATG ACG CAG TCG CAG ACC GTG ACG GTG – 3’
	Reverse	5’ – CGC CTC GAG TCA CGG GAG GCC ACC ACC CGG CGA TCC – 3’
R17 → A	Sense	5’ – GAG ATT TTG AAC GCG GCC AAC GAG GTG – 3’
	Anti-sense	3’ – CTC TAA AAC TTG CGC CGG TTG CTC CAC – 5’
H223 → A	Sense	5’ – GCA AGG CGG GAA GCT CCG ACT TAT GAA – 3’
	Anti-sense	3’ – CGA TCC GCC CTT CGA GGC TGA ATA CTT – 5’
F159 → R	Sense	5’ – GGG TGG AAC ACT CGC AAC CTG ACG CTG – 3’
	Anti-sense	3’ – CCC ACC TTG TGA GCG TTG GAC TGC GAC – 5’
I246 → R	Sense	5’ – GCC CGC GAC CAA CGT CTC CCG GTG TAC – 3’
	Anti-sense	3’ – CGG GCG CTG GTT GCA GAG GGC CAC ATG – 5’
K259 → A	Sense	5’ – CAG AGG TCG GAG GCG GTG CTG ACC GAA – 3’
	Anti-sense	3’ – GTC TCC AGC CTC CGC CAC GAC TGG CTT – 5’
K267 → A	Sense	5’ – GAA TAC AAC AAC GCG GCA GCC CTG GAA – 3’

	Anti-sense	3’ – CTT ATG TTG TTG CGC CGT CGG GAC TTC – 5’

3.2.1. Site-directed mutagenesis

The *espB*^{WT} gene fragment corresponding to the secreted isoform had been previously cloned into the pET28a plasmid (Chen et al., 2013). Site directed mutagenesis of the *espB*^{WT} gene was performed using Q5® Site-Directed Mutagenesis Kit (New England BioLabs). Annealing temperatures of the PCR cycles were adjusted to 3-5 °C lower than the melting temperatures of the primers that were used. Site-directed mutagenesis for a single residue replacement was first performed. The plasmid was purified from PCR products using Monarch® Plasmid Mini-Prep Kit (New England Biolabs) and quantified using NanoDrop™ One^{C} Spectrophotometer (Thermo Scientific). The purified plasmid was then transformed into TOP10 *E. coli* to prepare a larger quantity of plasmids. The plasmid with a single residue change was then used as a template for a second site-directed mutagenesis to construct a double mutant. PCR products were purified once again and transformed into TOP10 *E. coli* for higher yield plasmid preparation. The transformants were sequenced by Eurofins Genomics to confirm the mutations introduced into the *espB* gene.

Table 2: Parameters of site-directed mutagenesis to construct *espB* variants.

Segment	Cycles	Temperature (°C)	Time
1	1	98	2 minutes
2	18	98	30 seconds
		espB$^{R17A/H223A}$ – 67 *espB*$^{K259A/K267A}$ – 61	1 minute
		72	15 minutes
3	1	18	Hold

3.2.2. Ligation of synthesized *espB* into pET28a

The variants *espB*$^{F159R/I246R}$ and *espB*^{W176R} were commercially synthesized into a pUC19-based vector pUCIDT (Kan^{R}) by IDT with the addition of an NdeI cut-site at the C-terminus and an XhoI cut-site at the N-terminus of the gene. The plasmid was used for a double restriction digest with NdeI and XhoI (New England Biolabs). Next, 1 µL of each enzyme was added to 1 µL of the plasmid with 5 µL of 10X CutSmart Buffer (New England Biolabs). Water was added to the

mixture to a total volume of 50 µL. The double restriction digest was also performed on pET28a plasmid. The mixture was incubated for 2 hours at 37 °C, then was heated to 65 °C for 20 minutes for heat inactivation of the enzymes. The digests were resolved on a 0.8% agarose gel and the *espB* gene was excised from the gel for purification using the Monarch® DNA Gel Extraction Kit (New England Biolabs) according to manufacturer's instructions. The digested pET28a plasmid was also resolved and excised from the agarose gel for purification using the same kit. The purified *espB* gene and the cut pET28a plasmid was used for ligation using the T7 ligase (New England Biolabs). The ligation was performed using a molar ratio of 1:3 vector (pET28a) to purified DNA insert (*espB* gene) in 10 µL of 2X T7 DNA ligase reaction buffer (New England Biolabs) with 1 µL of T7 DNA ligase. Water was added to the mixture to a total volume of 20 µL. The mixture was incubater at room temperature for 30 minutes, then chilled on ice prior to transformation into TOP10 *E. coli*.

3.2.3. Preparation of plasmids

The constructed pET28a vectors containing the *espB* gene variants were transformed into TOP10 chemically competent *E. coli* (Invitrogen) for plasmid propagation and long-term storage. Heat shock transformation was performed by first adding 3 µL of purified plasmid or 10 µL of PCR products into a tube containing 50 µL of TOP10 *E. coli* and incubated on ice for 20 minutes. The mixture was heat shocked at 42 °C for 40 seconds and transferred back onto ice for 2 minutes. Then, 500 µL of fresh SOC media was added to the mixture and incubated at 37 °C for 1 hour with continuous shaking at 200 rpm. The culture was centrifuged at maximum speed and the pellet was resuspended with 100 µL of the LB media and plated on LB agar containing 50 µg/mL of kanamycin. The transformants were used to inoculate 10 mL of LB media containing 50 µg/mL of kanamycin and allowed to grow overnight at 37 °C, with continuous shaking at 200 rpm. The culture was centrifuged to harvest the cells. The pellet was obtained for plasmid purification using Monarch® Plasmid Miniprep Kit (New England BioLabs) following the manufacturer's instructions. The plasmid concentration was quantified using NanoDrop™ One^{C} Spectrophotometer (Thermo Scientific).

3.3. Purification of EspB

3.3.1. Transformation of pET28a into *E. coli* for recombinant EspB production

A volume of 3 µL of purified pET28a plasmid containing *espB* was added to 100 µL of chemically competent low background strain (LOBSTR) BL21 (DE3) *E.coli* and incubated on ice for 20 minutes. The mixture was then heat shocked at 42 °C for 40 seconds and placed back onto ice for 2 minutes. LB media was added to 500 µL to the bacterial cells and allowed to recover at 37 °C, with continuous shaking at 200 rpm for 1 hour. The recovered cells were plated onto LB agar containing 50 µg/mL of kanamycin and incubated at 37 °C overnight.

3.3.2. Growth and induction of cultures

The transformants were used to inoculate 200 mL of LB media and incubated at 37 °C, with agitation at 200 rpm for 12 hours (overnight) to establish a starter culture. The starter culture was added to 1 L of LB media to an OD of 0.1 and allowed to incubate at 37 °C until the culture had reached an OD of 0.5. The *E. coli* in the culture was induced with 1 mM of IPTG to allow vector protein expression for 4 hours at 37 °C. When the culture reached an OD of 1, *E. coli* was harvested by centrifugation at 5000 rpm for 10 minutes. The harvested cell pellet was resuspended in 150 mL of LEW (Lysis-Equilibrium-Wash) buffer (150 mM NaCl, 50 mM NaH_2PO_4, at pH 8) and were lysed using the Avestin EmulsiFlex-C3 homogenizer at 15,000 psi for 3 cycles. The lysate was centrifuged at 19,000 rpm, 4 °C for 40 minutes to remove cellular debris. The pellet was discarded, and the clarified lysate was used for further purification.

3.3.3. Ammonium sulfate precipitation

Ammonium sulfate ($(NH_4)_2SO_4$) (Sigma-Aldrich) was added to the clarified lysate 5% increments until a final saturation of 50% was reached (Table 3). The lysate was centrifuged at 10,000 rpm for 10 minutes to recover any precipitated protein after every addition of $(NH_4)_2SO_4$. The pellets collected from each fraction were resuspended in LEW buffer and resolved on an SDS-PAGE (Invitrogen) to confirm the presence of EspB in the pellets. The fractions that contained EspB were further diluted into 10 mL of LEW buffer prior to the next purification step.

Table 3: $(NH_4)_2SO_4$ added to 150 mL lysate at 25 °C

$(NH_4)_2SO_4$ saturation (%)	$(NH_4)_2SO_4$ added (g)
0	0
5	4.05

10	4.05
15	4.2
20	4.2
25	4.35
30	4.35
35	4.5
40	4.5
45	4.65
50	4.65

3.3.4. Ni-IDA column purification

Nickel column purification was performed by adding 1 g of Protino Ni-IDA Resin (Macherey-Nagel) to fractions containing EspB diluted into 10 mL of LEW buffer. The slurry was allowed to incubate overnight at 4 °C with continuous shaking. The slurry was poured into the column and the flow-through was collected. The resin was washed with 10 mL of LEW buffer and LEW buffer with increasing concentration of imidazole (10 – 30 mM) (Sigma-Aldrich). The binding protein was then eluted with LEW containing 250 mM or 500 mM imidazole. Each elution was collected in separate centrifuge tubes. The collected fractions were analyzed on SDS-PAGE and elutions containing purified EspB were concentrated and buffer exchanged using Vivaspin concentrator spin columns (Sartorius) until a volume of 1.5 mL was reached.

3.3.5. Quantification of purified EspB

Bovine serum albumin (BSA) standards were prepared at 500 μg/mL and diluted two-fold until the lowest concentration was at 31.25 μg/mL. The purified protein samples were diluted 1:10 in LEW buffer. The BSA standards and protein samples were prepared at a final volume of 50 μL and was quantified using the BCA Protein Assay Kit (Pierce) according to manufacturer's instructions. Quantified EspB samples were resolved on a SDS-PAGE gel. Equal amounts of purified EspB (10 μg) were added to NuPAGE™ 4 – 12% Bis-Tris gel (Invitrogen) and resolved at 200 V for 23 minutes. The gel was removed and stained with Coomassie blue. For antibody detection, 5 μg of EspB was resolved on the Bis-Tris gel using the same conditions. The gel was transferred onto a nitrocellulose membrane using the iBlot 2 Dry Blotting System (Invitrogen) at 25 V for 7 minutes. The nitrocellulose membrane was blocked with 10 mL of 5% skim milk in tris-buffered saline (TBS) for 1 hour in room temperature with continuous shaking. The membrane was washed 3 times using TBS (with 2 minute shaking in between washes) and incubated with 10 mL of 1:1,000 rat anti-EspB primary antibody in TBS with 0.05% TWEEN 20 (TBST) overnight

at 4 °C with continuous shaking. The next day, the membrane was washed 3 times with TBST and incubated with 1:10,000 IRDye® 800CW (fluorescently labelled) goat anti-rat secondary antibody (LI-COR Biotechnology) in TBST for 1 hour in room temperature. The membrane was washed 3 times with TBST and imaged on Odyssey CLx imaging system (LI-COR Biotechnology).

3.4. Native-PAGE

Purified EspB samples at 10 µg were prepared in 2X Novex™ Tris-Glycine Native Sample Buffer (Invitrogen) and water at a total volume of 40 µL. The samples were resolved on Novex™ WedgeWell™ 4- 12% Tris-Glycine protein gel (Invitrogen) at 4 °C for 2 hours at 80V. The gel was then rinsed with water and stained with Coomassie blue dye for 1 hour. The gel was destained overnight and was imaged on the Odyssey CLx imaging system (LI-COR Biotechnology).

3.5. Dynamic light scattering

3.5.1. EspB preparation

Purified EspB samples were filtered through 0.22 µm Costar Spin-X centrifuge tube filters (Corning) and were concentrated using 10k molecular weight cut-off (MWCO) Protein Concentrator Tubes (Pierce). A BCA assay was performed to quantify the concentration of the samples. The filtered and concentrated samples were prepared at a concentration of 2 mg/mL at 50 µL and kept at 4 °C until ready for use.

3.5.2. DLS measurement of EspB samples

Dynamic light scattering (DLS) analysis was performed at the Protein Characterization and Crystallization Facility (PCCF) which is supported by the College of Medicine, University of Saskatchewan, Saskatoon, Canada. This experiment was performed with the help of Dr. Michal Boniecki. The prepared samples were centrifuged at maximum speed for 5 minutes prior to DLS measurement of the samples. A volume of 50 µL was dispensed into the reading plate and inserted into the DynaPro Plate Reader II (Wyatt Technologies). Temperature of the instrument was set to 20 °C, acquisition time was set to 1 and number of acquisitions was set to 60. The data was analyzed on the DYNAMICS Software (Wyatt Technologies).

3.6. Transmission electron microscopy procedure

3.6.1. EspB preparation and staining

Purified EspB was diluted to 150 μg/mL in 500 μL of LEW buffer. Formvar/carbon coated copper grids were glow discharged with Quorum Q150T ES to make the surface of the grids hydrophilic. Next, 5 μL of sample was applied to the grid and allowed to be absorbed for 1 minute. The grid was washed with water for 20 seconds and stained with 2% uranyl acetate in water for 1 minute. The excess staining solution was removed using filter paper and the grid was allowed to dry prior to microscopy.

3.6.2. Microscopy procedure

Imaging of the prepared EspB samples were performed on the Hitachi HT7700 transmission electron microscope with the help of Dr. Eiko Kawamura. After inserting the sample into the microscope, the beam was switched on and aligned to the center of the field of view. A region of the grid was selected to image and the focus and contrast were adjusted. Images in this project were captured at 100k magnification.

3.7. Phospholipid binding assays

3.7.1. Custom made phospholipid spotted membrane preparation procedure

Phospholipid sodium salts 1,2-dilauroyl-sn-glycero-3-phosphate (DLPA) and 1,2-dipalmitoyl-sn-glycero-3-phosphoserine (DPPS) were purchased from Echelon Biosciences. The phospholipid sodium salts were dissolved in a mixture of 1:1:0.1 chloroform:methanol:water. The solubilized phospholipids were adjusted to a concentration of 80 μM and diluted two-fold until a concentration of 5 μM was reached. The mixtures were stored in -20 °C until ready for use. Next nitrocellulose membrane was soaked in phosphate buffered saline (PBS) briefly, then dried with Kimwipe before dispensing 5 μL spots onto the membrane. The spots were allowed to dry before blocking the membrane in PBS with 0.1% TWEEN® 20 (Sigma-Aldrich) (PBST) with 3% BSA for 1 hour. The membrane was processed in the same way as commercially produced phospholipid spotted membranes.

3.7.2. Phospholipid membrane overlay assay

Phospholipid spotted membranes were purchased from Echelon Biosciences and the assay was performed according to manufacturer's instructions. The membranes were incubated in PBST

with 3% BSA for 1 hour in room temperature with continuous shaking. Next, the membranes were incubated with 0.5 μg/mL of EspB in 10 mL of PBST with 3% BSA for 1 hour. The membranes were washed 3 times with PBST prior to incubating with 10 mL of 1:1,000 rat anti-EspB primary antibody in PBST for 1 hour in room temperature. The membranes were washed 3 times with PBST, then incubated in 10 mL of 1:10,000 secondary goat anti-rat antibody (fluorescently labelled) in PBST for 1 hour in room temperature. Lastly, the membranes were washed 3 times with PBST prior to imaging the membranes on the Odyssey CLx imaging system.

3.7.3. Phospholipid coated bead pull-down assay

Phospholipid coated agarose beads were purchased from Echelon Biosciences. Agarose beads were washed with 300 μL of PBS with addition of 0.25% IGEPAL® CA-630 (Sigma Aldrich) twice, centrifuged at 800 xg for 2 minutes in between washes. The wash buffer was removed and the beads were incubated with 1.5 μg of purified EspB in PBS with 0.25% IGEPAL® CA-630 overnight at 4 °C with continuous shaking. The next day, the beads were washed with 300 μL of washing buffer (PBS + 0.25% IGEPAL® CA-630) and centrifuged at 800 xg. Washes were repeated 4 times before removing most of the wash buffer, leaving approximately 20 μL in the sample tubes for elution. The bound protein was eluted with 2% 2-mercaptoethanol in NuPAGE™ LDS Sample Buffer (Invitrogen) and boiled at 100 °C for 15 minutes. The eluted protein and the beads were transferred into Costar 0.45 μM SpinX tubes (Corning) and centrifuged the samples at maximum speed to remove beads from the eluted sample. The elution was resolved on the NuPAGE™ 4 – 12% Bis-Tris gel system and a western blot was performed as previously described.

3.8. THP-1 macrophage infection

3.8.1. *M. tb* culture preparation

M. tb frozen glycerol stocks (-80 °C) of WT *M. tb* Erdman was streaked out on Difco 7H11 (Becton-Dickinson) agar plates supplemented with Middlebrook oleic albumin dextrose catalase (OADC) enrichment (Becton-Dickinson). The transposon mutant strains *M. tb espA*::Tn and *M. tb* 5'Tn::*pe35* were streaked out on 7H11 agar supplemented with OADC and containing 50 μg/mL hygromycin. The plates were incubated at 37 °C for approximately 2 weeks or until isolated colonies could be observed and picked for further culture in liquid media. A starter culture in liquid media was prepared by inoculating 10 mL of complete Difco Middlebrook 7H9 media (Becton-

Dickinson), supplemented with 10% Middlebrook albumin dextrose catalase (ADC) enrichment (Becton-Dickinson), 10% TWEEN®-80 and 50 μg/mL of hygromycin for transposon mutant strains. The starter culture was incubated at 37 °C, 100 rpm for 1 week. Prior to infection of THP-1 macrophages, a *M. tb* working culture was prepared. The starter culture was centrifuged at 300 xg for 3 minutes to remove bacterial aggregates. The starter culture was then used to inoculate 5 mL of fresh, complete 7H9 media to an OD of 1. This working culture was incubated at 37 °C, 100 rpm overnight.

3.8.2. THP-1 cell culture preparation and differentiation

Human THP-1 monocytes were obtained from the American Type Culture Collection (ATCC). Previously prepared frozen stocks of THP-1 monocytes stored in liquid nitrogen were thawed and revived in complete Roswell Park Memorial Institute (RPMI) (Gibco) supplemented with 10% heat inactivated fetal bovine serum (FBS) (SAFC Biosciences). The thawed monocytes were added to 10 mL of complete RPMI and centrifuged at 125 xg for 8 minutes to remove dimethyl sulfoxide (DMSO) in the freezing medium. The supernatant was discarded and the cell pellet was resuspended with 10 mL of fresh, complete RPMI in a vented, untreated T25 tissue culture flask. The THP-1 monocytes were maintained between a range of 3×10^5 cells/mL and 8×10^5 cells/mL until there was an adequate amount of cells for the infection experiment. The THP-1 monocytes were differentiated with 100 ng/mL phorbol 12-myristate 13-acetate (PMA) in complete RPMI media and seeded in a 48-well tissue culture plate at 1×10^5 cells/well with the final volume of 1 mL/well. The cells were allowed to differentiate for 3 days at 37 °C, followed by replacement of media containing PMA with fresh RPMI media. The differentiated macrophages were further allowed to recover in 37 °C for 2 days prior to infection.

3.8.3. Purified EspB preparation

Purified $EspB^{WT}$ and variants were diluted into a concentration of 1000 nM in 5 mL of LEW buffer. The diluted protein sample was then filtered using a 0.2 μm syringe filter. The filtered preparation was quantified using the BCA Protein Assay Kit similarly to Methods section 3.3.5. However, the filtered sample was measured without diluting. Prior to infection of THP-1 macrophages, the EspB preparations were diluted to 80 nM in complete RPMI media.

3.8.4. THP-1 infection procedure

Differentiated THP-1 macrophages were infected similarly to a previously published study (Chen et al., 2013). For the groups that contained $EspB^{WT}$ or variants, complete RPMI media was prepared with 80 nM of purified and filtered EspB protein first, then working cultures of the *M. tb* 5'Tn::*pe35* strain was diluted to 500,000 cells/mL (multiplicity of infection (MOI) of 5) into the RPMI media containing EspB. For the other groups containing only bacteria, the working cultures of the *M. tb* strains were diluted to 500,000 cells/mL in fresh RPMI media prior to infection of the macrophages. The conditioned RPMI media in the differentiated THP-1 macrophages was replaced with the RPMI containing *M. tb* and purified, filtered EspB. THP-1 macrophages were infected for 3 days before measuring cytotoxicity. Prior to measuring cytotoxicity, 775 µL of media was removed and 25 µL of PrestoBlue HS cell viability reagent (Invitrogen) was added to each of the wells. The plate was incubated at 37 °C in the dark for 15 minutes to allow for conversion of resazurin to resorufin, and cell viability was measured using the SpectraMax i3x (Molecular Devices). The plate was incubated for another 15 minutes (30 minutes total) in the dark, then cell viability was measured.

3.8.5. Statistical analysis of THP-1 infections

Statistical analysis of the cytotoxicity assays were performed on GraphPad Prism 9 software. Percent relative cytotoxicity plots were generated using this software. Statistical significance differences between experimental groups were determined using one-way ANOVA.

3.9. Localization of phospholipids with biosensors

3.9.1. Preparation of biosensor plasmids

Biosensor plasmids pGFP-LactC2 and pMGFP were obtained from Sergio Grinstein Laboratory at the University of Toronto, (Toronto, Canada) and Guangwei Du Laboratory at the University of Texas (Houston, TX) respectively. The plasmids were transformed into TOP10 *E. coli* by heat shock and plated onto LB agar plates. The transformants were inoculated into LB media and incubated overnight at 37 °C, 200 rpm. The plasmids were purified using the EndoFree Plasmid Maxi Kit (Bio Basic) according to manufacturer's instructions. Plasmids were stored in -20 °C prior to transfection into mammalian cells.

3.9.2. COS-7 cell culture preparation

COS-7 non-human primate kidney fibroblast-like cells were obtained from ATCC. Frozen stocks of COS-7 cells were stored in liquid nitrogen and were thawed and revived in Dulbecco's Modified Eagle's Medium (DMEM) (Sigma Aldrich) supplemented with 10% FBS and 0.05 mg/mL gentamicin. The thawed cells were centrifuged in complete DMEM at 800 rpm for 8 minutes to remove DMSO in the freezing medium. The cell pellet was resuspended in 15 mL of fresh, complete DMEM in a T75 treated tissue culture flask. To passage COS-7 cells, 2 mL of Trypsin was added to the T75 flask and incubated in 37 °C for 3-5 minutes for detachment of the cells. Complete DMEM was added to the cells and the cells were centrifuged at 800 rpm for 8 minutes. The cell pellet was resuspended with fresh, complete DMEM and the appropriate split ratio of cell suspension was added to the T75 flask to the final volume of 15 mL. Cells were seeded at a density of 2.5×10^5 cells in 2 mL of DMEM in a 35 mm petri dish. The seeded cells were allowed to incubate overnight at 37 °C prior to transfection.

3.9.3. Raw 264.7 cell culture preparation

Raw 264.7 murine macrophages were obtained from ATCC. Frozen stocks of Raw 264.7 macrophages stored in liquid nitrogen were thawed and revived in DMEM (Sigma Aldrich) supplemented with 10% heat inactivated FBS, 1 mM sodium pyruvate, and 0.05 mg/mL gentamicin. The thawed cells were centrifuged in complete DMEM at 800 rpm for 8 minutes to remove DMSO in the freezing medium. The cell pellet was resuspended in 15 mL of fresh, complete DMEM in a T75 untreated tissue culture flask. Cells were maintained for 1 week (with passages every 2 days) until the number of cells were adequate for seeding. The cells were seeded at a density of 2.5×10^5 cells in 2 mL of DMEM in a 35 mm petri dish. The seeded cells were allowed to incubate overnight at 37 °C prior to transfection.

3.9.4. Transfection of COS-7 cells and Raw 264.7 macrophages

The same transfection protocol was used for COS-7 and Raw 264.7 cells. Two tubes were set up prior to transfection: tube A with 2.0 μg of biosensor plasmid in 200 μL of Opti-MEM reduced serum media (Gibco) and tube B with 6 μL of Lipofectamine 2000 suspension (Invitrogen) in 200 μL of Opti-MEM. The contents of tube A and tube B were mixed by adding the plasmid to the Lipofectamine in a drop-wise fashion. This mixture was then incubated for 10 minutes in room temperature. During incubation of the DNA-Lipofectamine mixture, culture media was aspirated

from the cells and washed once with PBS and once with Opti-MEM to remove traces of serum and antibiotics. A volume of 400 μL of Opti-MEM was added to keep cells from drying. The DNA-Lipofectamine mixture was added to the cells in a drop-wise fashion to a final volume of 800 μL in the petri dish. The cells were incubated for 4 hours at 37 °C. After incubation, the media was replaced with 2 mL of DMEM (without serum or antibiotics) and incubated for 24 hours prior to imaging by confocal microscopy.

4. Results

4.1. Mapping amino acids postulated to be functionally important in EspB

Previously, EspB was found to have a virulence function that is distinct from other ESX-1 substrates (Chen et al., 2013). EspB was able to induce cytotoxicity in THP-1 macrophages in the presence of *M. tb* 5'Tn::*pe35* (Chen et al., 2013). In addition, it was found to bind phospholipids, specifically PA and PS (Chen et al., 2013). This led to the question if phospholipid binding is crucial for the virulence function of EspB. Furthermore, EspB was found to oligomerize into heptameric structures (Korotkova et al., 2015; Piton et al., 2020; Solomonson et al., 2015). However, it is currently unknown whether oligomerization of EspB plays an important role in phospholipid binding or the virulence function of EspB.

A multiple alignment of the amino acid sequence of EspB from several mycobacterial species was performed to identify conserved residues in the protein (Figure 4.1). Several residues in particular were hypothesized to be functionally important for EspB in terms of phospholipid binding and oligomerization. The residues R17, H223, F159, and I246 were predicted to be involved in phospholipid binding, whereas the residues K259, K267, and W176 were predicted to be involved in EspB oligomerization for reasons stated below. These targeted residues were then mapped onto the 3D model of EspB using the UCSF Chimera molecular modelling system to localize the potential phospholipid binding sites and oligomerization sites.

4.1.1. Residues hypothesized to be involved in phospholipid binding

The basic residues R17 and H223 were found to be highly conserved in the multiple sequence alignment. As anionic phospholipids such as PA and PS tend to interact with proteins with positive surface charges, the residues R17 and H223 were predicted to bind the negatively charged head groups of acidic phospholipids (Bohdanowicz and Grinstein, 2013; Chen et al., 2013; Stace and Ktistakis, 2006). Intriguingly, when R17 and H223 were mapped on a model of the EspB oligomer, the residues were located directly at the opening of either side of the EspB channel (Figure 4.2A). Two other residues, F159 and I246 were also predicted to be involved in phospholipid binding as they are located within two identified hydrophobic pockets on the EspB monomer (Korotkova et al., 2015). When these two residues were mapped, they were found to be located in close proximity to R17 and H223 (Figure 4.2B). I246 was located at the opening on one side of the channel, whereas F159 was located on the outer middle region of the oligomer.

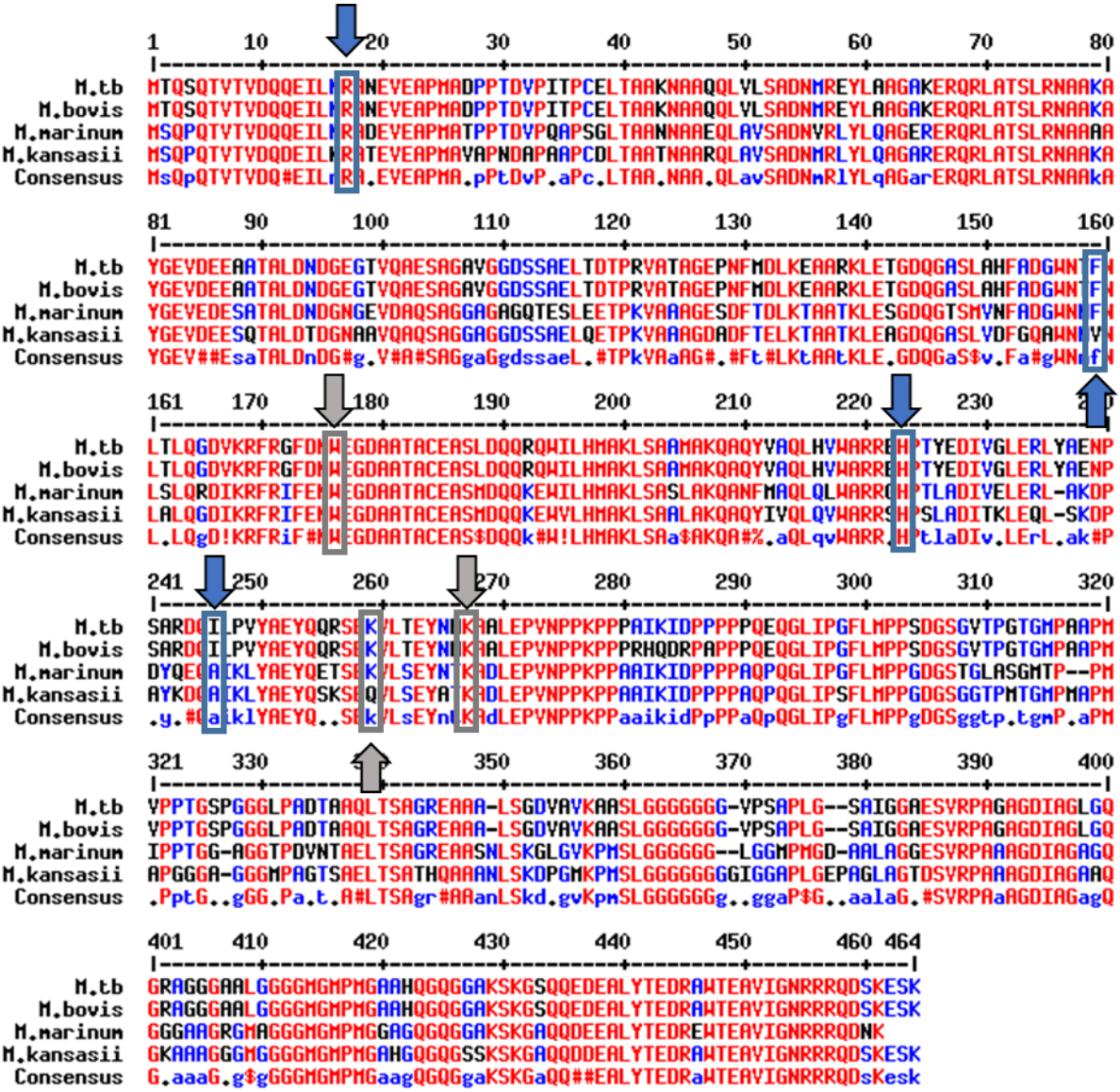

Figure 4.1. Multiple alignment of EspB amino acid sequences from multiple mycobacterial species. Alignment was performed using MultAlin. Residues hypothesized to be involved in phospholipid binding are indicated with a blue arrow, whereas residues predicted to be involved in oligomerization are indicated with a grey arrow.

4.1.2. Residues hypothesized to be involved in EspB oligomerization

The residues K259 and K267 were predicted to be involved in protein-protein interactions due to their close proximities in chemical cross-linking and mass spectrometry experiments (Solomonson et al., 2015). On the EspB oligomer model, K259 and K267 were found to be located in close proximity to each other within the same monomer but not from one monomer to another (Figure 4.3A). Next, the residue W176 is located in the WxG motif of EspB which may play a role

in stabilizing the monomeric hairpin structure, which in turn may be critical for oligomerization of EspB (Piton et al., 2020; Solomonson et al., 2015). Mapping W176 revealed that it was located at the opening of the channel and was shown to interact with Y81 of the YxxxD motif on the same EspB monomer to stabilize the hairpin structure (Figure 4.3B).

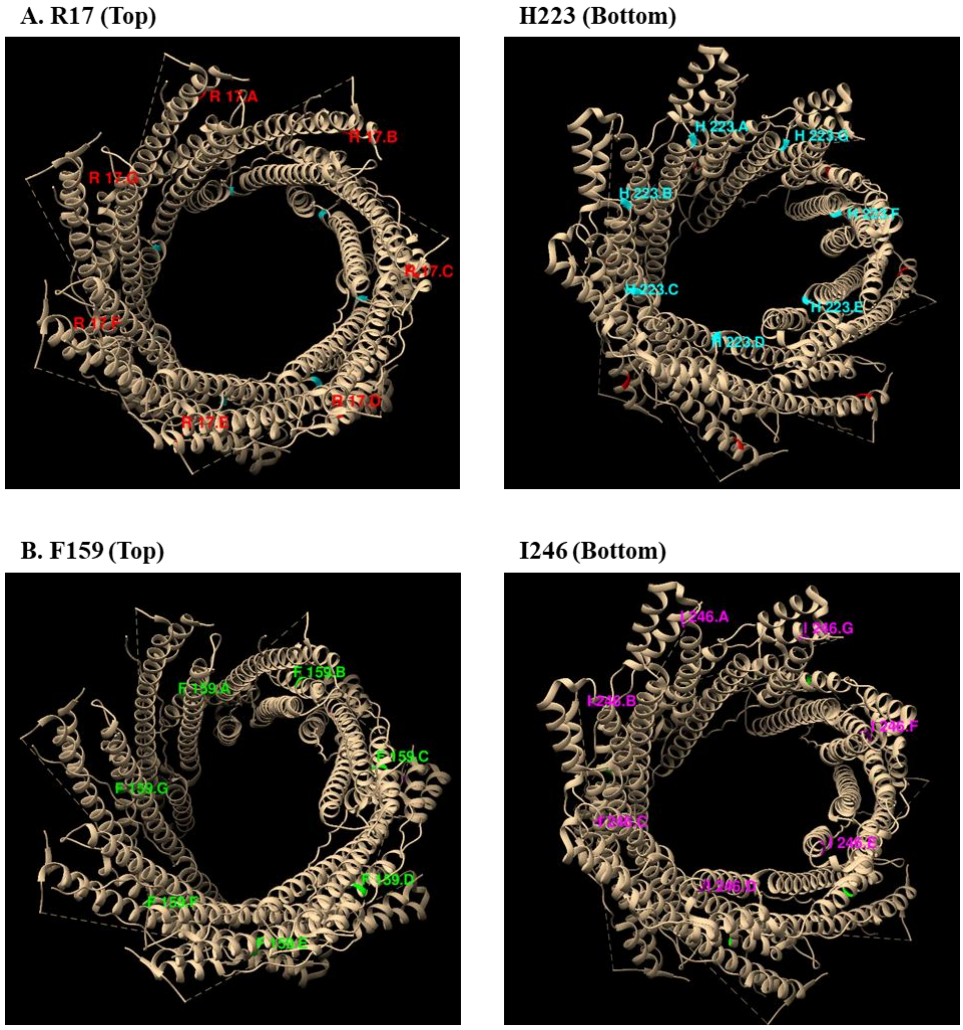

Figure 4.2. Labelled residues that are predicted to bind phospholipids targeted for mutation on 3D EspB model. Orientation of the oligomer was arbitrarily assigned as "Top" and "Bottom". A. R17 (red) and H223 (cyan), B. F159 (green) and I246 (magenta)

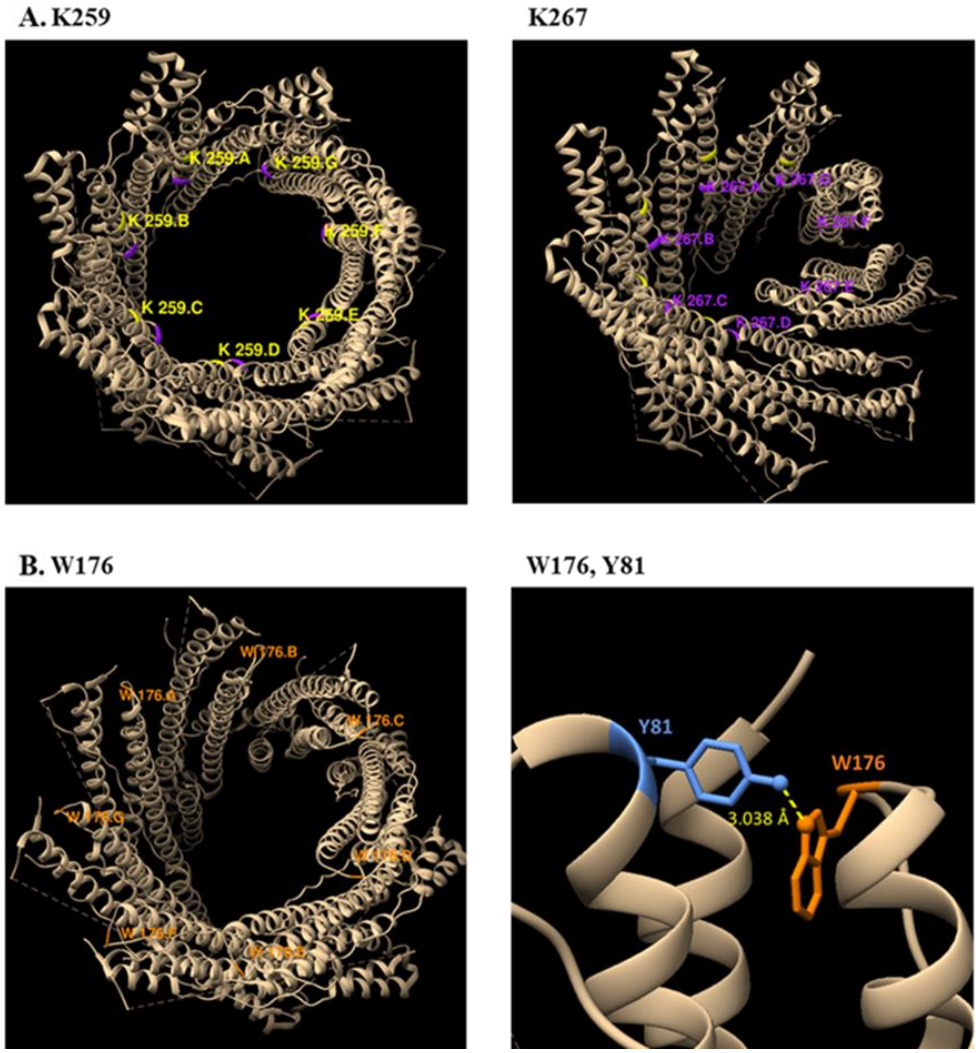

Figure 4.3. Labelled residues that are predicted to be involved in oligomerization targeted for mutation on 3D EspB model. Residues were labelled using UCSF Chimera molecular modelling system. **A.** K259 (yellow) and K267 (purple), and **B.** W176 (orange) and W176 interaction with Y81 (blue).

4.2. Purification of recombinant EspB

Production of a large amount of protein was required in order to characterize the molecular basis of EspB phospholipid binding and oligomerization and to define any association between these features with the virulence function of EspB. Accordingly, the *espB* gene was cloned into a pET28a expression system and transformed into *E. coli* to produce recombinant EspB protein. The bacteria were harvested and lysed for purification of EspB. Ammonium sulfate precipitation was used as a first step of purification to precipitate proteins within the solution at different levels of salt saturation. SDS-PAGE was used to detect the fractions containing EspB based on its known

size. Next, nickel affinity chromatography was used to further purify the protein. EspB was constructed to contain a histidine tag at the C-terminus of the protein and therefore would be captured within the column while contaminating proteins were allowed to exit the column. EspB was then eluted using imidazole.

The purification protocol was first established and optimized for $EspB^{WT}$, then was repeated with the EspB variants in the same manner. Ammonium sulfate precipitation experiments showed that EspB tends to precipitate out of solution at a range of 20-35% of the salt (Figure 4.4A). This was also observed in the other EspB variants. Next, nickel-iminodiacetic acid (Ni-IDA) affinity column revealed that EspB in elution fractions 1 and 2 were high in yield and purity (Figure 4.4B). The protein was mostly eluted from the column after the second elution as there were low levels of EspB detected in the third elution fraction. High yields of purified recombinant $EspB^{WT}$ and variants were produced using this purification method. The purified protein was then used for biochemical characterization to test for phospholipid binding and oligomerization.

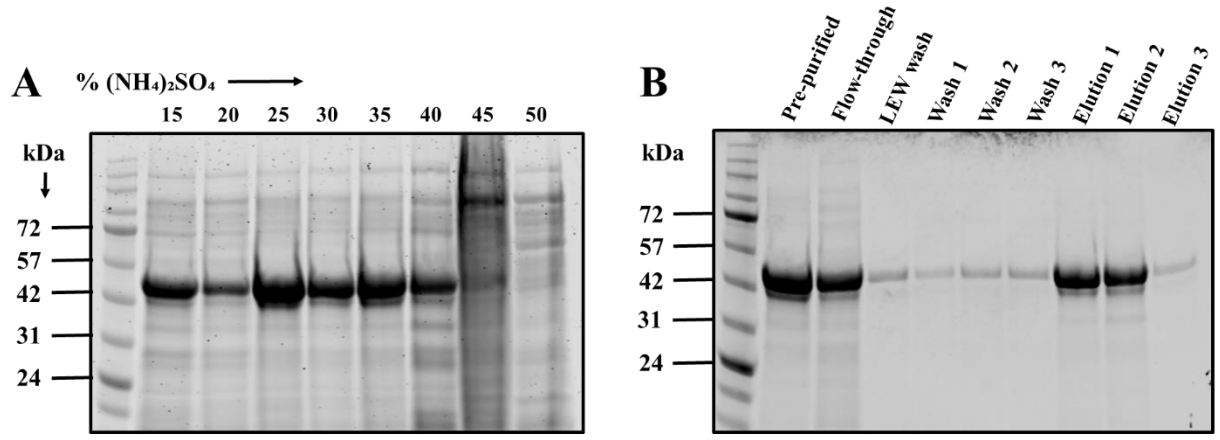

Figure 4.4. Purification process of recombinant $EspB^{WT}$. A. Ammonium sulfate precipitation of EspB. **B.** Ni-IDA column purification of recombinant EspB.

4.3. Characterization of recombinant EspB

Initially, single amino acid replacements at R17, H223, F159, I246, K259, and K267 in EspB were made. However, follow-up studies of these single amino acid mutants did not show significantly different phenotypes compared to $EspB^{WT}$. Therefore, double mutations of residues at hypothesized phospholipid binding sites ($EspB^{R17A/H2223A}$ and $EspB^{F159R/I246R}$) and hypothesized dimerization sites ($EspB^{K259A/K267A}$) were constructed. In addition, a single amino acid replacement at the W176 residue within the WxG motif was constructed as $EspB^{W176R}$. Similar sized non-polar

amino acid residues were chosen to replace the targeted polar residues within EspB (such as A to replace R17, H223, K259, and K267), and polar residues were chosen to replace the targeted residues (such as R to replace F159, I246, and W176). Following purification of $EspB^{WT}$ and variants, a BCA assay was performed to quantify each protein sample and equimolar amounts of $EspB^{WT}$ and variants were resolved on a denaturing gel. Each of the EspB samples were tested for purity of the preparations and detection by anti-EspB antibody. SDS-PAGE showed high purity of the EspB preparations with very small amounts of contaminating proteins (Figure 4.5A). Additionally, an immunoblot revealed that $EspB^{WT}$ and variants were all adequately detected by the anti-EspB antibody (Figure 4.5B).

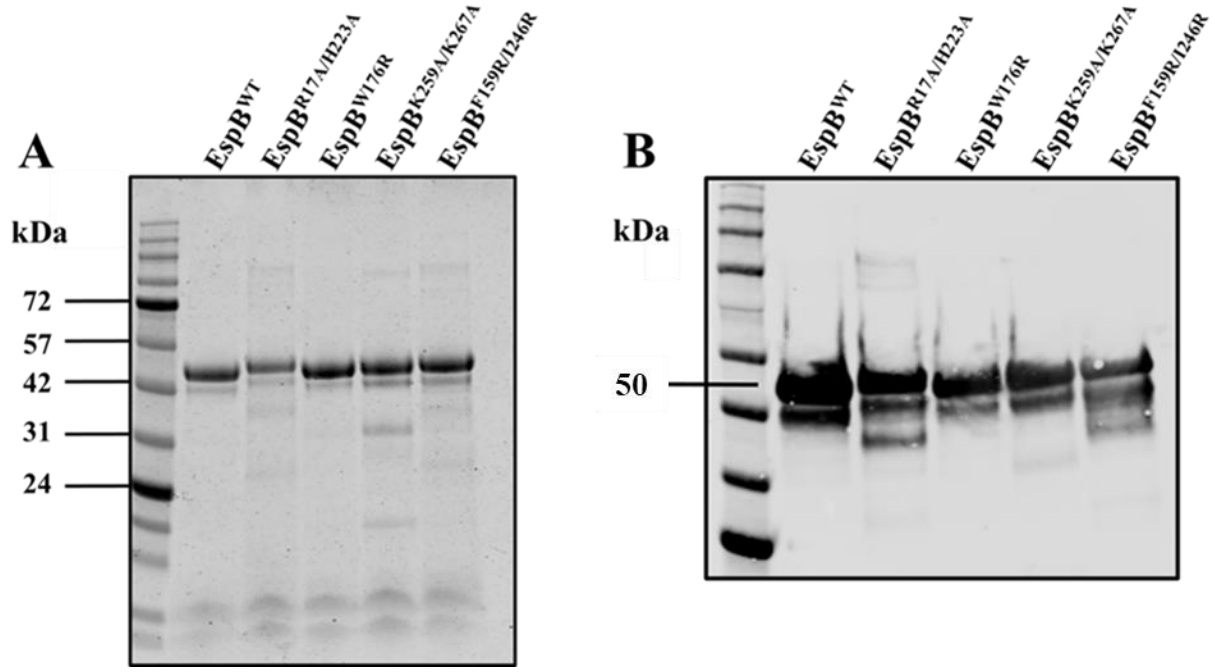

Figure 4.5. Purified $EspB^{WT}$ and variants resolved on SDS-PAGE. A. EspB samples resolved on SDS-PAGE and stained with Coomassie blue. **B.** EspB samples resolved on SDS-PAGE followed by western blot shows detection of $EspB^{WT}$ and variants by rat anti-EspB primary antibody.

4.3.1. Native-PAGE analysis of recombinant EspB

EspB monomers (50 kDa) oligomerizes into a 350 kDa heptameric barrel structure (Korotkova et al., 2015; Solomonson et al., 2015). Native-PAGE has previously been used to analyze the oligomeric states of EspB expressed by *M. tb* from CF and CL, as well as purified recombinant EspB (Korotkova et al., 2015). $EspB^{WT}$ showed higher oligomeric formation in CF

of *M. tb* in comparison to CL (Korotkova et al., 2015). In addition, purified EspB showed less tendency to form the heptameric structures in comparison to *M. tb* CF (Korotkova et al., 2015). Native-PAGE differs from SDS-PAGE in that it resolves proteins based on size in native conditions rather than denaturing conditions. Using this method, oligomeric states adopted by native EspB can be observed. In addition to confirming purified $EspB^{WT}$ oligomeric states in native-PAGE with previous publications, the newly constructed EspB variants were also examined.

Equimolar amounts of $EspB^{WT}$ and variants were resolved on a native-PAGE gel to observe differences in oligomeric states of the samples (Figure 4.6) $EspB^{WT}$ showed predominantly dimeric, trimeric, and pentameric species. Whereas, $EspB^{R17A/H223A}$ adopted a hyperoligomerized state. Some trimeric oligomers were observed but it was accompanied with a streaking pattern at the top of the gel. $EspB^{W176R}$ and $EspB^{K259A/K267A}$ formed mainly monomeric, dimeric and trimeric oligomers and did not show any hyperoligomerization. Lastly, $EspB^{F159R/I246R}$ showed an intense

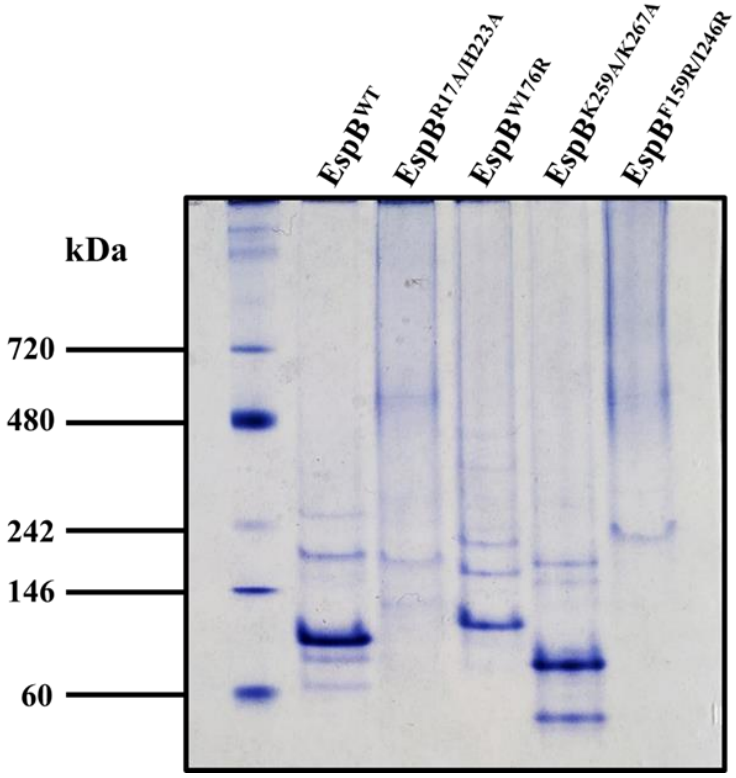

Figure 4.6. Purified recombinant $EspB^{WT}$ and variants resolved on native-PAGE. All EspB samples were added at a quantity of 10 µg and molecular weight markers in kDa are indicated on the left of the gel.

streaking pattern at the top of the gel similarly to EspB$^{R17A/H223A}$. However, it is unknown if there are differences in the large oligomeric structures between EspB$^{R17A/H223A}$.

4.3.2. Dynamic light scattering analysis of EspB

The next method used for EspB oligomeric characterization was dynamic light scattering (DLS). In brief, the principle of DLS is based on light diffracting off of the sample particles. Initially, an incident laser propagates through the sample containing particles in Brownian motion (Mailer et al., 2015; Stetefeld et al., 2016). The random movements of the particles results in fluctuations of measured light intensity due to Rayleigh scattering (Stetefeld et al., 2016) (Figure 4.7). The particle size is calculated based on the speed of the light decay (Mailer et al., 2015; Stetefeld et al., 2016). Smaller particles diffuse faster, corresponding to higher fluctuation of light intensity, whereas larger particles diffuse slower resulting in a lower fluctuation. The diffracted light is detected by a fast photon counter which takes measurements continuously with a preset interval called time delay. The data taken from each time point are compared to each other to obtain the correlation function (Mailer et al., 2015). The correlation of the light intensity between time points gives information on particle diffusion, which is related to the hydrodynamic radius of the particle by the Stokes-Einstein equation (refer to Appendix 1, Equation 1) (Mailer et al., 2015).

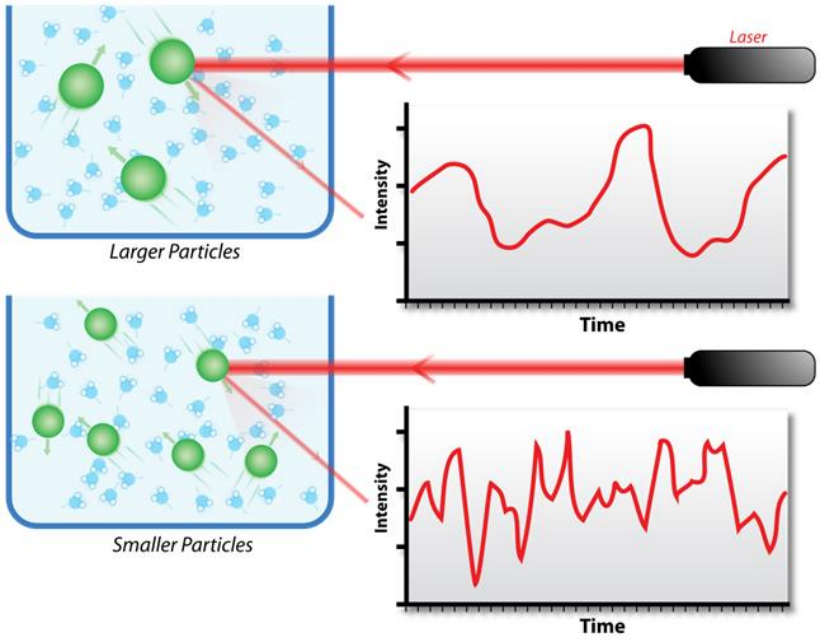

Figure 4.7. Principle of DLS. This diagram demonstrates that larger particles diffuse at a slower rate, resulting in a smoother intensity plot. Whereas smaller particles tend to diffuse faster will have a more erratic intensity plot (Jones, 2010).

The radius is then used to calculate the estimated molecular weight of the sample particles. In addition, the polydispersity index (PDI) was calculated for each sample to determine if they were monodispersed or polydispersed. A value above 20% indicates that the sample is polydispersed, meaning that there are several oligomeric species present in the sample. DLS was therefore used to determine oligomerization propensities of the EspB variants in comparison to $EspB^{WT}$.

The molecular weight estimation of approximately 226 kDa in the $EspB^{WT}$ sample was revealed to be the most abundant oligomeric species (Figure 4.8A). The PDI for $EspB^{WT}$ was estimated to be 23% which indicates that the sample was mainly monodispersed. $EspB^{R17A/H223A}$ showed an estimation of 53.9 kDa at 65% mass intensity as well as a very large oligomeric species of 1297 at 33.7% mass intensity (Figure 4.8B). The PDI was estimated to be 30% at the first peak and 67% at the second peak, indicating that there were various oligomeric species within the sample. $EspB^{W176R}$ showed an estimation of 163 kDa and did not show a tendency to form large oligomers (Figure 4.8C). The PDI was estimated to be 80%, showing high polydispersity. Like $EspB^{W176R}$, $EspB^{K259A/K267A}$ showed a molecular weight estimation of 193.0 kDa and also did not form an abundance of larger oligomeric species (Figure 4.8D). However, this variant was indicated to be monodispersed as the PDI was estimated to be 18%. Lastly, $EspB^{F159R/I246R}$ showed a molecular weight estimation upwards of 1458.5 kDa (Figure 4.8E). This variant had a strong tendency to form oligomeric species and was highly polydispersed, where PDI was estimated to be 88%.

A. EspB^{WT}

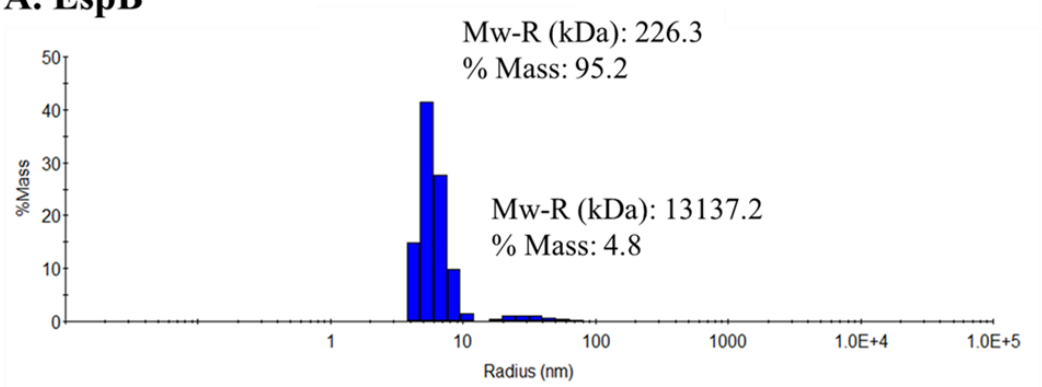

B. EspB$^{R17A/H223A}$

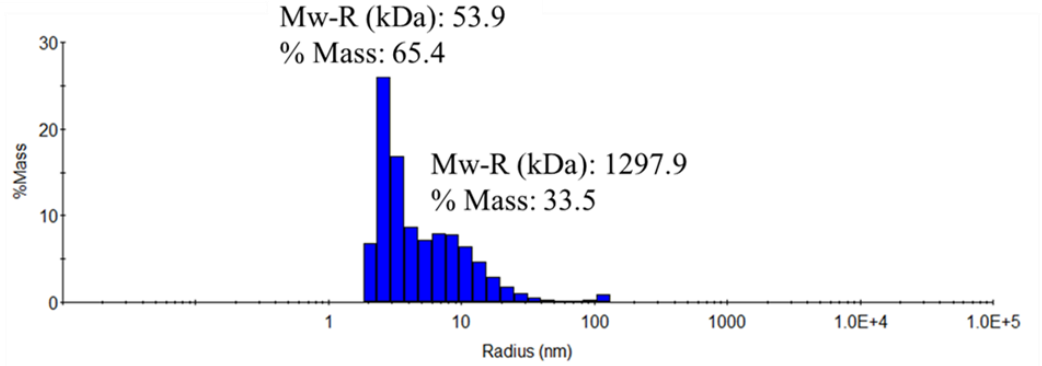

C. EspB^{W176R}

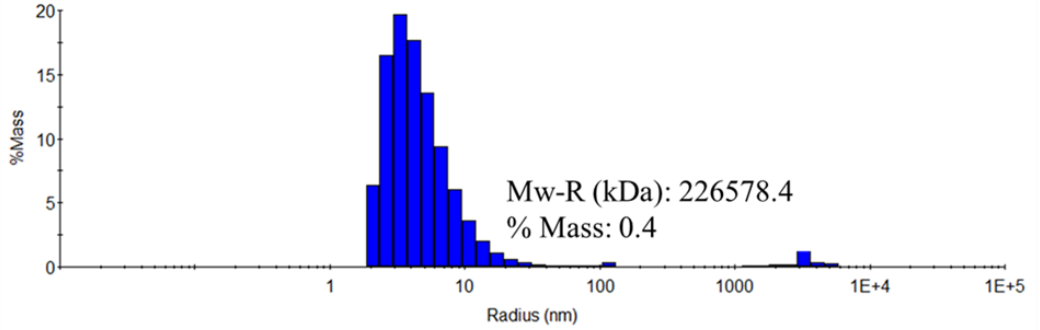

D. EspB$^{K259A/K267A}$

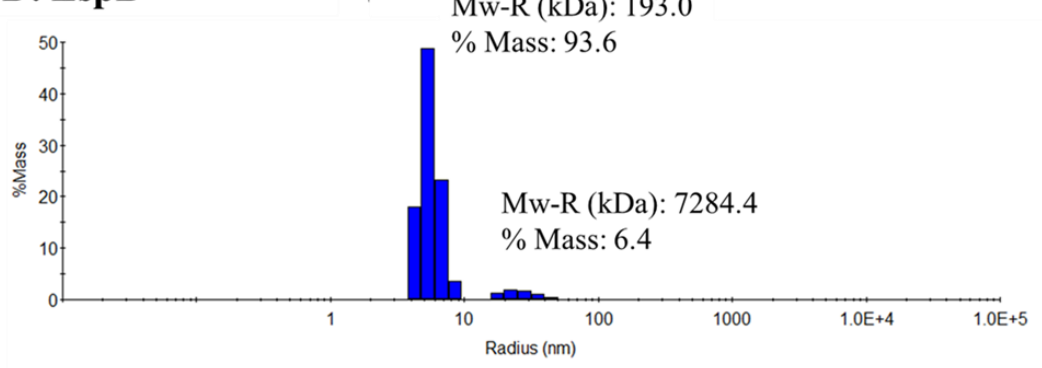

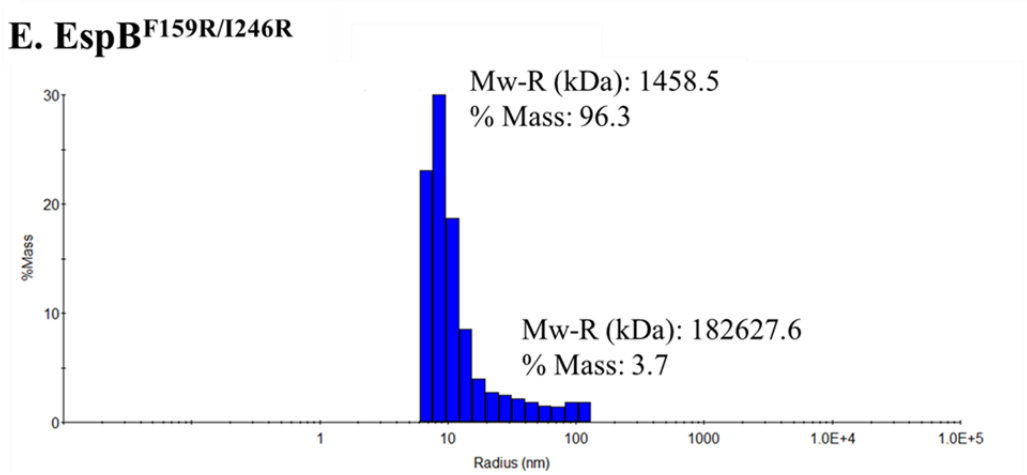

Figure 4.8. DLS analysis of EspB^{WT} and variants. Estimated molecular weight (Mw-R) of particles within the samples measurements are indicated in kDa. Mass distribution of each sample by oligomeric species are indicated in % Mass. Measurements were taken from samples containing **A.** EspB^{WT}, **B.** EspB$^{R17A/H223A}$, **C.** EspB^{W176R}, **D.** EspB$^{K259A/K267A}$, and **E.** EspB$^{F159R/I246R}$.

4.3.3. Transmission electron microscopy of EspB

To directly visualize the oligomeric states of EspB^{WT} and its variants, transmission electron microscopy (TEM) was performed. This method was previously used to visualize the EspB oligomer where it was found that EspB^{WT} formed heptameric barrel shaped oligomers (Korotkova et al., 2015; Piton et al., 2020; Solomonson et al., 2015).

EspB^{WT} formed heptameric oligomers that were consistent with previous publications (Figure 4.9A). The heptamers were dispersed evenly and separated from one another. EspB$^{R17A/H223A}$ also showed some similar oligomeric structures but the oligomers appeared to be more closely associated with one another, forming larger complexes (Figure 4.9B). EspB^{W176R} showed very few formations of heptameric barrels and the oligomers appeared incomplete and sparse (Figure 4.9C). However, EspB$^{K259A/K267A}$ formed very similar heptameric oligomers as EspB^{WT} did (Figure 4.9D). Lastly, EspB$^{F159R/I246R}$ appeared to rarely form the heptameric oligomers (Figure 4.9E). Rather, this variant formed large complexes of the protein associated with each other.

A. EspB^{WT}

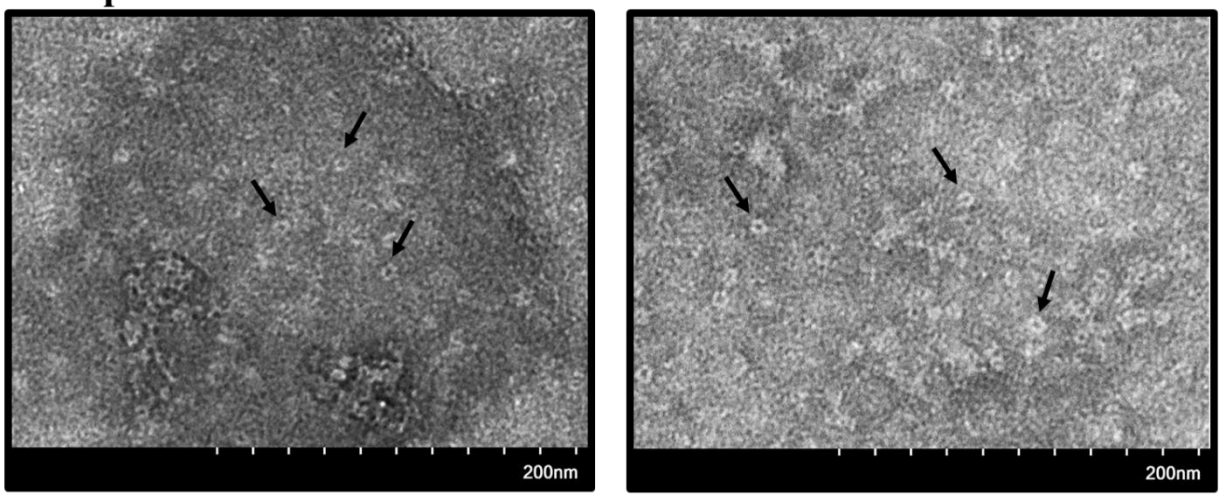

B. EspB$^{R17A/H223A}$

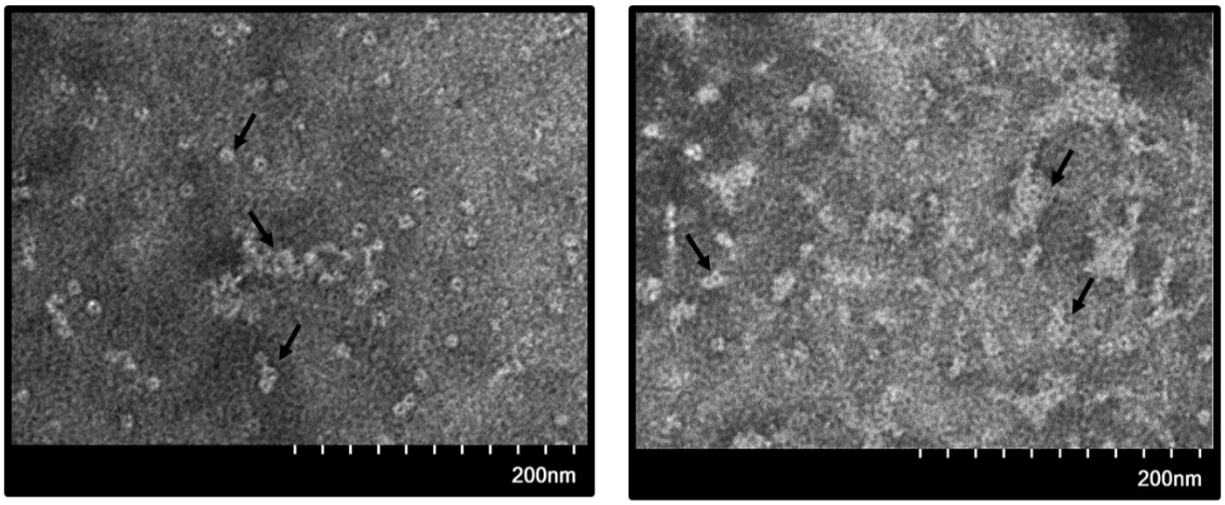

C. EspB^{W176R}

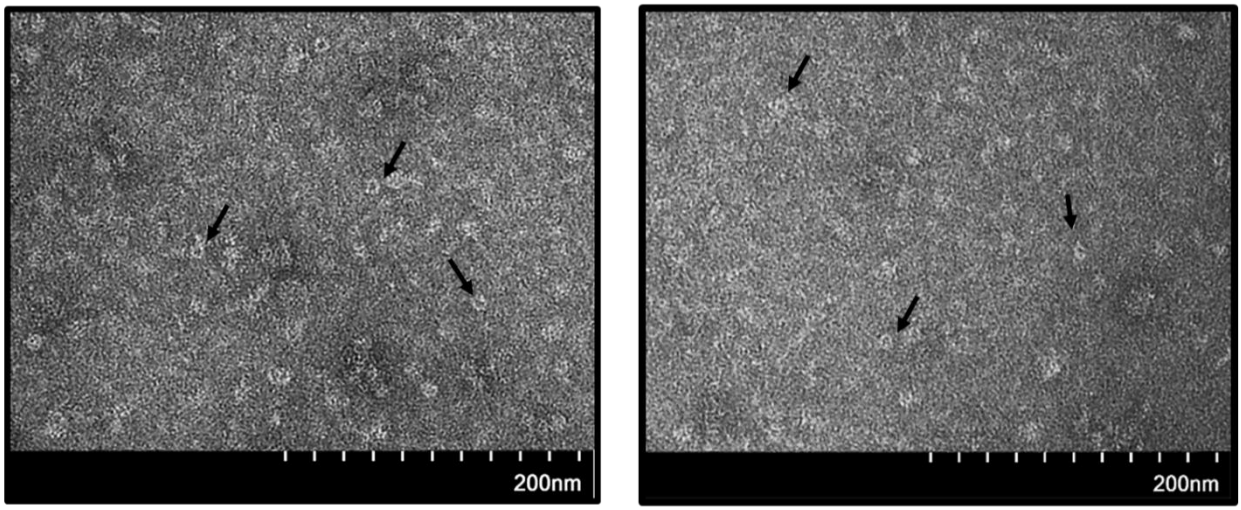

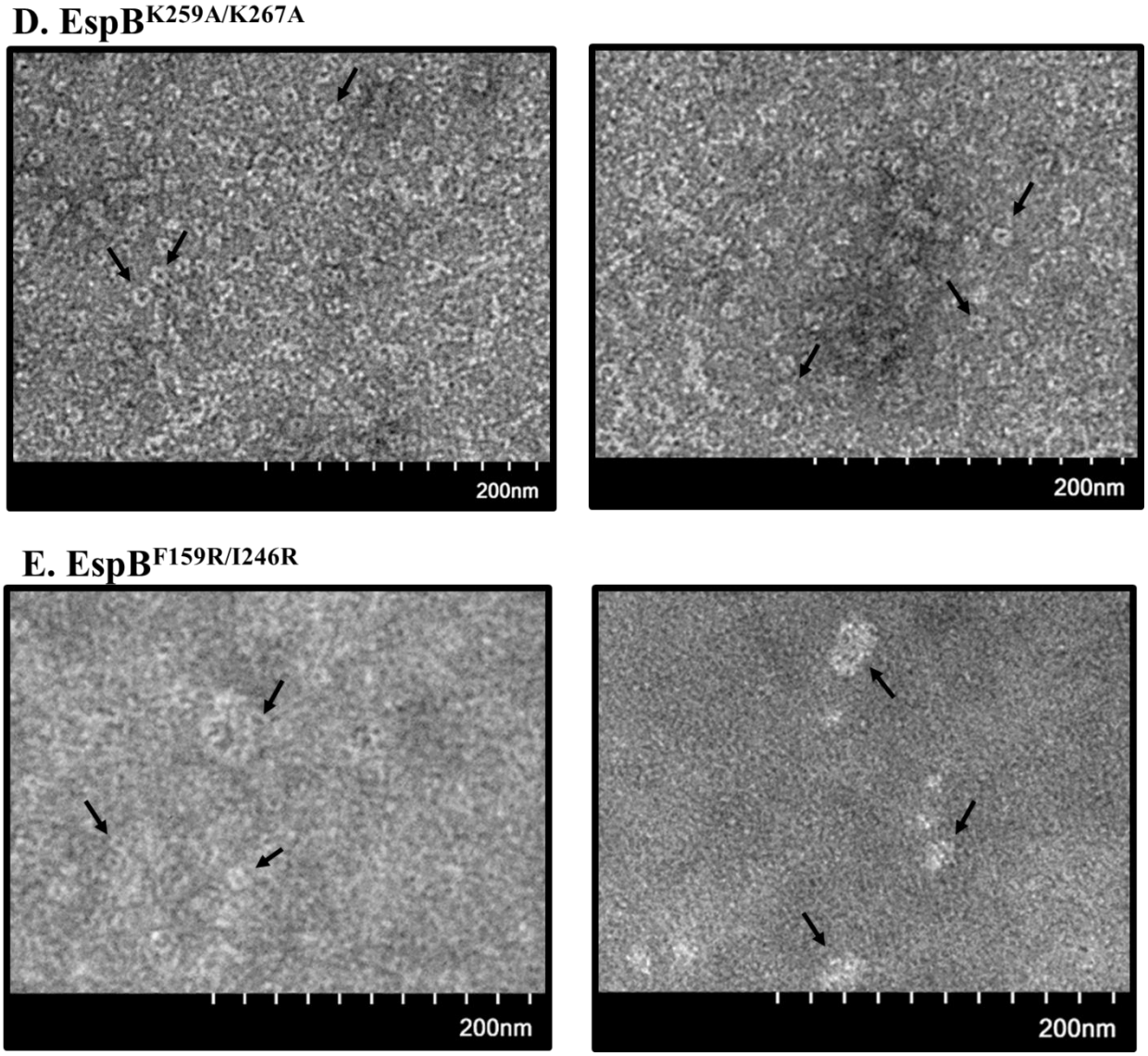

Figure 4.9. TEM imaging of EspB^{WT} and variants. All images were taken at 100K magnification. All protein samples **A.** EspB^{WT}, **B.** EspB$^{R17A/H223A}$, **C.** EspB^{W176R}, **D.** EspB$^{K259A/K267A}$, and **E.** EspB$^{F159R/I246R}$ were prepared at 150 µg/mL concentration.

Overall, the propensity of EspB$^{R17A/H223A}$ and EspB$^{F159R/I246R}$ to hyperoligomerize were found to be consistent throughout native-PAGE, DLS, and TEM analyses. Whereas, EspB^{W176R} and EspB$^{K259A/K267A}$ showed similar oligomeric formations as EspB^{WT}. However, the data obtained from native-PAGE and DLS analyses did not reveal how the oligomeric structures of each variant were formed. Therefore, TEM was used to directly visualize these oligomeric structures. Although the variants EspB$^{R17A/H223A}$ and EspB$^{F159R/I246R}$ both had the tendency to hyperoligomerize, their structures were vastly different. In addition, native-PAGE and DLS analyses revealed similar

molecular weights of the oligomers formed in $EspB^{W176R}$ and $EspB^{K259A/K267A}$ to $EspB^{WT}$. However, TEM analysis reveal some differences of the $EspB^{W176R}$ oligomeric structure from $EspB^{WT}$.

4.4. Characterization of EspB phospholipid binding

Pure EspB was previously found to bind phospholipids, specifically PA and PS *in vitro* (Chen et al., 2013). These phospholipids are involved in important macrophage processes such as phagosome maturation (Bohdanowicz and Grinstein, 2013). This led to the hypothesis that phospholipid binding may be critical for the virulence function of EspB. In addition, the EspB monomer was found to contain hydrophobic pockets predicted to bind the fatty acid region of phospholipids (Korotkova et al., 2015). The conserved basic residues R17 and H223 that were identified in a sequence alignment were also are predicted to be involved in binding the negatively charged head groups of acidic phospholipids. The EspB variants constructed in this project was tested for their phospholipid binding abilities.

4.4.1. Phospholipid membrane overlay assay

Phospholipid spotted membranes were used to assess $EspB^{WT}$ binding to specific phospholipids in comparison with the previous EspB study (Chen et al., 2013). In addition, phospholipid interactions of the newly constructed EspB variants were observed. Two types of phospholipid spotted membranes were used in this project: commercially made membranes were purchased from Echelon Biosciences and custom phospholipid arrays were made in the laboratory.

The commercially made phospholipid spotted membranes were used to assess the specificity of the phospholipid binding by EspB (Figure 4.10). $EspB^{WT}$ was observed to bind to PA similarly to the previous study (Chen et al., 2013). However, it was also detected to bind PI(3,5)P_2, PI(3)P, PI(4)P, and PI(5)P. $EspB^{R17A/H223A}$ showed a lack of PA binding as well as PI(3,5)P_2, PI(3)P, PI(4)P, and PI(5)P. $EspB^{W176R}$ showed similar phospholipid binding intensity as $EspB^{WT}$ to PA as well as the phosphoinositides. Interestingly, $EspB^{K259A/K267A}$ showed a slight reduction in binding these phospholipids. In contrast, $EspB^{F159R/I246R}$ was able to bind PA in the same manner as $EspB^{WT}$ but showed increased binding to PI(3,5)P_2, PI(3)P, PI(4)P, and PI(5)P.

Custom laboratory-made phospholipid membrane arrays were used to determine if there were differences of the EspB variants in terms of their affinity to PA binding (Figure 4.11). These

membranes were used as a more economical alternative in comparison to the costly commercially produced membranes. Each membrane was spotted with decreasing amounts of PA and PS starting at 400 pmol and diluted 2 fold. The spotted membranes were incubated with $EspB^{WT}$, $EspB^{R17A/H223A}$, $EspB^{W176R}$, $EspB^{K259A/K267A}$, or $EspB^{F159R/I246R}$, followed by immunoblotting. $EspB^{WT}$ showed strong binding to PA, whereas $EspB^{R17A/H223A}$ showed a very weak affinity to PA. $EspB^{W176R}$ showed a similar binding intensity to PA as $EspB^{WT}$. Consistently, $EspB^{K259A/K267A}$ showed a slight reduction in PA affinity. Lastly, $EspB^{F159R/I246R}$ showed similar affinity to PA as $EspB^{WT}$.

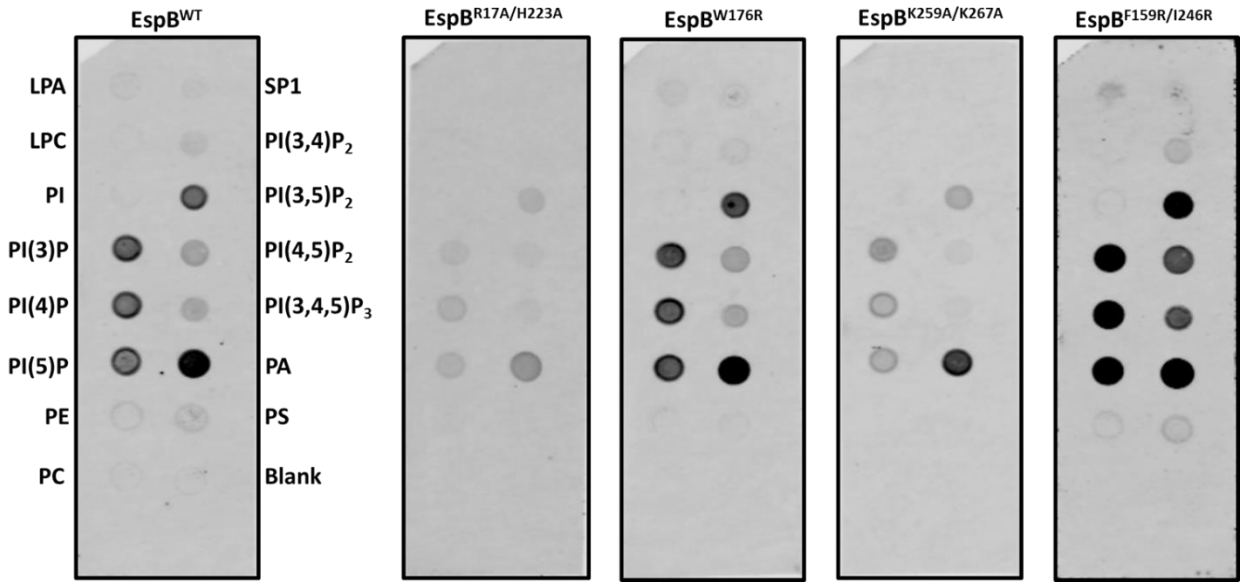

Figure 4.10. Commercially produced phospholipid membrane overlay assay of $EspB^{WT}$ and variants. Phospholipids used for this assay are indicated on the first membrane. Each membrane was incubated with either $EspB^{WT}$, $EspB^{R17A/H223A}$, $EspB^{W176R}$, $EspB^{K259A/K267A}$ or $EspB^{F159R/I246R}$.

4.4.2. Phospholipid bead pull-down assay

The second method used to test EspB-phospholipid interactions was the use of phospholipid coated agarose beads. These commercially produced beads were coated with a phospholipid of choice and incubated with the target protein to test phospholipid binding. PA and PS coated beads were used for each of these variants and control beads (without phospholipid coating) was used as a negative control. This experiment was repeated twice per variant comparing to $EspB^{WT}$ (Figure 4.12). $EspB^{WT}$ showed strong binding to PA beads, whereas $EspB^{R17A/H223A}$ was unable to bind PA. $EspB^{W176R}$ showed similar binding to PA as $EspB^{WT}$ and $EspB^{K259A/K267A}$ showed reduced binding. Lastly, $EspB^{F159R/I246R}$ showed similar PA binding as $EspB^{WT}$.

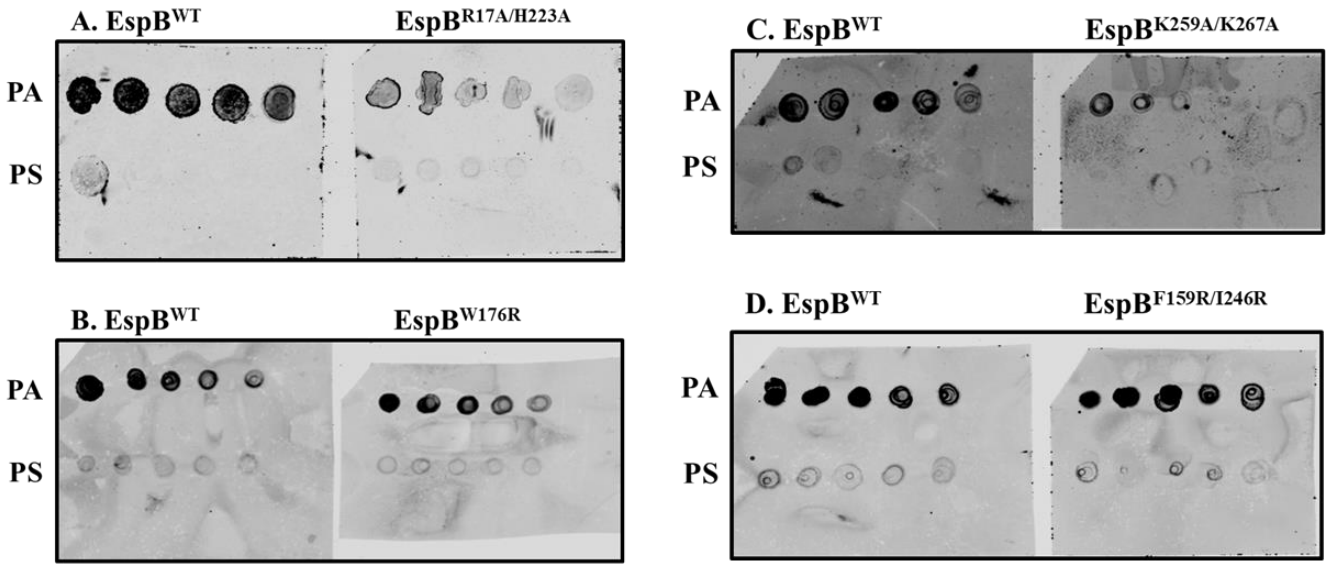

Figure 4.11. Phospholipid binding of EspB^{WT} and variants using custom laboratory-made lipid spotted membranes. Membranes were allowed to incubate with **A.** EspB^{WT} and EspB$^{R17A/H223A}$, **B.** EspB^{WT} and EspB^{W176R}, **C.** EspB^{WT} and EspB$^{K259A/K267A}$, and **D.** EspB^{WT} and EspB$^{F159R/I246R}$.

These phospholipid binding assays revealed that EspB^{WT} was able to bind PI(3,5)P_2, PI(3)P, PI(4)P, and PI(5)P in addition to the previously reported PA. The EspB mutants showed variable levels of phospholipid binding: EspB$^{R17A/H223A}$ lacked binding in all of the tested phospholipids, EspB^{W176R} showed similar phospholipid binding levels as EspB^{WT}, EspB$^{K259A/K267A}$ showed slightly reduced phospholipid binding, and interestingly, EspB$^{F159R/I246R}$ showed enhanced binding to PI(3,5)P_2, PI(3)P, PI(4)P, and PI(5)P. However, EspB$^{F159R/I246R}$ bound to PA at similar levels to EspB^{WT} as confirmed in the custom laboratory-made phospholipid spotted membranes and the phospholipid bead pull-down assay.

4.5. Enhancement of *M. tb* 5'Tn::*pe35* induction of cytotoxicity in macrophages

Previously, it was shown that EspB^{WT} was able to enhance *M. tb* 5'Tn::*pe35* induction of cytotoxicity in THP-1 macrophages (Chen et al., 2013). The transposon strain *M. tb* 5'Tn::*pe35* was unable to secrete EspB and did not induce high levels of cytotoxicity in macrophages (Chen et al., 2013). However, exogenous addition of purified recombinant EspB was able to restore its virulence to the same level as *M. tb espA*::Tn (Chen et al., 2013). It was hypothesized that the virulence function of EspB was due to its ability to bind phospholipids which caused the induction of cytotoxicity in THP-1 macrophages. Therefore, the next step was to observe if the inability of

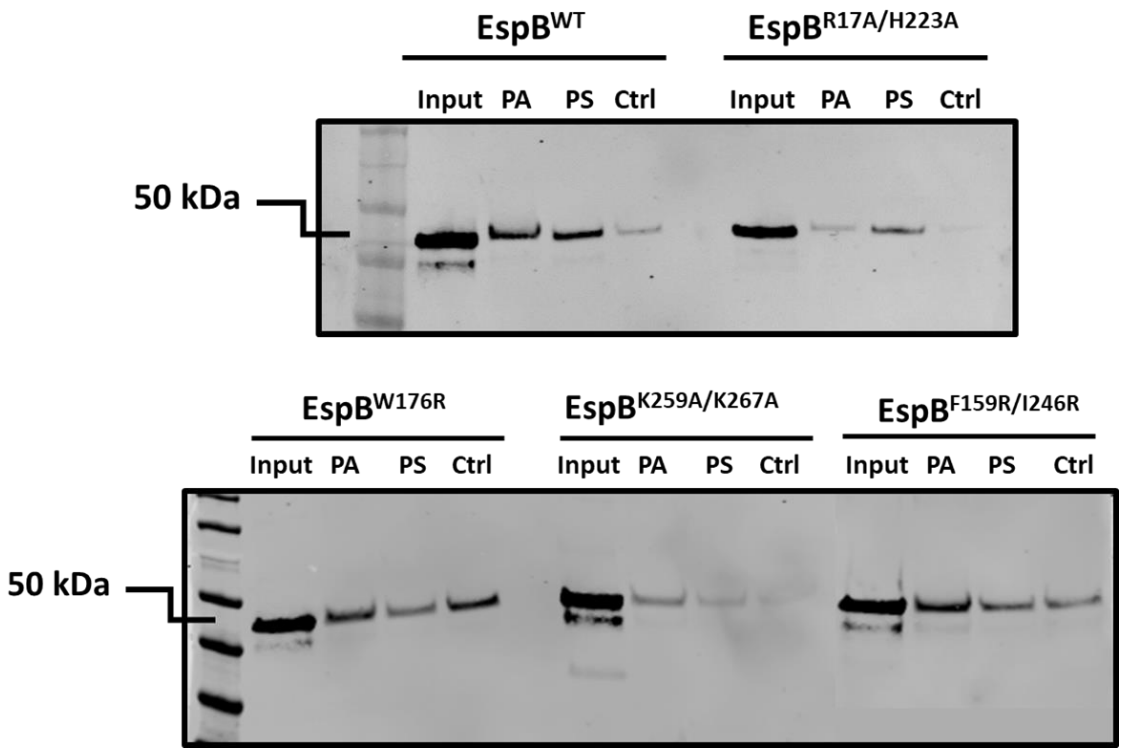

Figure 4.12. Phospholipid coated bead pull-down assay using EspB^{WT} and variants. Expected EspB molecular weight is indicated on the left of each western blot. Each EspB^{WT} or variant were incubated separately with either PA, PS or control beads and are indicated on the top of each western blot membrane.

EspB$^{R17A/H223A}$ to bind phospholipids has consequences to *M. tb* virulence during infections. In order to test this, purified EspB variants were added to *M. tb* 5'Tn::*pe35* prior to infecting THP-1 macrophages.

Prior to infection, THP-1 monocytes must first be differentiated into macrophage-like cells using an optimal concentration of PMA. Differentiation of THP-1 monocytes to macrophages has been previously described in many studies and is a recognized protocol. These differentiated macrophages are very similar to human peripheral blood mononuclear cell monocyte-derived macrophages and are adherent with lower proliferation rates (Starr et al., 2018). The THP-1 cells must be differentiated into macrophage-like cells in order to ensure that the infection experiment was performed on a biologically relevant cell type. However, since the differentiation process is a harsh treatment to the cells, the concentration of PMA must be adjusted to ensure optimal differentiation but healthy cells prior to infection with *M. tb*. The PMA concentration used for these experiments were 100 ng/mL for 3 days followed by 2 days of recovery in fresh RPMI media.

THP-1 monocytes 24 hours post treatment with PMA were not fully differentiated and displayed a round morphology with a defined membrane (Figure 4.13A). However, after treatment with PMA, the macrophage-like cells showed large and irregularly shaped cells with the membrane much less defined than undifferentiated cells (Figure 4.13B). These cells were also adherent and had very slow proliferation.

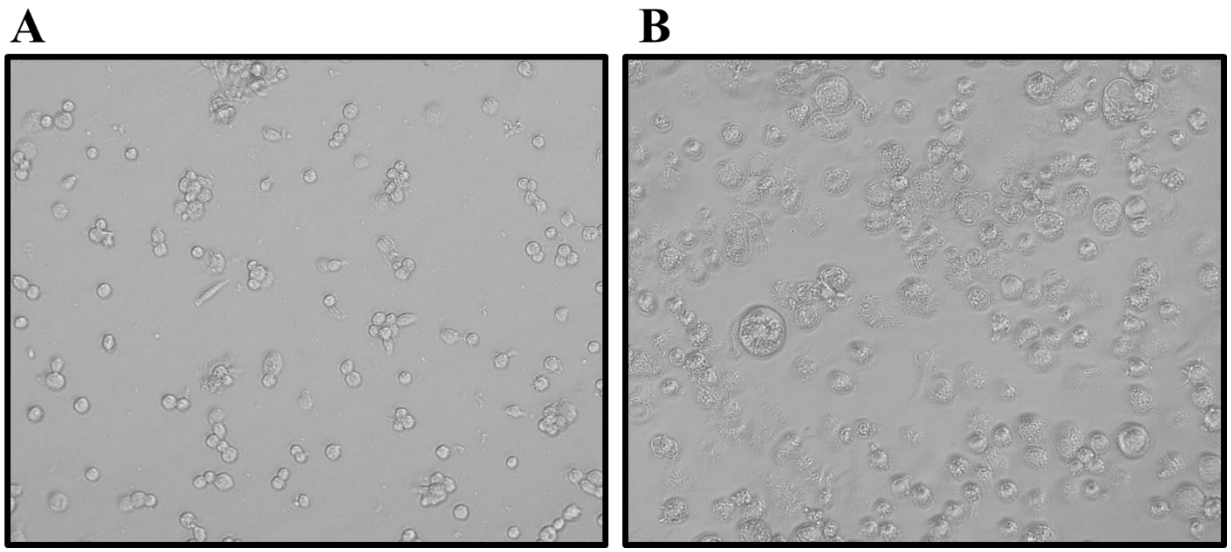

Figure 4.13. Differentiation of THP-1 cells using PMA treatment. A. Cells were imaged at 24 hours post-PMA treatment and **B.** at 72 hours post-PMA treatment.

After PMA treatment of the THP-1 cells, the media was replaced with fresh RPMI media for cells to recover for 48 hours prior to infection with *M. tb*. The THP-1 cells were infected with WT *M. tb* or *M. tb* transposon mutant at an MOI of 5. After infection for 72 hours, cell viability was measured using PrestoBlue viability reagent. This reagent is resazurin based where viable cells will convert resazurin to fluorescent resorufin to allow for direct measurement of cell viability as relative fluorescence units (RFU). The RFU values for each treatment group was compared to RFU values of uninfected THP-1 macrophages to calculate the % relative cytotoxicity using Equation 2 (refer to Appendix 1). The results were plotted as % relative cytotoxicity on Graphpad Prism 9 and statistical analysis was performed using one-way ANOVA with Tukey post-hoc test to determine significant differences between groups. There were no significant difference between $EspB^{WT}$ and $EspB^{R17A/H223A}$'s ability to enhance the virulence of 5'Tn::*pe35* (Figure 4.14) . This suggests that the virulence function of EspB may be more complex than previously hypothesized and that phospholipid binding may not be the only aspect to its virulence.

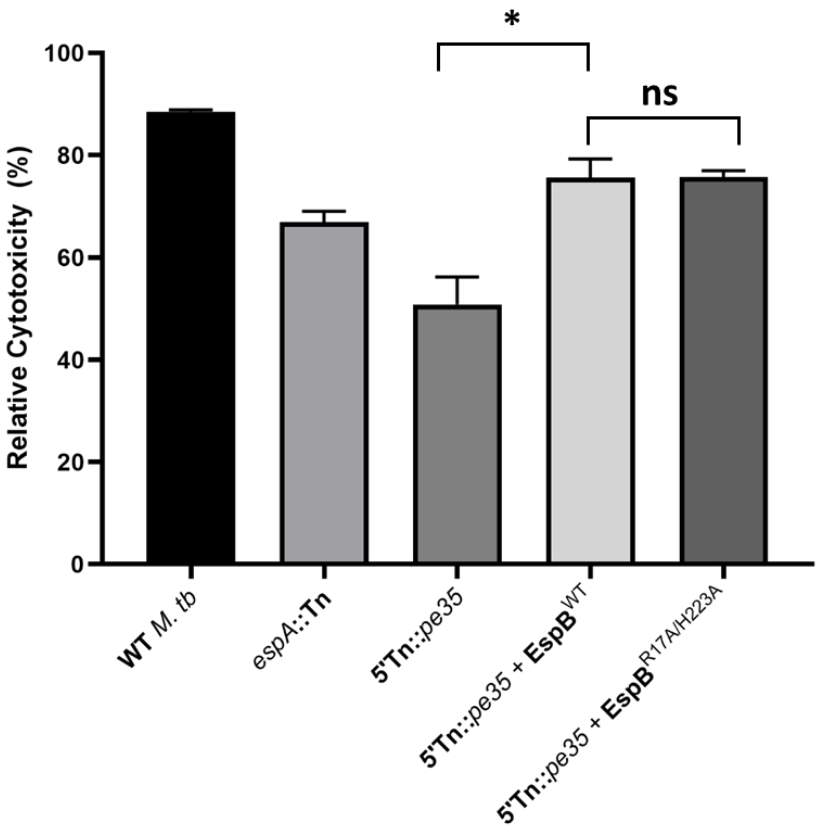

Figure 4.14. Cytotoxicity enhancement of *M. tb* 5'Tn::*pe35* by EspB$^{R17A/H223A}$ to infect THP-1 macrophages. The data in this figure represents an average of 3 independent experiments. One-way ANOVA was used to analyze differences between all the treatment groups $F_{4,10} = 60.47$, $p < 0.001$) and a Tukey post-hoc test was performed to compare differences between two of the treatment groups (α 0.05). There was no significant difference between *M. tb* 5'Tn::*pe35* + EspB^{WT} and *M. tb* 5'Tn::*pe35* + EspB$^{R17A/H223A}$ ($p > 0.999$) denoted with "ns". Whereas, there was a significant difference between *M. tb* 5'Tn::*pe35* + EspB^{WT} and *M. tb* 5'Tn::*pe35* alone ($p < 0.001$) denoted by an asterisk *.

The lack of difference in induction of cytotoxicity between EspB^{WT} and EspB$^{R17A/H223A}$ raised a question of whether the addition of EspB without the presence of bacteria would be able to induce cytotoxicity in the THP-1 macrophage. To address this, EspB^{WT} or EspB$^{R17A/H223A}$ was added to THP-1 macrophages without the presence of *M. tb*. The infection was performed in the same manner as the previous cytotoxicity experiment. Addition of either EspB^{WT} or EspB$^{R17A/H223A}$ alone to THP-1 macrophages demonstrated that EspB alone was unable to induce cytotoxicity in macrophages as EspB with *M. tb* 5'Tn::*pe35* did (Figure 4.15). The data was plotted using RFUs to better convey that there were no differences in cell viability between these groups and non-treated macrophages.

A cytotoxicity assay was also performed to compare the effects of $EspB^{W176R}$, $EspB^{K259A/K267A}$, or $EspB^{F159R/I246R}$ added to *M. tb* 5'Tn::*pe35* in comparison to $EspB^{WT}$ (Figure 4.16). However, this experiment was performed only once and therefore statistical analysis was not performed. From the results, addition of $EspB^{W176R}$, $EspB^{K259A/K267A}$, and $EspB^{F159R/I246R}$ does not appear to have a significant effect on cytotoxicity enhancement of *M. tb* 5'Tn::*pe35* in comparison to $EspB^{WT}$. However, it seems that $EspB^{W176R}$ and $EspB^{K259A/K267A}$ induced slightly lower levels of cytotoxicity and their effects may not be fully captured by this assay.

These infection assays revealed no significant differences between $EspB^{WT}$ and $EspB^{R17/H223A}$ to induce cytotoxicity to THP-1 macrophages when added to *M. tb* 5'Tn::*pe35*. There were also no differences found between $EspB^{W176R}$, $EspB^{K259A/K267A}$, and $EspB^{F159R/I246R}$ in comparison to $EspB^{WT}$. Furthermore, addition of purified $EspB^{R17A/H223A}$ or $EspB^{WT}$ to THP-1 macrophages alone was unable to induce cytotoxicity.

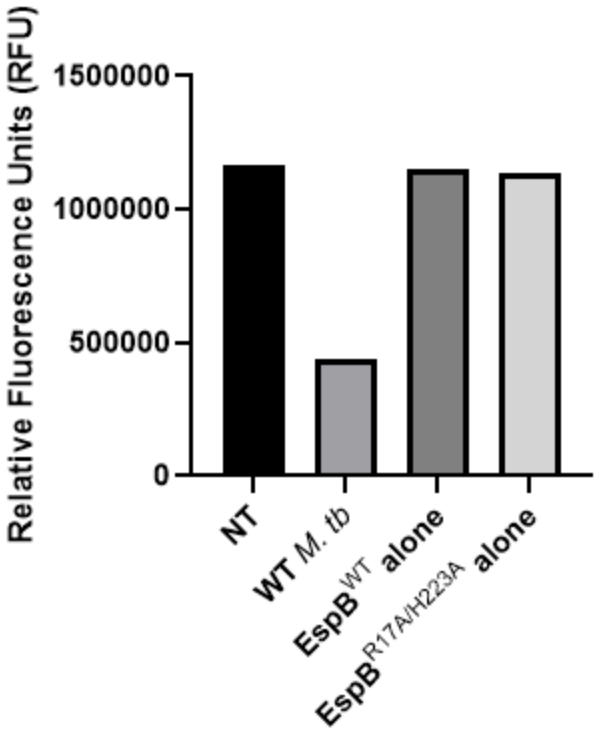

Figure 4.15. Effect of $EspB^{WT}$ or $EspB^{R17A/H223A}$ addition to THP-1 macrophages alone. Cell viability was measured in RFU. THP-1 macrophages either received no treatment (NT), infected with WT *M. tb*, or received addition of either $EspB^{WT}$ or $EspB^{R17A/H223A}$ alone.

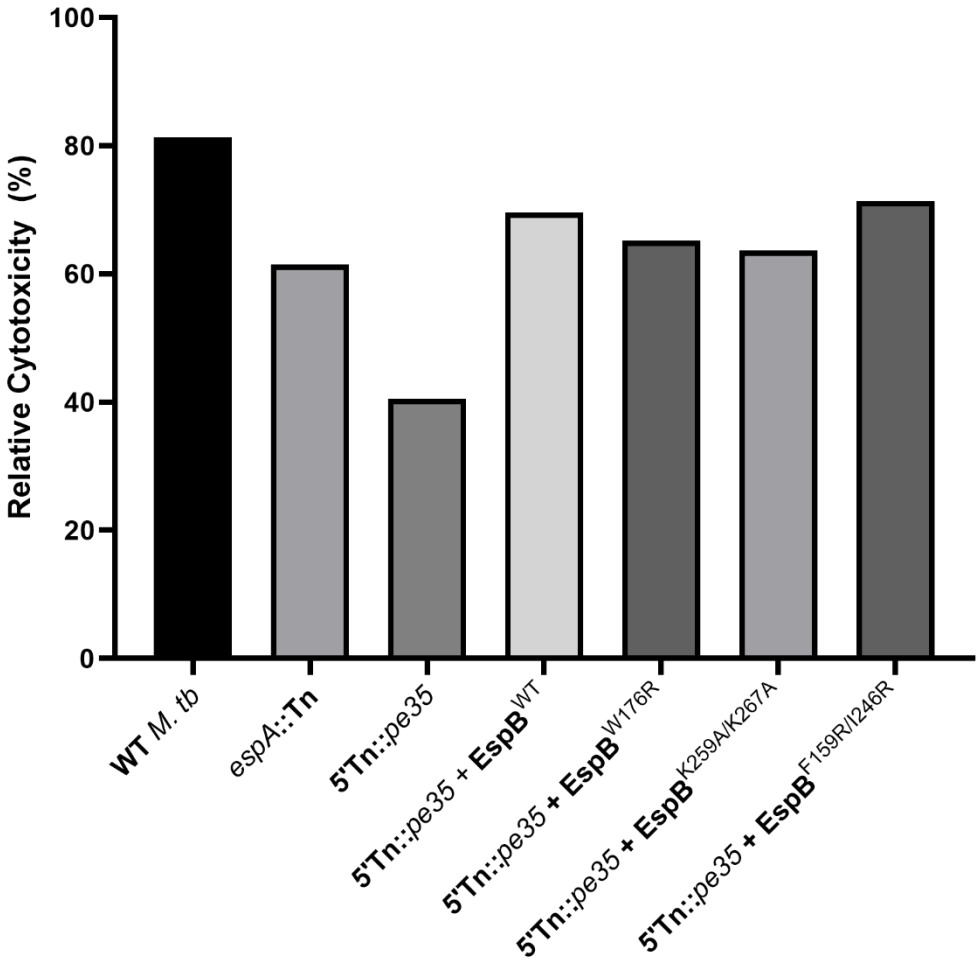

Figure 4.16. Cytotoxicity enhancement of *M. tb* 5'Tn::*pe35* by EspB^{W176R}, EspB$^{K259A/K267A}$, and EspB$^{F159R/I246R}$ in comparison to EspB^{WT}. Relative cytotoxicity of differentiated THP-1 macrophages infected with WT *M. tb*, *espA*::Tn, 5'Tn::*pe35* or 5'Tn::*pe35* with 80 nmol of EspB^{WT}, EspB^{W176R}, EspB$^{K259A/K267A}$ or EspB$^{F159R/I246R}$.

4.6. Preparation of PA and PS reporter macrophages

EspB was previously shown to bind mammalian phospholipids *in vitro*, this interaction was hypothesized to be important for the virulence function of EspB (Chen et al., 2013). During *M. tb* infection of macrophages, it is possible that EspB-phospholipid interactions can disrupt the signaling roles of these important phospholipids. Therefore, reporter macrophages can be used to directly observe EspB-phospholipid interactions at a cellular level. Plasmids used as PA and PS biosensors were obtained from the Guangwei Du Laboratory at the University of Texas (Houston, TX) and the Sergio Grinstein Laboratory at the University of Toronto (Toronto, Canada) respectively. These plasmids encode a probe that specifically binds PA or PS tagged with GFP for

visualization on confocal microscopy. The plasmid specific for PA (pMGFP-PASS) was an improved biosensor from its previous counterpart, GFP-Spo20-PABD, which was constructed from the PA binding domain of a *Saccharomyces cerevisiae* protein, Spo20 (Zhang et al., 2014). However, sensitivity in pGFP-PASS was improved by the addition of a nuclear export sequence (NES) from protein kinase A inhibitor α (PKI-α) (Zhang et al., 2014). Next, the plasmid specific for PS (pLact-C2) specific for PS was constructed from the C2 domain of lactadherin with the inclusion of a GFP tag (Yeung et al., 2008). The cell line initially used for this assay were COS-7 non-human primate kidney fibroblast-like cells in order to optimize the transfection procedure. These cells were transfected with pGFP-PASS or pLact-C2 plasmids and were imaged using confocal microscopy (Figure 4.17). GFP signal was present in both transfected groups which indicated that the transfection was successful and the plasmids were functional. Localization of PA was shown to be ubiquitous throughout the cell (Figure 4.17A). COS-7 cells transfected with pLact-C2 displayed a more specific localization of the GFP signal (Figure 4.17B).

While this experiment demonstrated that the transfection protocol was successful, COS-7 cells are not a biologically relevant cell line used to study *M. tb* infections. Therefore, the next objective was to transfect Raw 264.7 murine macrophages. Raw macrophages transfected with pMGFP-PASS also showed a ubiquitous GFP signal similarly to the COS-7 transfected cells (Figure 4.18A). However, the macrophages transfected with pLact-C2 showed similar specific localization of the GFP signal as COS-7 cells transfected with this plasmid (Figure 4.18B).

Ultimately, these reporter macrophages were generated in attempts to further the study of EspB-phospholipid interactions within the cell during *M. tb* infection. Future studies of this interaction would include construction of *M. tb* strains expressing $EspB^{WT}$ or other EspB variants and used to infect these reporter macrophages to monitor any differences in the intensity of GFP signal or localization of the phospholipids.

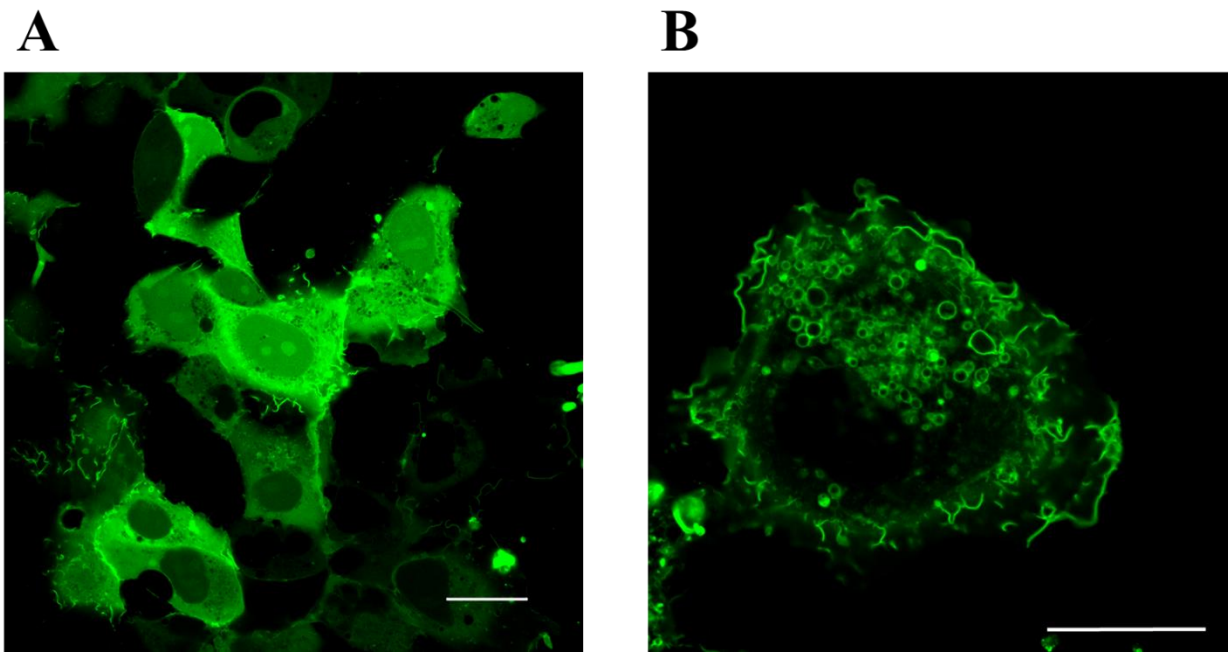

Figure 4.17. Transfection of COS-7 cells. Cells were transfected with **A.** pMGFP-PASS plasmid and **B.** pLact-C2 plasmid. Image was processed on Leica Application Suite (LasX). Scale bars are 25 μm.

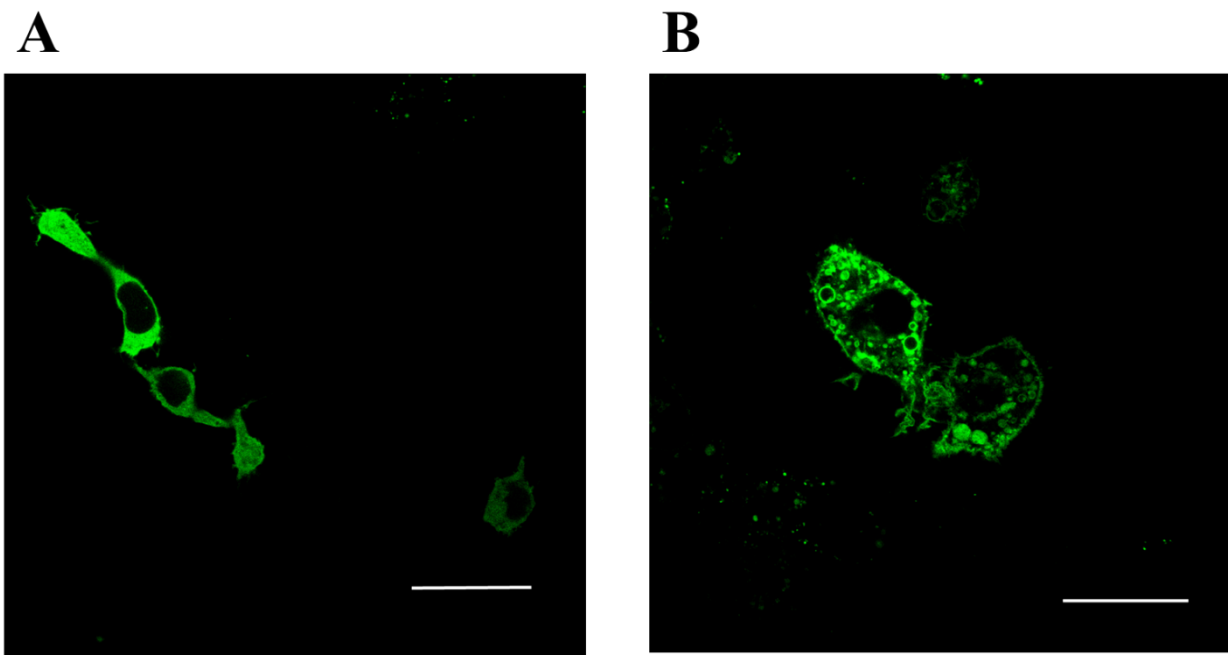

Figure 4.18. Transfection of Raw 264.7 murine macrophages. Cells were transfected with **A.** pMGFP-PASS and, **B.** pLact-C2. Images were processed using LasX and scale bars are set to 25 μm.

5. Discussion

5.1. Mapping residues presumed to be functionally important for EspB

Prior to characterization of the EspB variants, the residues that were hypothesized to be functionally important for EspB were targeted for mutagenesis. These residues were mapped on the 3D model of the EspB oligomer using the modelling software, Chimera. Through this exercise, the basic residues thought to be crucial for phospholipid binding, R17 and H223A were found to be localized at the immediate opening of the EspB channel. Furthermore, multiple sequence alignment of EspB from multiple mycobacterial species identified that these two residues were highly conserved. The localization of R17 and H223 at both sides of the EspB channel opening was significant as this may allow for easy access for phospholipid interaction by EspB. In addition, these residues are basic which would have the capacity to bind the negatively charged head groups of acidic phospholipids such as PA and other phosphoinositides. This is consistent with the specificity of the phospholipid interaction by EspB that was previously reported (Chen et al., 2013). Two other residues predicted to bind the fatty acid region of EspB, F159 and I246, are localized at the interior of the EspB oligomeric channel (Korotkova et al., 2015). It was previously shown that the overall charge of the EspB interior channel is positive which is consistent with the placement of these two residues. It is possible that R17 and H223 are responsible for binding negatively charged head groups of acidic phospholipids, while F159 and I246 binds the fatty acid regions of the phospholipids.

Residues that were predicted to be involved the oligomerization of EspB, K259 and K267, were found to be localized to the interior of the EspB channel (Solomonson et al., 2015). Although these residues were hypothesized to be involved in oligomerization of EspB, they may not be involved in oligomerization. Through chemical cross-linking coupled mass spectrometry using cyanur-biotin-dimercapto-propionyl-succinimide (CBDPS), it was found that K259 and K267 residues were located within 25 Å with one another (Solomonson et al., 2015). However, it was found that the intermolecular contacts (crystal contacts) within the crystallized protein differs from the ones mediating EspB oligomerization. Therefore, it is possible that these residues are not involved in EspB oligomerization which was reflected in the native-PAGE, DLS, and TEM results. The residue W176 that is involved in stabilization of the EspB monomer hairpin was found to be located at one end of the EspB channel, and was demonstrated to interact with Y81 within the same monomer (Piton et al., 2020; Solomonson et al., 2015). It was hypothesized that if the

interaction between W176 and Y81 was abolished, it may affect the formation of the monomer hairpin structure and as a result, may compromise the oligomeric structure of EspB. These results thus motivated the construction and characterization of EspB with mutations in these residues predicted to be important for EspB.

5.2. Purification and antibody detection of EspB^{WT} and variants

EspB variants were purified prior to performing any biochemical assays for characterization. Previously, single amino acid replacements of R17, H223, F159, I246, K259, and K267 were made in EspB. However, due to the mild phenotypes revealed from follow-up biochemical characterization assays, double mutations in EspB were constructed for further assessment. During purification, two of the four variants, EspB$^{R17A/H223A}$ and EspB$^{F159R/I246R}$ consistently had lower purification yields compared to EspB^{WT}, EspB^{W176R}, and EspB$^{K259A/K267A}$. This is intriguing as EspB$^{R17A/H223A}$ and EspB$^{F159R/I246R}$ showed a tendency to hyperoligomerize under native-PAGE conditions as well as in DLS and TEM results. Therefore, the quantification step following purification of the variants was crucial to ensure that equivalent amounts of protein variants were used in each assay. In addition, all of the EspB variants were detected by the α-EspB primary antibody equivalently and therefore, the results obtained in the following experiments were due to the phenotypes of the EspB variants themselves and not due to differential detection by the anti-EspB antibody.

5.3. Oligomerization of EspB

Native-PAGE was first used to observe oligomerization of EspB^{WT} and variants. The variants, EspB$^{R17A/H223A}$ and EspB$^{F159R/I246R}$ both showed the tendency to hyperoligomerize under native-PAGE conditions. It was observed during the purification process of EspB$^{R17A/H223A}$ and EspB$^{F159R/I246R}$ resulted in a lower yield compared to other EspB variants. This could have resulted from inefficient elution from the Ni-IDA purification columns due to their hyperoligomeric properties. The two variants EspB^{W176R} and EspB$^{K259A/K267A}$ were observed to form similar oligomeric patterns as EspB^{WT}. Although these variants were constructed in order to eliminate oligomerization of EspB, this experiment demonstrated that the residues K259 and K267 were most likely not involved in oligomerization of EspB. However, it is possible that replacement of the residue W176 did not fully abrogate the interaction between the WxG and the YxxxD motif on the EspB monomer and therefore did not affect the oligomerization of this variant.

In order to verify the results observed in the native-PAGE assay, DLS was used as another method to characterize EspB oligomerization. The results obtained using DLS showed similar trends to the native-PAGE results. Both $EspB^{R17A/H223A}$ and $EspB^{F159R/I246R}$ showed hyperoligomerization, whereas $EspB^{W176R}$ and $EspB^{K259A/K267A}$ showed similar oligomeric species as $EspB^{WT}$. In addition, all variants showed a PDI of above 20%, suggesting that there were multiple oligomeric species present in all samples. However, the molecular weight values estimated through DLS did not correspond to previously published values of the molecular size of EspB. The inconsistencies in molecular weight estimation here compared to previously reported values may be due to the method in which DLS uses to approximate particle size. Since DLS estimates particle size based on hypothetical perfect spheres that would scatter light the same way the sample particles would, this could lead to overestimation or underestimation of the molecular weight (Figure 5.1).

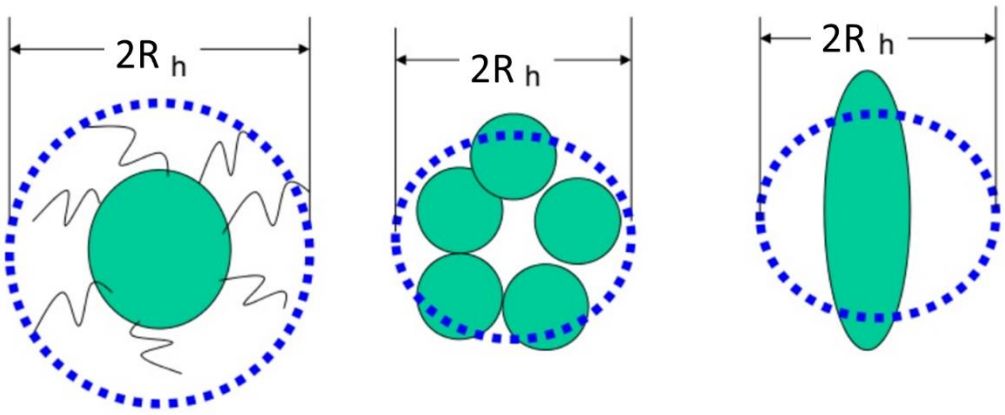

Figure 5.1. DLS estimation of sample particle size based on hydrodynamic radii. Particle size is estimated by the dotted blue circle denoted with the hydrodynamic radius (R_h) which can result in either over- or under-estimation (Kundu, 2019).

Both native-PAGE and DLS demonstrated that $EspB^{R17A/H223A}$ and $EspB^{F159R/I246R}$ had a tendency to hyperoligomerize, whereas $EspB^{W176R}$ and $EspB^{K259A/K267A}$ showed similar oligomeric patterns as $EspB^{WT}$. However, these assays did not confirm if the oligomers that the EspB variants formed were the same as $EspB^{WT}$. Therefore, TEM was used to directly visualize the oligomers that EspB variants were forming. $EspB^{R17A/H223A}$ was observed to form heptameric barrel structures similar to that of $EspB^{WT}$. However, the heptamers were clustered together to form a larger, more complex oligomer that was likely reflected in the results of the native-PAGE and DLS assays. In contrast, $EspB^{F159R/I246R}$ formed large complexes that did not resemble heptameric barrels observed

in $EspB^{WT}$. $EspB^{W176R}$ was observed to form very sparse heptameric oligomers that were similar to $EspB^{WT}$. It is possible that altering W176 that is involved in stabilization of the EspB hairpin may have slightly compromised the oligomerization. Lastly, $EspB^{K259A/K267A}$ showed similar heptameric structures as $EspB^{WT}$. This variant was not compromised in its oligomeric formation in native-PAGE, DLS, or TEM analyses. Therefore, it could be possible that these residues were not involved in oligomeric formation of EspB.

5.4. Phospholipid interactions of EspB

As $EspB^{WT}$ was previously found to bind specifically to PA, the variants that were constructed in this project were examined for their phospholipid binding abilities using a phospholipid membrane overlay assay (Chen et al., 2013). Two types of membranes were used for this experiment: commercially produced phospholipid spotted membranes to observe specificity of the phospholipid binding and custom made phospholipid spotted arrays to observe the affinity of EspB-PA binding.

Interestingly, $EspB^{WT}$ was observed to bind to $PI(3,5)P_2$, PI(3)P, PI(4)P, and PI(5)P in addition to binding PA. However, $EspB^{R17A/H223A}$ lacked binding to all of these phospholipids. It appeared that the residues R17 and H223 played a significant role in EspB phospholipid binding, and mutation of these residues to uncharged residues resulted in its inability to bind phospholipids. On the contrary, $EspB^{F159R/I246R}$ was observed to bind PA similarly to $EspB^{WT}$, but also had enhanced binding to the phosphoinositides. It is possible that the change from F159 and I246 to a basic residue is contributing to increased binding to the acidic phospholipids. Although both the $EspB^{R17A/H223A}$ and $EspB^{F159R/I246R}$ variants showed hyperoligomerization, these variants differed in their oligomeric patterns as well as their abilities to bind phospholipids. It suggested that the oligomeric structure that EspB forms does not dictate its ability to bind phospholipids. $EspB^{W176R}$ had similar binding to phospholipids as $EspB^{WT}$, suggesting that the residue W176 may not be involved in phospholipid binding. Interestingly, $EspB^{K259A/K267A}$ showed a reduction in phospholipid binding in comparison to $EspB^{WT}$. It is possible that a mutation at the residues K259 and K267 introduced a structural hindrance to the residues that were involved in phospholipid binding.

The results obtained from the phospholipid membrane overlay assay were verified using another method, phospholipid bead pull-down assay. Agarose beads that were coated with specific phospholipids were used to detect EspB binding. Using this method, similar findings were obtained. $EspB^{R17A/H223A}$ was unable to bind PA, whereas $EspB^{F159R/I246R}$ and $EspB^{W176R}$ showed similar PA binding intensity as $EspB^{WT}$. $EspB^{K259A/K267A}$ also showed reduced PA binding using this method. EspB non-specifically binding to control beads were observed in performing this assay. However, the pattern of EspB-PA binding was consistent within repetitions of this assay as well as consistent with the membrane overlay assay. For further studies, it is possible to use a non-interacting phospholipid coated bead as negative control rather than control beads.

5.5. THP-1 infection

It was previously shown that addition of purified $EspB^{WT}$ to *M. tb* 5'Tn::*pe35* enhanced its virulence to the same level as that of the *M. tb espA*::Tn mutant (Chen et al., 2013). Following biochemical characterization of $EspB^{WT}$ and variants constructed in this project, a cytotoxicity assay was performed to observe if EspB variants would be able to enhance the virulence of *M. tb* 5'Tn::*pe35*. It was previously demonstrated that $EspB^{R17A/H223A}$ was unable to bind phospholipids. Therefore, this variant was used to determine if lack of phospholipid binding would affect its virulence function. Like $EspB^{WT}$, addition of $EspB^{R17A/H223A}$ was able to enhance the cytotoxic potential of *M. tb* 5'Tn::*pe35* towards THP-1 macrophages. Likewise $EspB^{F159R/I246R}$, $EspB^{W176R}$, and $EspB^{K259A/K267A}$ also enhanced *M. tb* 5'Tn::*pe35* cytotoxicity towards THP-1 macrophages.

These results suggests that the virulence function of EspB may be more complex than previously appreciated and may not solely depend on phospholipid binding. Addition of $EspB^{WT}$ or $EspB^{R17A/H223}$ alone to THP-1 macrophages did not induce cytotoxicity. This suggests that EspB requires the presence of *M. tb* in order to have a virulence function. Furthermore, none of the variants in this project were truly abolished in its ability to oligomerize. It was demonstrated from a pre-print study from bioRxiv by Gijsbers et al., that EspB from pathogenic mycobacteria are able to oligomerize whereas EspB from non-pathogenic species such as *M. smegmatis* did not show oligomerization (Gijsbers et al., 2021). Therefore, future testing on an EspB variant completely abolished in oligomerization may be necessary to determine if it is crucial to EspB's virulence function. Although phospholipid binding may not strictly correlate with the virulence function of

EspB, this function may be due to another factor such as mitochondrial damage of the infected host cell.

M. tb was previously found to induce mitochondrial damage and fragmentation in the infected host cell, and leading to necrotic cell death (Spier et al., 2019; Wiens and Ernst, 2016a, 2016b). Infection with *M. tb* causes mitochondrial stress which contributes to IFN-β induction as well as mitochondrial membrane disruption, leading to mitochondrial outer membrane permeabilization (MOMP) and cytochrome c release (Spier et al., 2019; Wiens and Ernst, 2016a). The increase in mitochondrial membrane permeability leads to damage and fragmentation of the mitochondria, resulting in induction of necrotic cell death (Spier et al., 2019; Wiens and Ernst, 2016a). Although it is currently unclear how this is caused, it is possible that EspB contributes to mitochondrial damage. It was reported that *M. africanum* induces less mitochondrial stress and less IFN-β than the virulent *M. tb* (Wiens and Ernst, 2016a, 2016b). The inability of *M. africanum* to induce mitochondrial damage could be due to it containing a premature stop codon at the *espK* gene, leading to lack of secretion of EspB (Wiens and Ernst, 2016a). Current work at the Chen Laboratory has also revealed that an *M. tb* strain lacking in EspK expression is unable to secrete EspB and furthermore, induces less mitochondrial damage compared to WT *M. tb* (unpublished data). In addition, as it is known that PA has a crucial role in regulating mitochondrial fission and fusion, EspB interaction with PA may interfere with this function (Chen et al., 2013; Yang and Frohman, 2012). This mechanism of the mitochondria is important especially during cellular metabolic or environmental stress (Youle and Van Der Bliek, 2012).

5.6. Preparation of PA and PS reporter macrophages

As EspB was found to interact with mammalian phospholipids within the cell, reporter macrophages specific for sensing PA and PS was constructed in this project. Plasmids encoding probes that specifically interact with PA or PS and tagged with GFP were used for transfecting mammalian cells. This would be a promising tool for further studying the interaction of EspB and specific phospholipids within an intracellular environment. Two cell lines were used: COS-7 kidney fibroblast-like cells and Raw 264.7 murine macrophages. GFP signal was detected in both transfected COS-7 cells and Raw 264.7 cells. Although the transfection was successful, GFP signal observed in pGFP-PASS transfected reporter macrophages was ubiquitous and did not show specific localization. As this assay is in its early stages of development, the transfection procedure

should be optimized with some considerations: ratio of transfection reagents and the transfection duration. During the transfection procedure, the ratio of plasmids and Lipofectamine 2000 used should be optimized in order for the transfected cells to express an optimal level of the biosensing probe. Determining the best time point to image the cells in order to capture a more specific localization of the biosensor within the cells.

The goal of generating reporter macrophages was to observe any difference between phospholipid levels or localizations during infection with *M. tb*. Therefore, the logistics of the transfection procedure in conjunction with *M. tb* infection should be considered. Since *M. tb* is a biosafety level 3 pathogen, the reporter macrophages must be transported into containment in order to perform the infection. Taken together with the optimal time point for imaging post-transfected cells, this could pose some difficulty in the experiment. Furthermore, the transfection procedure itself is a harsh treatment to the cells. Therefore, necessary controls must be included to account for the health of the reporter macrophages that may have been compromised by the transfection treatment.

6. Conclusions and Future Directions

The aim of this project was to further characterize the virulence function of EspB in its secreted form. Several mutations were made at residues predicted to be functionally important for EspB. These constructed variants were used for characterizing oligomerization and phospholipid binding of EspB. Two variants in particular, $EspB^{R17A/H223A}$ and $EspB^{F159R/I246R}$ were found to hyperoligomerize in native-PAGE, DLS, and TEM analyses. Whereas, $EspB^{W176R}$ and $EspB^{K259A/K267A}$ showed similar heptameric formation as $EspB^{WT}$. Altering the residue W176 appeared to have little effect on oligomerization of EspB. It is possible that a variant containing mutations in both W176 and its interacting residue Y81 may show a more significant difference in its oligomerization properties. In addition, it was reported by Gijsbers et al. that double mutation of the residues N55 (at the core of monomer) and T119 (at the PE-PPE linker) to C abolished oligomerization of EspB (Gijsbers et al., 2021). This mutation was found to prevent the linker from adopting a different conformation needed for oligomerization (Gijsbers et al., 2021). Therefore, this variant would be a good candidate to determine if the ability of EspB dimerization is crucial for its interaction with phospholipids.

Although the two variants $EspB^{R17A/H223A}$ and $EspB^{F159R/I246R}$ both displayed hyperoligomerization, they revealed opposite phenotypes in terms of phospholipid binding. Therefore, it is possible how EspB forms its oligomers does not necessarily affect phospholipid binding. Interestingly, $EspB^{K259A/K267A}$ showed reduced phospholipid binding. It is possible that a change from a basic residue (such as lysine) to a non-polar residue (alanine) affected the ability of this variant to bind phospholipids. An assay testing phospholipid binding strength could potentially give more information on the reason why this variant displayed this phenotype.

A more recent study on EspB shows evidence that EspB may be a structural component to the ESX-1 secretion system (Gijsbers et al., 2021). It is possible that in addition to forming a heptameric structure, the oligomers themselves may organize into a tubular structure summarized in Figure 6.1. However, mutation of certain residues may result in irregular complex formations that may hinder EspB function. Further studies are needed to determine if these EspB variants function differently from $EspB^{WT}$.

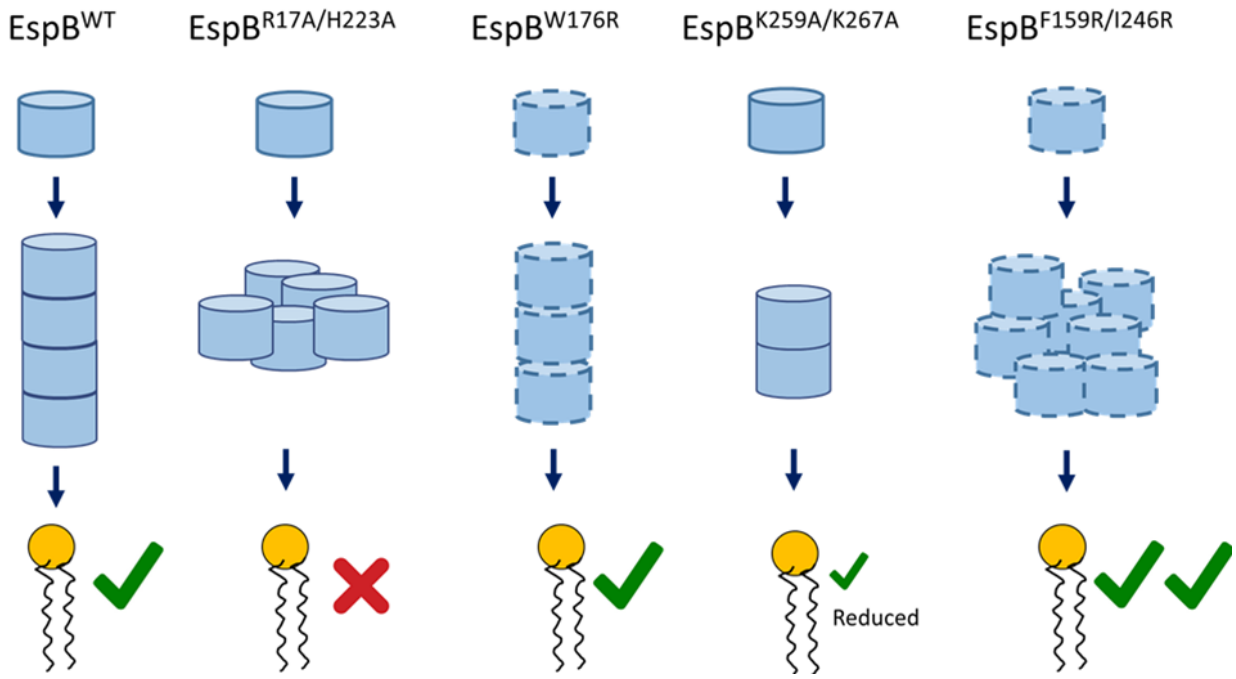

Figure 6.1. Summary of EspB^{WT} and variants oligomerization and phospholipid binding patterns. This schematic summarizes the different oligomeric formations and phospholipid binding ability of each EspB variant found in this project. Each cylinder structure represents one EspB heptamer. Dashed lines indicates that the variant may not be readily forming heptameric oligomers similarly to EspB^{WT}. However, the exact conformations that these variants are adopting have yet to be confirmed.

Future experiments to further this project would be to construct an *M. tb* strain with an *espB* knockout. A plasmid encoding espB variants constructed in this project can be used to complement the *espB M. tb* knockout strain. These constructed strains would be used to study secretion of the EspB variants, induction of cytotoxicity in macrophages, as well as cytokine analysis. In addition, they would be used to infect reporter macrophages generated in this project to observe for differences in levels and localization of GFP signals. Since an EspB variant that is unable to oligomerize was demonstrated by Gijsbers et al. in a pre-print article in bioRxiv, this variant can be constructed to further define if monomeric EspB is able to bind phospholipids and also induce cytotoxicity in THP-1 macrophages (Gijsbers et al., 2021).

7. REFERENCES

Andersen, P., and Doherty, T.M. (2005). The success and failure of BCG - implications for a novel tuberculosis vaccine. Nat. Rev. Microbiol. 3, 656–662.

Barber-Mayer, K.D., and Barber, D.L. (2015). Innate and adaptive cellular immune responses to *Mycobacterium tuberculosis* infection. Cold Spring Harb. Perspect. Med. 5, 1–20.

Beckham, K.S.H., Ciccarelli, L., Bunduc, C.M., Mertens, H.D.T., Ummels, R., Lugmayr, W., Mayr, J., Rettel, M., Savitski, M.M., Svergun, D.I., et al. (2017). Structure of the mycobacterial ESX-5 type VII secretion system membrane complex by single-particle analysis. Nat. Microbiol. 2, 1–7.

Bento, C.F., Renna, M., Ghislat, G., Puri, C., Ashkenazi, A., Vicinanza, M., Menzies, F.M., and Rubinsztein, D.C. (2016). Mammalian Autophagy: How Does It Work? Annu. Rev. Biochem. 85, 685–713.

Bohdanowicz, M., and Grinstein, S. (2013). Role of phospholipids in endocytosis, phagocytosis, and macropinocytosis. Physiol. Rev. 93, 69–106.

Brodin, P., Majlessi, L., Marsollier, L., Jonge, M.I. De, Bottai, D., Demangel, C., Hinds, J., Neyrolles, O., Butcher, P.D., Leclerc, C., et al. (2006). Dissection of ESAT-6 System 1 of *Mycobacterium tuberculosis* and Impact on Immunogenicity and Virulence. 74, 88–98.

Chen, J.M., Boy-Röttger, S., Dhar, N., Sweeney, N., Buxton, R.S., Pojer, F., Rosenkrands, I., and Cole, S.T. (2012). EspD is critical for the virulence-mediating ESX-1 secretion system in *Mycobacterium tuberculosis*. J. Bacteriol. 194, 884–893.

Chen, J.M., Zhang, M., Rybniker, J., Boy-Röttger, S., Dhar, N., Pojer, F., and Cole, S.T. (2013). *Mycobacterium tuberculosis* EspB binds phospholipids and mediates EsxA-independent virulence. Mol. Microbiol. 89, 1154–1166.

Daleke, M.H., Ummels, R., Bawono, P., Heringa, J., Vandenbroucke-Grauls, C.M.J.E., Luirink, J., and Bitter, W. (2012). General secretion signal for the mycobacterial type VII secretion pathway. Proc. Natl. Acad. Sci. U. S. A. 109, 11342–11347.

Davenne, T., and Mcshane, H. (2016). Why don't we have an effective tuberculosis vaccine yet? Expert Rev. Vaccines 15, 1009–1013.

Delogu, G., and Fadda, G. (2009). The quest for a new vaccine against tuberculosis. J. Infect. Dev. Ctries. 3, 5–15.

Dey, B., and Bishai, W.R. (2014). Crosstalk between *Mycobacterium tuberculosis* and the host cell. Semin. Immunol. 26, 486–496.

DiGiuseppe Champion, P.A., Champion, M.M., Manzanillo, P., and Cox, J.S. (2009). ESX-1 secreted virulence factors are recognized by multiple cytosolic AAA ATPases in mycobacteria. Mol. Microbiol. 73, 950–962.

Ekiert, D.C., and Cox, J.S. (2014). Structure of a PE-PPE-EspG complex from *Mycobacterium tuberculosis* reveals molecular specificity of ESX protein secretion. Proc. Natl. Acad. Sci. U. S. A. 111, 14758–14763.

Elmore, S. (2007). Apoptosis: A Review of Programmed Cell Death. Toxicol. Pathol. 35, 495–516.

Ernst, J.D. (2018). Mechanisms of *M. tuberculosis* Immune Evasion as Challenges to TB Vaccine Design. Cell Host Microbe 24, 34–42.

Flynn, J.L., and Chan, J. (2001). Tuberculosis : Latency and Reactivation. Infect. Immun. 69, 4195–4201.

Forrellad, M.A., Klepp, L.I., Gioffré, A., García, J.S., Morbidoni, H.R., de la Paz Santangelo, M., Cataldi, A.A., and Bigi, F. (2013). Virulence factors of the *Mycobacterium tuberculosis* complex. Virulence 4, 3–66.

Geneva: World Health Organization (2020). Global Tuberculosis Report 2020.

Gijsbers, A., Vinciauskaite, V., Siroy, A., Gao, Y., Tria, G., and Mathew, A. (2021). Priming mycobacterial ESX-secreted protein B to form a channel-like structure. BioRxiv Biochem. 3–13.

Glickman, M.S., and Jacobs, W.R. (2001). Microbial pathogenesis of *Mycobacterium tuberculosis*: Dawn of a discipline. Cell 104, 477–485.

Gröschel, M.I., Sayes, F., Simeone, R., Majlessi, L., and Brosch, R. (2016). ESX secretion systems: Mycobacterial evolution to counter host immunity. Nat. Rev. Microbiol. 14, 677–691.

Houben, D., Demangel, C., van Ingen, J., Perez, J., Baldeón, L., Abdallah, A.M., Caleechurn, L., Bottai, D., van Zon, M., de Punder, K., et al. (2012). ESX-1-mediated translocation to the cytosol controls virulence of mycobacteria. Cell. Microbiol. 14, 1287–1298.

Houben, E.N.G., Korotkov, K. V., and Bitter, W. (2014). Take five - Type VII secretion systems of Mycobacteria. Biochim. Biophys. Acta - Mol. Cell Res. 1843, 1707–1716.

Huang, D.D., and Bao, L. (2016). *Mycobacterium tuberculosis* EspB protein suppresses interferon-γ-induced autophagy in murine macrophages. J. Microbiol. Immunol. Infect. 49, 859–865.

Iacobino, A., Fattorini, L., and Giannoni, F. (2020). Drug-resistant tuberculosis 2020: Where we stand. Appl. Sci. 10, 1–17.

Jones, M., 2010. Dynamic Light Scattering [WWW Document]. Wikipedia. URL https://en.wikipedia.org/wiki/File:DLS.svg (accessed 6.27.21).

de Jong, B.C., Antonio, M., and Gagneux, S. (2010). *Mycobacterium africanum*-review of an important cause of human tuberculosis in West Africa. PLoS Negl. Trop. Dis. 4, 1–9.

Korotkova, N., Piton, J., Wagner, J.M., Boy-Röttger, S., Japaridze, A., Evans, T.J., Cole, S.T., Pojer, F., and Korotkov, K. V. (2015). Structure of EspB, a secreted substrate of the ESX-1 secretion system of *Mycobacterium tuberculosis*. J. Struct. Biol. 191, 236–244.

Kroesen, V.M., Madacki, J., Frigui, W., Sayes, F., and Brosch, R. (2019). Mycobacterial virulence: impact on immunogenicity and vaccine research. F1000Research 8, 1–14.

Kundu, S., 2019. Dynamic light scattering (dls) [WWW Document]. SlideShare. URL https://www.slideshare.net/SumanKundu40/dynamic-light-scattering-dls-133535694 (accessed 6.27.21).

Lawn, S.D., and Zumla, A.I. (2011). Tuberculosis. In The Lancet, pp. 57–72.

Lerner, T.R., Borel, S., and Gutierrez, M.G. (2015). The innate immune response in human tuberculosis. Cell. Microbiol. 17, 1277–1285.

Levin, R., Grinstein, S., and Schlam, D. (2015). Phosphoinositides in phagocytosis and macropinocytosis. Biochim. Biophys. Acta - Mol. Cell Biol. Lipids 1851, 805–823.

Lin, P.L., and Flynn, J.L. (2018). The End of the Binary Era: Revisiting the Spectrum of Tuberculosis. J. Immunol. 201, 2541–2548.

Ma, Y., Keil, V., and Sun, J. (2015). Characterization of *Mycobacterium tuberculosis* EsxA membrane insertion: Roles of N- and C-terminal flexible arms and central helix-turn-helix motif. J. Biol. Chem. 290, 7314–7322.

Mailer, A.G., Clegg, P.S., and Pusey, P.N. (2015). Particle sizing by dynamic light scattering: Non-linear cumulant analysis. J. Phys. Condens. Matter 27.

Majlessi, L., Prados-Rosales, R., Casadevall, A., and Brosch, R. (2015). Release of mycobacterial antigens. Immunol. Rev. 264, 25–45.

de Martino, M., Lodi, L., Galli, L., and Chiappini, E. (2019). Immune Response to *Mycobacterium tuberculosis*: A Narrative Review. Front. Pediatr. 7, 1–8.

Mattow, J., Schaible, U.E., Schmidt, F., Hagens, K., Siejak, F., Brestrich, G., Haeselbarth, G., Müller, E.C., Jungblut, P.R., and Kaufmann, S.H.E. (2003). Comparative proteome analysis of culture supernatant proteins from virulent Mycobacterium tuberculosis H37Rv and attenuated *M. bovis* BCG Copenhagen. Electrophoresis 24, 3405–3420.

McLaughlin, B., Chon, J.S., MacGurn, J.A., Carlsson, F., Cheng, T.L., Cox, J.S., and Brown, E.J. (2007). A Mycobacterium ESX-1-Secreted Virulence Factor with Unique Requirements for Export. PLoS Pathog. 3, 1051–1061.

Mishra, S.K., Shankar, U., Jain, N., Sikri, K., Tyagi, J.S., Sharma, T.K., Mergny, J.L., and Kumar, A. (2019). Characterization of G-Quadruplex Motifs in espB, espK, and cyp51 Genes of *Mycobacterium tuberculosis* as Potential Drug Targets. Mol. Ther. - Nucleic Acids 16, 698–706.

Moraco, A.H., and Kornfeld, H. (2014). Cell Death and Authophagy in TB. Semin. Immunol. 26, 497–511.

Ohol, Y.M., Goetz, D.H., Chan, K., Shiloh, M.U., Craik, C.S., and Cox, J.S. (2010). *Mycobacterium tuberculosis* MycP1 Protease Plays a Dual Role in Regulation of ESX-1 Secretion and Virulence. Cell Host Microbe 7, 210–220.

Pai, M., Behr, M.A., Dowdy, D., Dheda, K., Divangahi, M., Boehme, C.C., Ginsberg, A., Swaminathan, S., Spigelman, M., Getahun, H., et al. (2016). Tuberculosis. Nat. Rev. Dis. Prim. 2, 1–23.

Pettersen, E.F., Goddard, T.D., Huang, C.C., Couch, G.S., Greenblatt, D.M., Meng, E.C., and Ferrin, T.E. (2004). UCSF Chimera — A Visualization System for Exploratory Research and Analysis. J. Comput. Chem. 25, 1605-1612.

Piton, J., Pojer, F., Wakatsuki, S., Gati, C., and Cole, S.T. (2020). High resolution CryoEM structure of the ring-shaped virulence factor EspB from *Mycobacterium tuberculosis*. J. Struct. Biol. X 4, 100029.

Poirier, V., and Av-Gay, Y. (2012). *Mycobacterium tuberculosis* modulators of the macrophage's cellular events. Microbes Infect. 14, 1211–1219.

Silva Miranda, M., Breiman, A., Allain, S., Deknuydt, F., and Altare, F. (2012). The Tuberculous Granuloma: An Unsuccessful Host Defence Mechanism Providing a Safety Shelter for the Bacteria? Clin. Dev. Immunol. 2012, 1–14.

Simeone, R., Bottai, D., and Brosch, R. (2009). ESX/type VII secretion systems and their role in host-pathogen interaction. Curr. Opin. Microbiol. 12, 4–10.

Simeone, R., Bobard, A., Lippmann, J., Bitter, W., Majlessi, L., Brosch, R., and Enninga, J. (2012). Phagosomal Rupture by *Mycobacterium tuberculosis* Results in Toxicity and Host Cell Death. PLoS Pathog. 8, 1–13.

Solomonson, M., Setiaputra, D., Makepeace, K.A.T., Lameignere, E., Petrotchenko, E. V., Conrady, D.G., Bergeron, J.R., Vuckovic, M., Dimaio, F., Borchers, C.H., et al. (2015). Structure of EspB from the ESX-1 Type VII secretion System and Insights into its Export Mechanism. Structure 23, 571–583.

Spier, A., Stavru, F., and Cossart, P. (2019). Interaction between Intracellular Bacterial Pathogens and Host Cell Mitochondria. Microbiol. Spectr. 7, 1–11.

Stace, C.L., and Ktistakis, N.T. (2006). Phosphatidic acid- and phosphatidylserine-binding proteins. Biochim. Biophys. Acta - Mol. Cell Biol. Lipids 1761, 913–926.

Starr, T., Bauler, T.J., Malik-Kale, P., and Steele-Mortimer, O. (2018). The phorbol 12-myristate-13-acetate differentiation protocol is critical to the interaction of THP-1 macrophages with *Salmonella typhimurium*. PLoS One 13, 1–13.

Stetefeld, J., McKenna, S.A., and Patel, T.R. (2016). Dynamic light scattering: a practical guide and applications in biomedical sciences. Biophys. Rev. 8, 409–427.

Stoop, E.J.M., Bitter, W., and van der Sar, A.M. (2012). Tubercle bacilli rely on a type VII army for pathogenicity. Trends Microbiol. 20, 477–484.

Strong, M., Sawaya, M.R., Wang, S., Phillips, M., Cascio, D., and Eisenberg, D. (2006). Toward the structural genomics of complexes: Crystal structure of a PE/PPE protein complex from *Mycobacterium tuberculosis*. Proc. Natl. Acad. Sci. U. S. A. 103, 8060–8065.

Stutz, M.D., Clark, M.P., Doerflinger, M., and Pellegrini, M. (2017). *Mycobacterium tuberculosis*: Rewiring host cell signaling to promote infection. J. Leukoc. Biol. 103, 259–268.

Tan, T., Lee, W.L., Alexander, D.C., Grinstein, S., and Liu, J. (2006). The ESAT-6/CFP-10 secretion system of *Mycobacterium marinum* modulates phagosome maturation. Cell. Microbiol. 8, 1417–1429.

Vieira, O. V., Botelho, R.J., and Grinstein, S. (2002). Phagosome maturation: Aging gracefully. Biochem. J. 366, 689–704.

Wang, Q., Boshoff, H.I.M., Harrison, J.R., Ray, P.C., Green, S.R., Wyatt, P.G., and Barry, C.E. (2020). PE/PPE proteins mediate nutrient transport across the outer membrane of *Mycobacterium tuberculosis*. Science. 367, 1147–1151.

Wiens, K.E., and Ernst, J.D. (2016a). The Mechanism for Type I Interferon Induction by *Mycobacterium tuberculosis* is Bacterial Strain-Dependent. PLoS Pathog. 12, 1–20.

Wiens, K.E., and Ernst, J.D. (2016b). Type I interferon is pathogenic during chronic *Mycobacterium africanum* infection. J. Infect. Dis. 214, 1893–1896.

Wong, K.-W. (2017). The Role of ESX-1 in *Mycobacterium tuberculosis* Pathogenesis. Microbiol. Spectr. 5, 1–8.

Yang, C.Y., and Frohman, M.A. (2012). Mitochondria: Signaling with phosphatidic acid. Int. J. Biochem. Cell Biol. 44, 1346–1350.

Yeung, T., Gilbert, G.E., Shi, J., Silvius, J., Kapus, A., and Grinstein, S. (2008). Membrane Phosphatidylserine Regulates Surface Charge and Protein Localization. Science. 319, 210–213.

Youle, R.J., and Van Der Bliek, A.M. (2012). Mitochondrial Fission, Fusion, and Stress. Science. 337, 1062–1065.

Zhang, F., Wang, Z., Lu, M., Yonekubo, Y., Liang, X., Zhang, Y., Wu, P., Zhou, Y., Grinstein, S., Hancock, J.F., et al. (2014). Temporal Production of the Signaling Lipid Phosphatidic Acid by Phospholipase D2 Determines the Output of Extracellular Signal-Regulated Kinase Signaling in Cancer Cells. Mol. Cell. Biol. 34, 84–95.

Zhang, Q., Wang, D., Jiang, G., Liu, W., Deng, Q., Li, X., Qian, W., Ouellet, H., and Sun, J. (2016). EsxA membrane-permeabilizing activity plays a key role in mycobacterial cytosolic translocation and virulence: Effects of single-residue mutations at glutamine 5. Sci. Rep. 6, 1–15.

APPENDIX 1

$$R = \frac{k_B T}{6\pi\eta D}$$

Equation 1: Radius of particles within sample calculated by DLS instrument where R is the radius of the particles, k_B is the Boltzmann constant, T is the temperature, η is the viscosity of the medium and D is the diffusion coefficient.

$$\frac{Uninfected - Treatment}{Uninfected} \times 100\% = \%\ Relative\ Cytotoxicity$$

Equation 2: RFU values obtained from treatment groups were compared to RFU values from uninfected THP-1 macrophages to calculate the percent relative cytotoxicity.